การประดิษฐ์ขั้วไฟฟ้าระดับจุลภาคของอนุภาคนาโนเงินและทองด้วย

เทคนิคโฟลดิโพซิชันสำหรับการประยุกต์แลบออนชิพ

นางสาวผาณิตมาส กำลังดัสนะ

วิทยานิพนธ์นี้เป็นส่วนหนึ่งของการศึกษาตามหลักสูตรปริญญาวิทยาศาสตรดุษฎีบัณฑิต
สาขาวิชาวิทยาศาสตร์นาโนและเทคโนโลยี (สหสาขาวิชา)
บัณฑิตวิทยาลัย จุฬาลงกรณ์มหาวิทยาลัย
ปีการศึกษา 2554

FABRICATION OF SILVER AND GOLD NANOPARTICLES MICROELECTRODE BY FLOW DEPOSITION TECHNIQUE FOR LAB ON A CHIP APPLICATION

Miss Panittamat Kumlangdudsana

A Dissertation Submitted in Partial Fulfillment of the Requirements

for the Degree of Doctor of Philosophy Program in Nanoscience and Technology

(Interdisciplinary Program)

Graduate School

Chulalongkorn University

Academic Year 2011

Thesis Title	FABRICATION OF SILVER AND GOLD NANOPARTICLES MICROELECTRODE BY FLOW DEPOSITION TECHNIQUE FOR LAB ON A CHIP APPLICATION
Thesis Advisor	Luxsana Dubas, Ph.D.
Thesis Co-advisor	Stephan Thierry Dubas, Ph.D. Adisorn Tuantranont, Ph.D

Accepted by the Graduate School, Chulalongkorn University in Partial Fulfillment of the Requirements for the Doctoral Degree

…….. Dean of the Graduate School

(Associate Professor Pornpote Piumsomboon,Ph.D.)

THESIS COMMITTEE

…….. Chairman

(Associate Professor Vudhichai Parasuk, Ph.D.)

…….. Thesis Advisor

(Luxsana Dubas, Ph.D.)

…….. Thesis Co-advisor

(Stephan Thierry Dubas, Ph.D.)

…….. Thesis Co-advisor

(Adisorn Tuantranont, Ph.D.)

…….. Examiner

(Assistant Professor Sukkaneste Tungasmita, Ph.D.)

…….. Examiner

(Ratthapol Rangkupan, Ph.D.)

…….. External Examiner

(Assistant Professor Supattanapong Dumrongrattana, Ph.D.)

ผาณิตมาส กำลังดัสนะ : การประดิษฐ์ขั้วไฟฟ้าระดับจุลภาคของอนุภาคนาโนเงินและทองด้วยเทคนิคโฟลดิโพซิชันสำหรับการประยุกต์แลบออนชิพ. (FABRICATION OF SILVER AND GOLD NANOPARTICLES MICROELECTRODE BY FLOW DEPOSITION TECHNIQUE FOR LAB ON A CHIP APPLICATION) อ. ที่ปรึกษาวิทยานิพนธ์หลัก: ดร.ลักษณา ดูบาส, อ. ที่ปรึกษาวิทยานิพนธ์ร่วม: ดร.สเตฟาน เทียรี่ ดูบาส, ดร.อดิสร เตือนตรานนท์, 150 หน้า.

งานวิจัยนี้เป็นการประดิษฐ์ขั้วไฟฟ้าจากอนุภาคนาโนเงินและทอง โดยใช้กระบวนการโฟลดิโพซิชันร่วมกับเทคนิคเลเยอร์บายเลเยอร์ โดยเทคนิคนี้ใช้พีดีเอ็มเอสเป็นแบบสำหรับการประดิษฐ์ขั้วไฟฟ้าที่ต้องการ ซึ่งอนุภาคนาโนจะไหลผ่านแบบสลับกับพอลีไดแอลลิลไดเมทิลแอมโมเนียมคลอไรด์ ในการเตรียมอนุภาคนาโนเงินจะใช้ฮิวมิคแอซิด, พอลิสไตรีนซัลโฟนิคแอซิดโคมาเลอิคแอซิด และแอลจินิกแอซิด เป็นสเตบิไลเซอร์ ในขณะที่อนุภาคนาโนทองใช้โซเดียมซิเตรทเป็นตัวสเตบิไลเซอร์ เมื่อเตรียมเป็นฟิล์มบาง พบว่าฟิล์มที่เตรียมจากอนุภาคนาโนทองที่เตรียมจากโซเดียมซิเตรทที่ความเข้มข้น 30 มิลลิโมลาร์จะแสดงคุณสมบัติการนำไฟฟ้าที่ดีที่สุด ซึ่งค่าสภาพต้านทานของฟิล์มที่สร้างจะถูกวัดด้วยเทคนิค โฟร์พอยท์โพรบ โดยขั้วที่เคลือบด้วยฟิล์มที่สร้างจากอนุภาคนาโนทองจำนวน 6 ชั้นให้ค่าสภาพต้านทานใกล้เคียงกับโลหะทองซึ่งมีค่าเท่ากับ 2.44×10^{-6} โอห์ม เซนติเมตร ในขณะที่ ความหนาและลักษณะทางสัณฐานวิทยาของขั้วไฟฟ้าจากอนุภาคโลหะนาโนทองถูกวิเคราะห์ด้วยกล้องจุลทรรศน์แรงอะตอมและกล้องจุลทรรศน์อิเล็กตรอน นอกจากนี้ในการศึกษานี้ได้มีการทดสอบประสิทธิภาพของขั้วไฟฟ้าที่เตรียมโดยวัดค่าการนำไฟฟ้าของสารละลายโพแทสเซียมคลอไรด์ด้วยกระบวนการวัดค่านำไฟฟ้าจากกระแสสลับนอกจากนี้พบว่าค่าการนำไฟฟ้าของสารละลายโพแทสเซียมคลอไรด์ที่ได้จากขั้วไฟฟ้าทอง 10 ขั้วที่เตรียมขึ้นให้ค่าความแปรปรวนของผลการวัดที่ดี โดยมีค่าร้อยละการกระจายสัมพัทธ์เป็น 0.29, 0.13 และ 0.28 สำหรับการวัดค่าการนำไฟฟ้าของสารละลายโพแทสเซียมคลอไรด์ความเข้มข้น 1, 10 และ 100 มิลลิโมลาร์ ตามลำดับ นอกจากนี้ได้มีการประเมินประสิทธิภาพการทำงานของขั้วไฟฟ้าต่อการวัดค่าการนำไฟฟ้าซ้ำๆ พบว่า ความแม่นยำในการวัดดี โดยมีค่า % RSD เท่ากับ 0.21, 2.18 และ 0.08 สำหรับความเข้มข้นสารละลายโพแทสเซียมคลอไรด์เป็น 1, 10 และ 100 มิลลิโมลาร์ ตามลำดับ ทั้งนี้ได้มีการทดสอบความแข็งแรงในการยึดเกาะพื้นผิวของขั้วไฟฟ้าโดยเปรียบเทียบกับขั้วที่มีการเคลือบฟิล์มบางหลายชั้นด้วยกระบวนการประยุกต์จาก ASTM D3359 พบว่าการเคลือบฟิล์มบางหลายชั้นบนขั้วไฟฟ้าสามารถช่วยปกป้องขั้วไฟฟ้าจากการหลุดลอกได้ โดยไม่ส่งผลต่อการวัดค่าการนำไฟฟ้าของสารละลายโพแทสเซียมคลอไรด์ ในการศึกษาครั้งนี้ ได้ประยุกต์ขั้วไฟฟ้าจึงได้ทำการเคลือบฮิวมิคแอซิดบนชั้นของฟิล์มบางหลายชั้นที่เคลือบอยู่บนขั้วไฟฟ้าเพื่อใช้ในการตรวจวัดคาร์บาริล โดยค่ากระแสที่วัดได้ลดลง 7 เปอร์เซ็นต์หลังจากคาร์บาริลดูดซับลงบนขั้วที่เคลือบด้วยฮิวมิคแอซิดและมัลติเลเยอร์ฟิล์ม นอกจากนี้งานวิจัยนี้ยังได้ทำการปรับปรุงพื้นผิวของวัสดุพอลิเมทิลเมทาคริเลตและพีดีเอ็มเอสซึ่งเป็นวัสดุในการสร้างอุปกรณ์ไมโครฟลูอิดิกด้วย พอลิไดแอลลิลไดเมทิลแอมโมเนียมคลอไรด์-พอลิสไตรีนซัลโฟเนต หรือ ไคโตซาน-แอลจิเนต โดยใช้เทคนิคเลเยอร์บายเลเยอร์ เพื่อปกป้องวัสดุจากตัวทำละลายอินทรีย์ ร้อยละการส่งผ่านแสงใช้ในการบอกถึงประสิทธิภาพของวัสดุพอลิเมทิลเมทาคริเลตที่ทำการปรับปรุงพื้นผิวเมื่อจุ่มในสารละลายอะซิโตไนไตรล์ ในขณะการปรับปรุงพื้นผิวของพีดีเอ็มเอสติดตามด้วยการวัดการเปลี่ยนแปลงน้ำหนักเมื่อสัมผัสไอของคลอโรฟอร์มโดยผลแสดงถึงความสามารถในการปกป้องพื้นผิวจากสารละลายอินทรีย์ได้เป็นอย่างดี

สาขาวิชา วิทยาศาสตร์นาโนและเทคโนโลยี ลายมือชื่อนิสิต .....

ปีการศึกษา 2011 ลายมือชื่อ อ.ที่ปรึกษาวิทยานิพนธ์หลัก.....

ลายมือชื่อ อ.ที่ปรึกษาวิทยานิพนธ์ร่วม .....

.....

4989732420 : MAJOR NANOSCIENCE AND TECHNOLOGY

KEYWORDS: GOLD NANOPARTICLES / MICROFLUIDIC/ MICROELECTRODE

PANITTAMAT KUMLANGDUDSANA: FABRICATION OF SILVER AND GOLD NANOPARTICLES MICROELECTRODE BY FLOW DEPOSITION TECHNIQUE FOR LAB ON A CHIP APPLICATION. ADVISOR: LUXSANA DUBAS, Ph.D., CO-ADVISORS: STEPHAN THIERRY DUBAS, Ph.D., ADISORN TUANTRANONT, Ph.D. 150 pp.

In this research, silver and gold nanoparticles electrodes were fabricated using layer-by-layer technique combining with the flow deposition methods. Pre-designed microfluidic channels were used as templates for the desired electrode. The nanoparticles was alternatively flow with poly(diallyldimethyl amonium chloride) (PDADMAC) through the template. First, the silver nanoparticles were synthesized using either humic acid (HA), poly(4-styrenesulfonic acid-co-maleic acid) (PSS-co-MA) or alginic acid as a stabilizing agent. Sodium citrate was used as stabilizing agent and reducing agent for gold nanoparticles preparation. The multilayer thin film electrode fabricated with the gold nanoparticles using 30 mM sodium citrate as reducing and stabilizing reagents shown the best conductivity. The resistivity of the film was measured using 4 points probe. The resistivity as low as 10-6 ohm.cm was achieved after the deposition of only 6 layers of gold nanoparticles preparing with 30 mM sodium citrate. The thickness and morphology of the flow-printed multilayer microelectrode was characterized by atomic force microscopy (AFM) and field emission scanning electron microscope (FE-SEM). The performance of gold nanoparticles electrodes was then tested using AC current detection of potassium chloride (KCl) solution. The current detection of KCl solution of the ten different gold nanoparticles electrodes revealed good reproducibility with 0.29, 0.13 and 0.28 %RSD for detection of 1, 10 and 100 mM KCl concentrations. Moreover, the performance of an electrode was also tested, which showed a good precision (0.21, 2.18 and 0.08 % RSD for 1, 10 and 100 mM KCl concentrations, respectively). The physical contact test adapted from ASTM D3359 was also performed on the uncoated gold nanoparticles electrode comparing with the gold nanoparticles electrode coated polyelectrolyte multilayers thin films (PEMs). The PEMs coating on gold nanoparticles electrodes could prevent scratching of electrodes and did not affect its detection performace. The detection of carbaryl was investigated as the potential application for the fabricated electrode. First, humic acid was deposited on the PEMs-gold nanoparticles electrodes. When, the carbaryl binding with HA-PEMs-gold nanoparticles electrode, the 7 % drop of current was obtained. Moreover, in this study, the organic solvent resistance substrate was also developed. The poly(methyl methacrylate) (PMMA) and poly(dimethyl siloxane) (PDMS) substrates were coated with either PDADMAC/poly(sodium 4-styrenesulfonate)/(PSS) or chitosan/alginate. %Transmission was used to evaluate the performance of the developed surface of PMMA after dipping to the acetonitrile solution, while the modified PDMS substrate was evaluated by observation of the changing weight under exposing to chloroform vapor. The results showed that the substrate could be protected from organic solvent by simply coating technique as LBL technique.

Field of Study : Nanoscience and technology Student's Signature .....

Academic Year : 2011 Advisor's Signature .....

Co-advisor's Signature .....

.....

ACKNOWLEDGEMENTS

I would like to express my gratitude to all those who gave me the possibility to complete this dissertation. First of all, I would like to express my deepest gratitude to Dr. Luxsana Dubas, Dr. Stephan Thierry Dubas and Dr. Adisorn Tuantranont, my advisor team, for their kind supervision, valuable advice, and helpful criticism throughout my studied.

I would also like to express my sincere thanks to committee; Associate Professor Dr. Vudhichai Parasuk, Assistant Professor Sukkaneste Tungasmita, Dr. Ratthapol Rangkupan, and Associate Professor Dr. Supattanapong Dumrongrattana for their helpful comments and participation as dissertation committees.

I would like to acknowledge the Thailand Graduate Institute of Science and Technology (TGIST: TG-44-09-50-085D) and Nanoscience and Technology (International Program), Nanoscience and Technology Interdisciplinary Program, Graduate School, Chulalongkorn University for providing financial support. I would also like to acknowledge Metallurgy and Materials Science Research Institute for all providing facilities.

I would like to thanks Dr. Kanokporn Boonsong for her kindness and valuable advice. Thank for my lovely friends in PEMs lab and Miss Chindarat Pinkeaw for their friendship, encouragement and help along my study.

Last but not the least, I would express my deepest gratitude to my parents for their love, moral support, great encouragement, blessing and always stand by me in time of need.

CONTENTS

LIST OF TABLES

LIST OF FIGURES

CHAPTER I
INTRODUCTION

The recent advances in fabrication technology have led to reduction in size of devices by several orders of magnitude. One area that benefits in particular from this trend is the area of microfluidic system. Microfluidic devices can be used to obtain a variety of interesting application such as DNA and protein separation, immunoassay, and biosensors. Microfluidic devices have potential in a reduction of cost per analysis, a decreasing of sample amount, and shorter analysis time.

Microfluidic chips used in lab-on-chip applications usually include a detection stage used to quantify the concentration of a compound or to monitor the separation of a mixture of solutes [1-2]. Although potentiometric method are often used for electrochemical detection, impedance spectroscopy or contactless conductivity detection were preferred for portable applications [3-6]. These electrical detection methods require miniaturized electrodes positioned across in the microfluidic channel and connected to either a potentiostat or a function generator and multimeter [7-8]. The design of miniaturized electrodes is a challenge considering that they need to be precisely adjusted in the channel and be sufficiently thin and do not obstruct the flow in the microfluidic channels [9]. Gold wires sandwiched between the two sections of a microchip were firstly used but tend to be replaced with printed micro-electrode which can have very complex shape and more precise positioning [10-11]. These microelctrodes were first prepared by chemical vapor deposition but the wet screen printing of micro-electrode is now being developed as an alternative of vacuum methods [12-14]. The reported methods are based on the flow of the solutions though the micro-channels which were left to dry to form a self assembled coating of conducting particles such as silica nanoparticles or carbon particles solution. In recent developments, carbon based solution are being replaced with dispersed metallic nanoparticles of gold or silver [12, 15-18]. However, the thick electrode was obtained which trend to crack after bonding of substrate. [19-20]. The layer-by-layer deposition of nanoparticles

appears to be a good alternative mainly because it allows an excellent control over the amount of nanoparticles deposited after each cycles.

Polyelectrolyte multilayers can be prepared using an alternating sequence of positively and negatively charged polyelectrolytes. Polyelectrolyte multilayers (PEM) are obtained by means of electrostatic layer-by-layer deposition. Layer-by-layer deposition has been successful in producing thin films with unique optical, electrical, and mechanical properties. Layer-by-layer nanoparticle assemblies can also be prepared by alternately dipping a substrate into nanoparticles and polyelectrolyte solutions. The resulting material is a nanoparticle-polymer hybrid, which combines the unique properties of nanoparticles and the mechanical properties of polymers.

Objective of this study

The study is aimed to develop an electrode fabrication method, which is simple, low cost and can be done under ambient condition by employing layer-by-layer technique combining with flow deposition method. The technique used PDMS as a mold to fabricate electrode, which was reversible seal to glass substrate, to define the size of electrode. The electrodes were prepared through layer-by-layer deposition of metallic nanoparticles and cationic polyelectrolyte. The electrode performances were evaluated by Atomic Force Microscopy (AFM), Field Emission Scanning Electron Microscope (FE-SEM), four point probe and conductivity detection of potassium chloride solution. Lastly, the novel surface modification method to protect polymer substrate from organic solvent penetration was developed via layer-by-layer (LbL) technique.

Scope of this study

Silver and gold nanoparticles were used to fabricate electrodes. Three types of polyelectrolyte, humic acid, poly(4-styrenesulfonic acid-*co*-maleic acid) sodium salt and alginic acid, were chosen to synthesis silver nanoparticles as stabilizing agents. Sodium citrate was used to stabilize gold nanoparticles. The metallic nanoparticles electrodes were integrated with conductivity detector.

The prepared electrodes were characterized by four point probe apparatus and their potential usage in the detection of potassium chloride (KCl) solution was confirmed by AC current detection. The electrodes were used to detect the conductivity of humic acid after binding with carbaryl insecticide.

For the development of organic solvent resistance surface, the poly(methyl methacrylate) (PMMA) and poly(dimethylsiloxane) (PDMS) substrates were protected by polyelectrolyte multilayers (PEM) thin films of either poly(diallydimethyl ammonium chloride)/ poly(styrene sulfonate) (PDADMAC/PSS) pair or chitosan/alginate pair. The PEMs deposited on the PMMA and PDMS substrates was used to improve the resistance toward the organic solvent.

CHAPTER II
THEORY AND LITERATURE REVIEW

2.1 Metallic Nanoparticles

2.1.1. Introduction to metallic nanoparticles [54]

Nanoparticles are defined as particles having sizes between 1 to 100 nanometers. Depending on the application of interest, nanoparticles may be known by a number of alternative and other specific names, including ultrafine particles, clusters, nanocrystals, quantum dots, colloids, aerosols, hydrosols, organosols [21-28]. The increase in the surface area to volume ratio can lead to an increasing dominance of the behavior of atoms on the surface of particle. This affects particles properties in isolation and interaction with other material. High surface area is an important factor in performance of catalysis and structures such as electrodes, allowing improvement in performance of some technologies. There is growing interest in utilizing metal nanoparticles because of their unique properties such as optical, electrical, and thermal properties [29-32]. Moreover, metal nanopartilces are being incorporated into products that range from the antimicrobial activity of surgical sutures to chemical sensors [33-34]. The metal nanoparticles can be combined into solid without sintering process, leading to improve especially in electronic applications. There are different types of nanomaterial according to the shape of particles such as sphere nanoparticles (Figure 2.1 [a]), nanorods (Figure 2.1[b]), and nanowires (Figure 2.1 [c] [35-37].

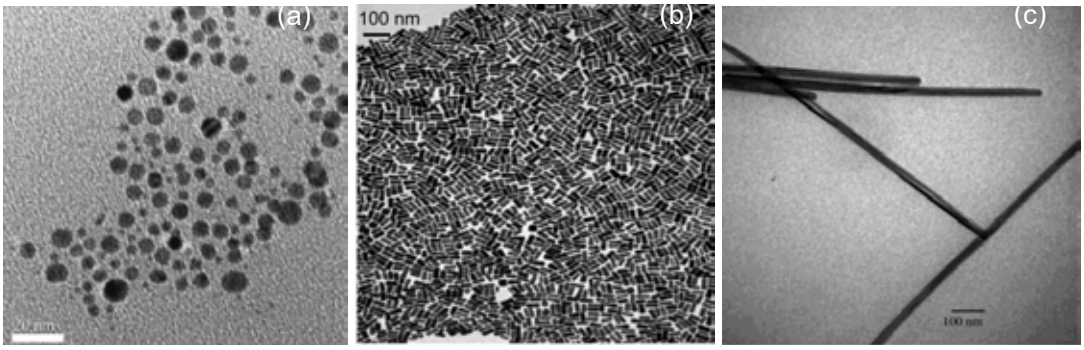

Figure 2.1 TEM images of nanoparticles (a), nanorods (b) and nanowires (c) [35-37].

2.1.2. Properties of metallic nanoparticles

2.1.2.1 Optical property

The optical properties of metal nanoparticles have long been of interest in physical chemistry for long time. Gold colloidal nanoparticles are responsible for the brilliant reds seen in stained glass windows. Silver particles are typically yellow. These properties have been of interest for centuries, and scientific research on metal nanoparticles dates at least to Michael Faraday. Mie presented a solution to Maxwell's equations that describes the extinction spectra (extinction) (scattering + absorption) of spherical particles of arbitrary size. Mie's theory has remained important for so long is that it is the only simple, exact solution to Maxwell's equations that is relevant to particles. In addition, most of the standard colloidal preparations yield particles that are approximately spherical, and most of the optical methods for characterizing nanoparticles spectra probe a large ensemble of these particles [38]. Recently, however, there has been growing interest in characterizing the optical properties of metal nanoparticles that are made using lithographic methods such as nanosphere lithography, e-beam lithography, and other methods, which produce well-defined sizes and nonspherical shapes without aggregation. In addition, variations on classical wet chemistry techniques have been developed that give high yields of nonspherical particles, especially rods and triangles [38]. The shapes and sizes of these particles are better characterized than in the past using electron and scanning probe microscopy and in some cases, the optical properties of individual nanoparticles have been determined.

The free electrons in the metal are free to travel through the material. The mean free path of metal nanoparticles are very small, nevertheless, in nanoparticles smaller than bulk metal, no scattering is expected from the bulk. The wavelength of light is much larger than the nanoparticle size it can set up standing resonance conditions as represented in figure 2.2. Light in resonance with the surface plasmon oscillation causes the free-electrons in the metal to oscillate. As the wave front of the light passes, the electron density in the particle is polarized to one surface and oscillates in resonance with the light's frequency causing a standing oscillation. The resonance condition is

determined from absorption and scattering spectroscopy and is found to depend on the shape, size, and dielectric constants of both the metal and the surrounding material. This is referred to as the surface plasmon resonance (SPR), since it is located at the surface. As the shape or size of the nanoparticles changes, the surface geometry change causing a shift in the electric field density on the surface. This causes a change in the oscillation frequency of the electrons, generating different cross-sections for the optical properties including absorption and scattering. When the electron cloud is displaced relative to the nuclei, a restoring force arises from Coulomb attraction between electrons and nuclei that results in oscillation of the electron cloud relative to the nuclear framework. The oscillation frequency is determined by four factors: the density of electrons, the effective electron mass, and the shape and size of the charge distribution. The collective oscillation of the electrons is called the dipole plasmon resonance of the particle.

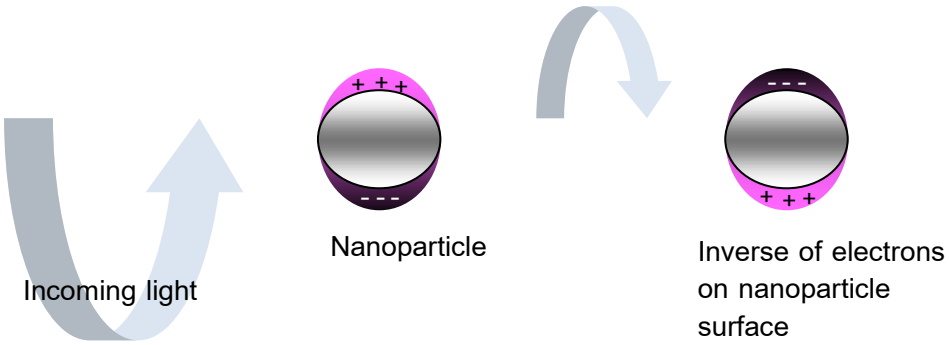

Figure 2.2 Origin of surface plasmon resonance due to coherent interaction of the electrons in the conduction band with light [39].

The size and shape of metal nanoparticles are typically measured by analytical techniques such as TEM, scanning electron microscopy (SEM) or atomic force microscopy (AFM). Measuring the aggregation state of the particles requires a technique to measure the effective size of the particles in solution such as dynamic light scattering (DLS) or analytical disc centrifugation. However, due to the unique optical properties of silver nanoparticles, a great deal of information about the physical state of

the nanoparticles can be obtained by analyzing the spectral properties of silver nanoparticles in solution [40].

Changing the dielectric constant of the surrounding material will have an effect on the oscillation frequency due to the varying ability of the surface to accommodate electron charge density from the nanoparticles. Changing the solvent will change the dielectric constant, but the capping material is most important in determining the shift of the plasmon resonance due to the local nature of its effect on the surface of the nanoparticles. Chemically bonded molecules can be detected by the observed change they induce in the electron density on the surface, which results in a shift in the surface plasmon absorption maximum. This is the basis for the use of noble metal nanoparticles as sensitive sensors.

By controlling the dielectric constant of the surrounding medium, the wavelength of the SPR can be fine tuned to a desired position, as is shown in figure 2.3. In the first panel, the SPR is shifted to shorter wavelengths due to the decrease in the dielectric constant from that of isopropanol to that of Teflon AF [41].

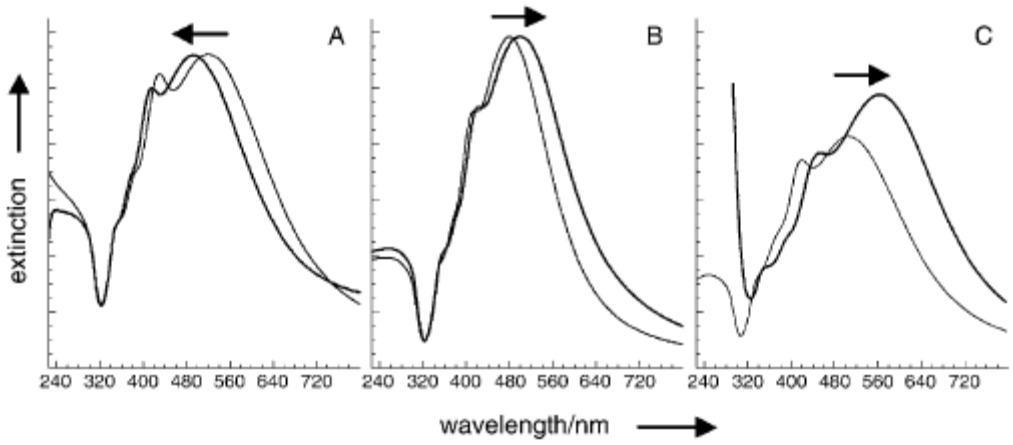

Figure 2.3 UV/Vis extinction spectra of silver nanoparticles suspensions before (——) and after (——) changes were made to the dielectric environment from A) isopropanol to Teflon AF, B) water to silica, and C) water to titania [41].

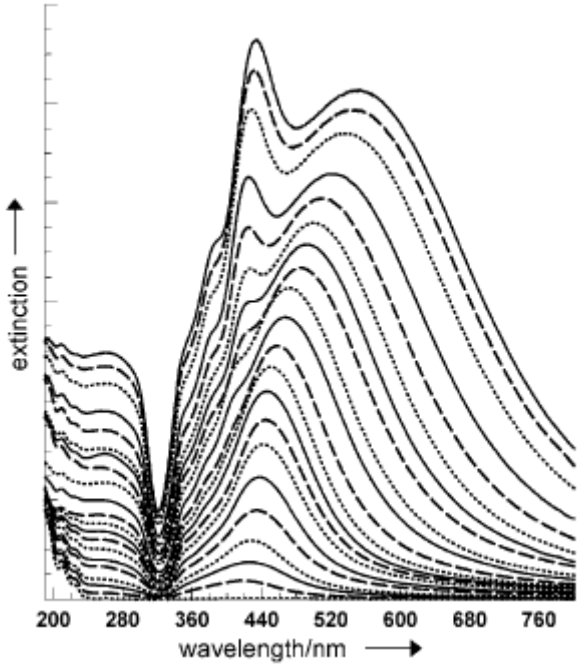

Figure 2.4 UV/Vis extinction spectra of silver nanoparticles suspensions of 20 different particle diameters [41].

In figure 2.4, the SPR extinction spectra of Ag suspensions of different particle diameters are shown. It is apparent that the dipole maximum rapidly shifts to longer wavelengths as the particle size increases beyond 70 nm (450 nm spectral maximum) revealing the quadrupole peak at about 420 nm. The observed spectral shift results from the “spreading” of the particle’s surface charge over a larger surface area so that the surrounding medium better compensates the restoring force thus slowing the electron oscillations [41].

2.1.2.2 Electrical property

Nanoparticles may exhibit size-related properties that differ significantly from those observed in fine particles or bulk materials. The effects of size on electrical property of nanoparticles are complex, since they are based on distinct mechanisms. This mechanism can be generated some groups of categories: quantized conduction including ballistic conduction, Coulomb charging and tunneling and widening and discrete of band gap and change of microstructures. Moreover, increased perfection,

such as reduced impurity, structure defects and dislocations would affect the electrical conductivity of nanomaterials [42].

A reduction in characteristic dimension below a critical size would result in a change of electronic structure, leading to widening and discrete band gap. Tunneling conduction is another charge transport mechanism important in the nanometer range. Tunneling involves charge transport through an insulating medium separating two conductors that are extremely closed spaced. It is because the electron wave functions from two conductors overlap inside the insulating material, when its thickness is extremely thin.

2.1.2.3 Catalytic property

The catalytic properties metal nanoparticles have generated great interest. In fact, these new catalysts often combine the precious characteristics of higher reactivity and selectivity. This can be explained by the structural specificities of the colloidal state of the catalyst: these materials have a very large specific surface, and consequently a large percentage of catalyst's metal atoms are available to the substrates [43]. Several studies in metal particle catalysis research area have been performed to know the true number of catalytically active surface sites.

Lehnert A. and co-workers prepared catalytic properties of bimetallic colloids consisting of a ligand-stabilized Pt shell on Au or Pd cores supported by alumina [44]. Bailly A. and co-workers investigated the relationship between catalytic activity and size/shape of gold nanoparticles supported on TiO_2(110) during CO oxidation [45]. The dependence of the catalytic activity on the particle size is presented in figure 2.5. The activity increases as the diameter of the gold particles decreases below 5-6 nm. It passes through a maximum at 2.0 nm where the height of the particles is one atomic layer.

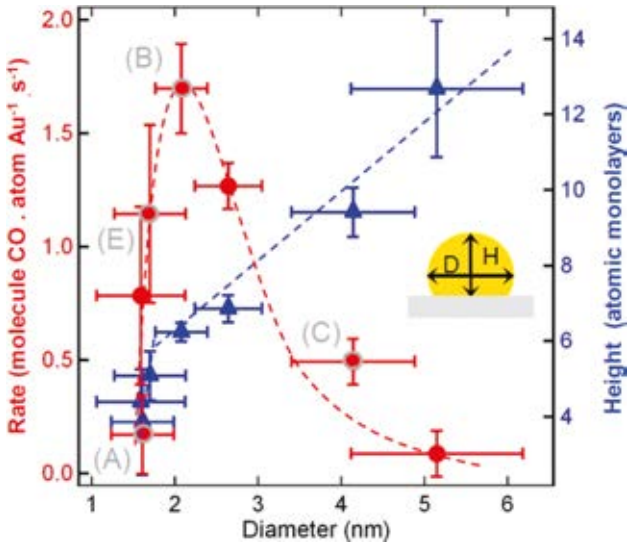

Figure 2.5 Reaction rate as a function of the mean particle diameter (red circles). The labels correspond to the different samples mentioned in the text. Blue triangles: variation of the measured mean height (in number of atomic layers) as a function of the diameter. The dashed lines are guide for eyes, and the error bars represent the width of the size distribution [45].

Chattopadhyay A and co-workers presented Catalytic gold nanoparticles driven pH specific chemical locomotion [46]. The pH-dependence of rate constants of H_2O_2 decomposition measured both in the presence and in absence of the catalytic beads is shown in figure 2.6. As can be seen, in the pH range of 9.1–10.8, the rate constant for the decomposition of H_2O_2 in the presence of Au NP deposited beads was higher at all (measured) pH than the same measured with non-catalytic polymer beads.

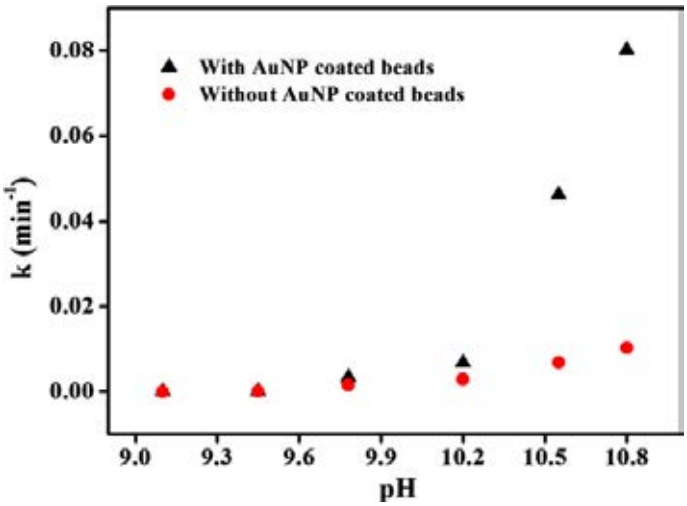

Figure 2.6 Variation of decomposition rate constants of H_2O_2 with pH, in the presence and absence of Au NPs [46].

2.1.3 Synthesis of metal nanoparticles [43]

The formation of metal nanoparticles can be obtained by two ways (Figure 2.7): (I) physical method or (II) chemical method.

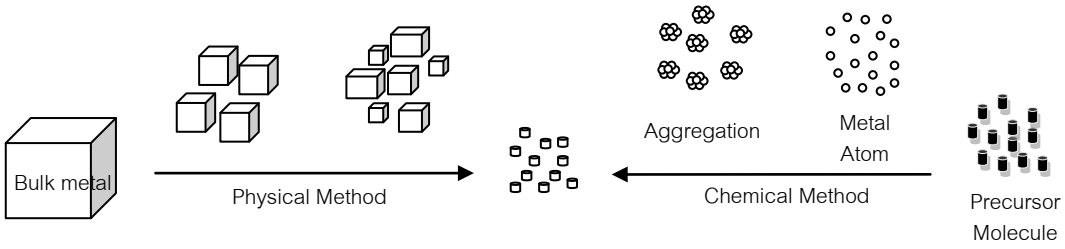

Figure 2.7 The illustration of preparative methods of metal nanoparticles.

The very broad size of metal nanoparticles is found from the physical methods preparation. Chemical methods are the most convenient ways to control the particles. The dispersion of colloids in liquid media can be obtained variously leading to various particles size distributions. Nevertheless, the method used a stabilizing agent is always necessary to prevent the aggregation of the colloids formed into larger particles.

Five general synthetic methods are mainly used to synthesize transition metal colloids: (i) chemical reduction of transition metal salts, (ii) thermal, photochemical, or

sonochemical decomposition, (iii) ligand reduction and displacement from organometallics, (iv) metal vapor synthesis, and (v) electrochemical reduction.

2.1.3.1 Chemical reduction of transition metal salts

The reduction of metal salts in solution is the most widely used method to generate metal nanoparticles. In fact, this method is generally very simple to achieve. A wide range of reducing agents have been used to obtain colloidal materials: gas such as hydrogen or carbon monoxide, hydrides or salts such as sodium borohydride or sodium citrate, or even oxidable solvents such as alcohols.

The borohydrides ($NaBH_4$ or KBH_4) reduction of metal salts is the most widely used hydride reduction method of generating aqueous suspensions of metals. The stabilizing agents used in these cases are generally surfactants or water-soluble polymers in order to prevent agglomeration of particles. These method silver nanoparticles were generated in the presence of water-soluble nonionic polymers and anionic polyelectrolytes [47]. Hausner SH and co-workers presented the investigation of the ability and stability of silver nanoparticles by an anionic sulfonate polyelectrolyte and three polyacids (which are partially deprotonated in aqueous medium). They found that the choice of the type of the protective polymer can have a large influence on the nanoparticles features, the optical properties, and the colloidal stability of the samples [47]. Murphy CJ and co-workers reported the chemical reaction of gold salts to gold nanoparticles [48]. They studied the effect of 12 nm gold seed concentration in the solution-phase preparation of gold nanoparticles for a range of reducing agents. Central to the concept of seed-mediated growth of nanoparticles is that small nanoparticles seeds serve as nucleation centers to grow nanoparticles to a desired size. They have examined this common assumption in a model system, the wet chemical synthesis of gold nanoparticles via reduction of a gold salt. We found that changing the seed concentration does affect the size of the product nanoparticles, but the method of reagent addition drastically affects the outcome even more. For fast addition of reducing agent, the presence of seeds appears to promote the formation of more seeds instead of growth. The observed nucleations were drastically enhanced (99%) compared to

particle growth. For slow addition of reducing agent, the seeds do grow, but the product nanoparticle's degree of homogeneity in shape was compromised. For higher concentrations of seeds, nanoparticles growth was better controlled for slow addition of reducing agent compared to fast addition of reducing agent. We propose a mechanistic step to explain the commonly observed size distribution [48].

Surfactants are also generally used as stabilizers of metal nanoparticles by $NaBH_4$ or KBH_4. They can be cationic, anionic, or nonionic. Stephen R. Leone and co-workers presented the imaging of cetyl trimethyl ammonium bromide (CTAB) capped and uncapped spherical gold nanoparticles by the aperture less near-field scanning optical microscope (ANSOM) technique [48-49]. The measurements investigated the gold-particle size-dependent signals and the modification of those signals by the CTAB layer in the visible at λ = 633 nm.

Other reducing agents such as hydrazine or sodium citrate have efficiently been used in colloidal metal preparation. Hydrazine can be used in all its forms to reduce transition metals. Sodium citrate was also used as reducing agent to obtain colloidal suspension of transition metals [43]. Turkevitch and co-workers studied the nucleation and growth of Au nanoparticles reduced by sodium citrate [50]. In this case, the citrate is not only a reducing agent but also an ionic stabilizer. Citrate reduction has also been used to prepare Ir and Pt nanoparticles [51-52]. However, citrate anion is a non-innocent ligand and has one significant disadvantage because of the simultaneously formation of the intermediate acetone dicarboxylic acid.

2.1.3.2 Thermal, photochemical, or sonochemical decomposition

Many organometallic compounds are thermally decomposed to their respective zerovalent element. The syntheses of Pd and Pt organosols by thermolysis of precursors such as palladium acetate palladium acetylacetonate have been reported in the literature [53-55]. The solvents used had high boiling points such as methyl-isobutylcetone. These syntheses were performed without stabilizing agents, and as a result broad size distributions and large particles were observed.

Photochemical method of colloid particle preparation using UV radiation yields the particles with properties similar to the particles produced by the above mentioned radiolytic method, its advantage being the simpler and cost effective experimental equipment. Mercury discharge lamp is often used as the source of UV radiation. In addition to silver salt and eventual stabilizers the reaction mixture contains suitable organic substance whose interaction with UV radiation generates radicals which reduce silver ions [56].

The usage of ultrasound in a dispersion method of colloid particle preparation it can be used also as a condensation method. The ultrasound is capable to decompose water into hydrogen and hydroxyl radicals. Subsequent reactions with suitable additives yield organic radicals which act as reducing agents. By sonisication of aqueous silver salts solutions in the presence of surfactants (the frequency of ultrasound was 200 kHz) the silver particles of 13±3 nm size were prepared [57].

2.1.3.3 Ligand reduction and displacement from organometallics

Some zerovalent organometallic complexes can be converted into colloidal suspension of metals by reduction or ligands displacements. Using this procedure, Bradley and co-workers generated Pt and Pd (PVP) stabilized organosols [58-59]. The olefinic ligand reduction of zerovalent complexes can also be applied to the preparation of colloidal suspensions.

2.1.3.4 Metal vapor synthesis

The use of metal vapors co-condensed with organic vapors to synthesized colloidal metals in nonaqueous media is known since the dawn of the last century. However, this procedure was only extensively studied in the 70s. This method consists of the evaporation at reduced pressure of relatively volatile metals and a subsequent co-condensation at low temperature of these metals with the vapors of organic solvents. A colloidal dispersion of the metal was then obtained by warming the frozen metal/organic mixture. The colloidal particles nucleate and grow as the frozen mixture is warmed to melting [43].

2.1.3.5 Electrochemical reduction

A sacrificial anode is used as a metal source. This anode is oxidized in the presence of quaternary ammonium salts, which are both the electrolyte and the stabilizing agent. The ions are then reduced at the cathode to yield the metallic nanoparticles [43]. This process presents several advantages: (i) particle size can be controlled by varying the current intensity (higher current intensity gives smaller particles); (ii) isolation of the nanoparticles is simple as they precipitate out of the solvent when formed; and finally (iii) the synthesis occurs with good yields (>95%) [43].

2.1.4 Characterization of nanomaterial

Characterizations of nanomaterials require not only extreme sensitivity and accuracy, but also atomic level resolution. It leads to various microscopic properties that will play the important role in characterization and measurements of nanostructure materials. Transmission electron microscopy (TEM), scanning electron microscopy (SEM), surface plasmon resonance detection (SPR) is most widely used in the characterization nanoparticles.

Transmission Electron Microscopy (TEM)

The transmission electron microscope (TEM) operates on the same basic principles as the light microscope but uses electrons instead of light. What you can see with a light microscope is limited by the wavelength of light. TEMs use electrons as light source and their much lower wavelength make it possible to get a resolution a thousand times better than with a light microscope. The layout of component is presented in figure 2.8. A light source at the top of the microscope emits the electrons that travel through vacuum in the column of the microscope. Instead of glass lenses focusing the light in the light microscope, the TEM uses electromagnetic lenses to focus the electrons into a very thin beam. The electron beam then travels through the specimen you want to study. Depending on the density of the material present, some of the electrons are scattered and disappear from the beam. At the bottom of the microscope the unscattered electrons hit a fluorescent screen, which gives rise to a shadow image of the specimen

with its different parts displayed in varied darkness according to their density. The image can be studied directly by the operator or photographed with a camera.

The useful range of the transmission electron microscope for particle size measurement is 1 nm- 5 μm diameter. Owing to the complexity of calculating the degree of magnification directly, this is usually determined by calibration using characterized polystyrene latex particles or a diffraction grating.

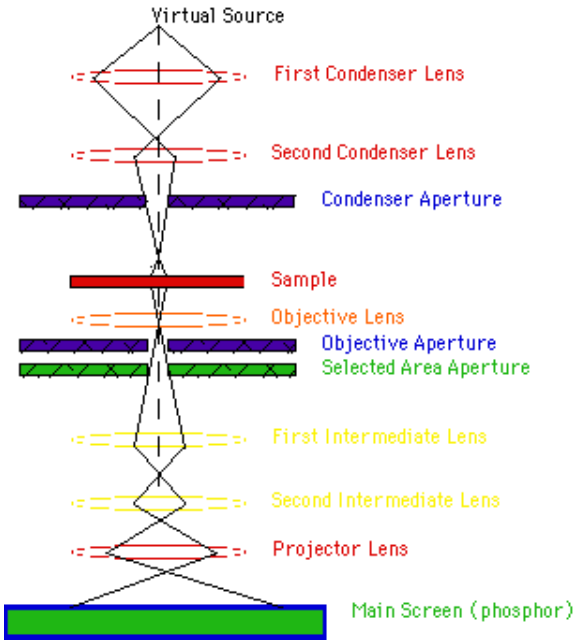

Figure 2.8 Schematic presentation of the transmission electron microscope.

Scanning Electron Microscope (SEM)

In the scanning electron microscope a fine beam of medium-energy electrons scans across the sample in a series of parallel tracks. These interact with the sample to produce various signals, including secondary electron emission (SEE), back-scattered electrons (BSE), cathodoluminescence and X-rays, each of which (with their varying characteristics) can be detected, displayed on a fluorescent screen and photographed. In the SEE mode the particles appear to be diffusely illuminated, particle size can be measured and aggregation behavior can be studied, but there is little indication of

height. In the BSE mode the particles appear to be illuminated from a point source and the resulting shadows lead to a good impression of height.

The magnification achieved in a scanning electron microscope (resolution limit of c. 5 nm) is, in general, less than that in a transmission electron microscope, but the major advantage of the technique (which is a consequence of the low numerical aperture) is the great depth of focus which can be achieved. At magnifications in the range of optical microscopy the scanning electron microscope can give a depth of focus several hundred times greater than that of the optical microscope. In colloid and surface science this large depth of focus is extremely valuable in the study of the contours of solid surfaces and in the study of particle shape and orientation.

Spectrophotometer[60]

Spectrophotometers are instruments that measure the reflectance from, or the transmittance through, materials as a function of wavelength. They have many uses besides color measurement. The visible region (380 – 780 nm) is always used for color measurement.

The main components of all spectrophotometers for color measurement are a source of optical radiation, an optical system for defining the geometric conditions of measurement, some means of dispersing light, and a detector and signal processing systems that converts light into signals suitable for analysis.

Physical properties of the specimens to be measured ultimately determine instrument design. In particular, many materials are fluorescent, using fluorescent colorants or fluorescent whitening agents: this affects the design of the illumination system. The absorption and scattering characteristics of colorants lead to slowly varying reflectance and transmittances as a function of wavelength thin the visible spectrum; this affects the design of the dispersing and detector and signal processing systems. Furthermore, because the visual system is such an excellent null detector signal processing requirements are stringent. That is, the instrument should be at least as sensitive in detecting small differences in color as an observer.

2.1.5 Application of silver and gold nanoparticles

Fernando Silva and co-workers [61]reported electrochemical characterization of polyelectrolyte/gold nanoparticles multilayers self-assembled on gold electrodes. Two different redox pairs $[Fe(CN)6]^{3-/4-}$ and $[Ru(NH3)6]3^{+/2+}$ were used to study Charge transport through the multilayer. The result showed a large sensitivity to the charge of the outermost layer for the permeability of these assemblies to the probe ions. The changes in the impedance response were obtained for thin multilayers each time a new layer was deposited. The multilayer behaved as a conductor exhibiting a strikingly lower impedance response, the electric current being enhanced as more layers were added for Au NP terminated multilayers. Litong Jin and co-workers[62] also reported silver nanoparticles modified electrode and its application to the electroanalysis of Cytochrome *c*. They could be efficiently immobilized on the surface of a silver electrode. The result showed that the CSNs could clearly enhance the electron transfer process between Cyt. c and the electrode compared with bulk silver electrode. Linear sweep voltammetric measurement of Cyt. c at the chemical modified electrode indicated that the oxidative peak current of Cyt. c was linear to its concentration ranging from 8.0 nmol L^{-1} to 3.0_mol L^{-1} with the calculated detection limit was about 2.6 nmol L^{-1}.

2.2 Formation of Polyelectrolyte Multilayer Thin film [63]

2.2.1 Polyelectrolytes [64]

The term “polyelectrolyte” is employed for polymer systems consisting of a macroion i.e., a macromolecule carrying covalently bound anionic or cationic groups, and low molecular “counterions” securing for electroneutrality. Example of an anionic and a cationic polyelectrolyte (PEL) are presented in figure 2.9.

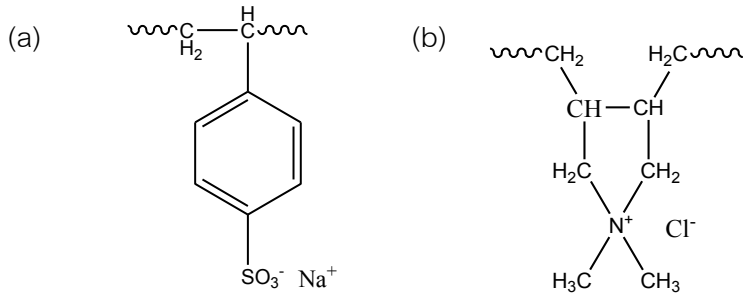

Figure 2.9 Chemical structure of (a) sodium poly(styrene sulfonate) and (b) poly(diallyldimethylammonium chloride).

Both Na-polystyrene sulfonate and poly(diallyldimethylammonium chloride) are dissociated into macroion and counterion in aqueous solution in the total pH range between 0 and 14. Also polymers like poly(acrylic acid) and poly(ethylene imine) are usually classified as polyelectrolytes, in spite of the fact that they form a polyion-counterion system only in a limited pH range, and remain as an undissociated polyacid in the acid range or undissociated polybase in the alkaline range, respectively(Figure 2.10), a behavior typical for weak polyelectrolytes and quite analogous to weak low molecular electrolytes.

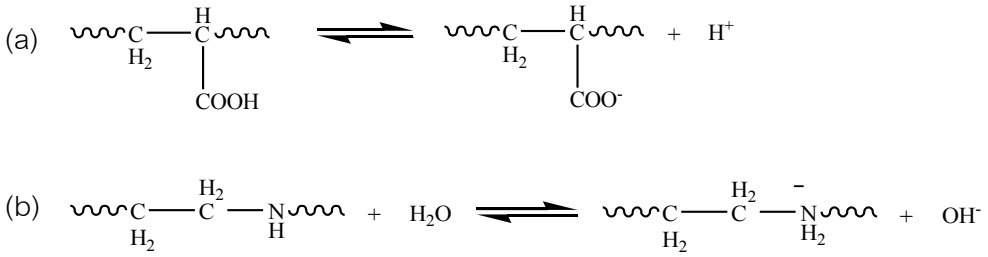

Figure 2.10 Dissociation equilibrium of the weak polyelectrolytes (a) poly(acrylic acid) and (b) poly(ethylene imine).

On the other hand, a polymer like cellulose capable of dissociating partially into cellulosate anions and counterions at extremely alkaline conditions (pH > 14) cannot be classified as a poyelectrolyte, as in the conventional pH range of dilute aqueous systems the OH groups of polymer are not ionized.

A special case of polyelectrolytes, the “polyampholytes,” carrying both anionic and cationic groups covalently bound to the macromolecule, are presented in nature by an abundant number of proteins but can also be obtained by various synthetic routes. An example is presented in figure 2.11 as a typical polyampholytes where carries both cationic charges in an acid and anionic charges in an alkaline medium.

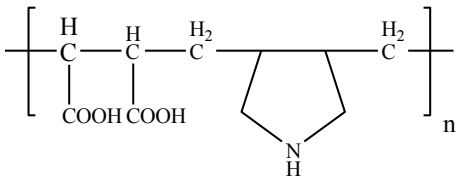

Figure 2.11 Chemical structure of a maleic acid-diallylamine copolymer.

In principle, any macromolecular chemical structure can be transform into a polyelectrolyte structure by covalently attaching a reasonable number of ionic groups to the polymer backbone, with linear or branched macromolecules at a compound soluble in an aqueous medium of appropriate pH after introducing a sufficient number of ionic groups. In the case of a cross linked polymer its swell ability in aqueous media is enhanced by transferring into a PEL. A vast number of polyelectrolyte types known today are listed in table 2.1.

Table 2.1 Selected types of polyelectrolytes

Anionic and cationic polysaccharides and polysaccharidic derivatives
Nucleic acids
Gelatin
Lignosulfonic acids
Polyacrylic and polymethacrylic acid and its copolymers
Maleic acid anhydride copolymers
Polystyrene sulfonic acid
Polyethylene imine
Polyamines and polyamidamines
Ionenes
Poly(diallyldimethylammonium chloride)
Homo- and copolymers of cationic acrylic acid esters

Table 2.1 demonstrates the remarkable variability of polyelectrolyte chemical structure, resulting from the tremendous number of polymer backbone structures. Today's commercial polyelectrolytes are predominantly obtained by a polymerization, polycondensation, or polyaddition process. Also numerous important PEL also originate from nature, such as gelatin, as a representative of the widespread class of proteins or pectins belonging to the group of anionic polysaccharides. Furthermore, some PEL of practical importance result from a chemical modification of nonionic natural polymers such as cellulose or starch.

In contrast to the huge variability of the polymer backbone structure, the number of different chemical structures of anionic or cationic sites responsible for the preculiar behavior of PEL in solution is rather small (Table 2.2)

Table 2.2 Structures of ionic sites of polyelectrolyte

$-COO^-$	$-NH_3^+$
$-CSS^-$	$=NH_2^+$
$-OSO_3^-$	$\equiv NH^+$
$-SO_3^-$	$-NR_3^+$
$-OPO_3^{2-}$	

These ionic groups are usually classified as anionic and cationic; a further subdivision into weakly and strongly acid and basic groups is reasonable in analogy to “strong” and “weak” acids and bases of low molecular chemistry with the sulfonate, the sulfonate-half ester, and the tetraalkylammonium group being representative for the so-called “strong PEL.”

Besides the acid or base strength of the ionic site, the average distance between the adjacent anionic or cationic charges along the polymer chain is a decisive parameter determining PEL behavior, especially in the dissolved state. This charge carrier density or charge density is defined as the average distance between ionic sites, taking into account chain bond geometry, or as the average number of ionic sites per monomer unit in the case of copolymers, with the latter definition yielding comparable data only within the same class of copolymer with an ionic component. Besides this average charge density, the regularity of distribution of ionic sites along the chain can also influence PEL properties significantly, for example, with regard to solubility. As a rule, typical PEL behavior can be expected if more than 1 ionic site per 10 monomeric units is present in a copolymer.

In addition to acid or base strength and charge density a third important point determining PEL properties is the location of the charged sites within the molecular geometry of the macroion. According to figure 2.12, principally distinguish between an integral type of PEL with the ionic sites being part of the polymer backbone and the pendant type with the ionic sites being attached to the backbone as a side chain with a broad variability in spacer length. The geometric position of the charged sites is relevant especially in polyanion - polycation complex formation.

(a) 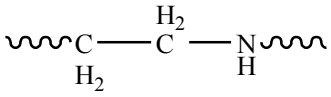

(b) 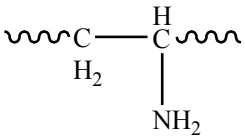

Figure 2.12 PEL of the integral of pendant type: (a) linear poly(ethylene imine) as an example of the integral type and (b) poly(vinylamine) as an example of the pendant type.

Besides these three parameters characterizing the macroion, the species of low molecular counterions has a strong influence on the properties of the whole system in solution, especially on solubility and structure formation. Two examples may illustrate this and demonstrate that the counterion is not just an anonymous particle securing elctroneutrality: The chloride of the poly(diallyldimethylammonium) (polycation) is easily soluble in water, while the corresponding iodide is rather insoluble. The K^+ salt of some water-soluble high molecular cellulose sulfates forms a stiff, cuttable thermoreversible gel at a polymer concentration between 1 and 2 %, while the Na^+ salt of the same sample at the same concentration gives quite a normal polymer solution of the expected viscosity.

2.2.2 Behavior of polyelectrolyte in solution

Polyelectrolyte can be dispersed in aqueous solution. It can ionize and transform into charged chains with electrostatic interaction. Polyelectrolytes are normally linear in structure because of the repulsive interaction between each ion within polyelectrolyte chains as shown figure 2.13.

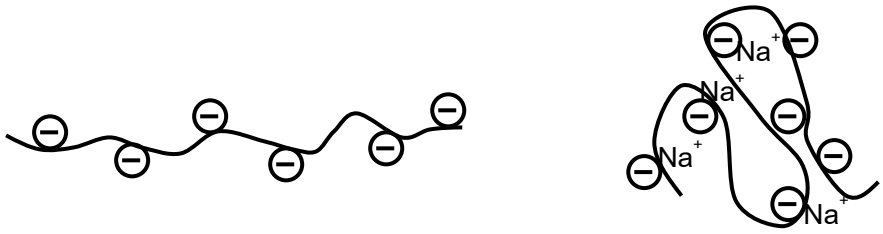

(a) (b)

Figure 2.13 Represent of behavior of polyelectrolyte in solution (a) the absence of salt in solution (b) the presence of salt in solution.

Single chain of polyelectrolyte in aqueous solution has weak interaction with another chain which can be mentioned as isolated chain dispersed in solution. Normally, charged chains are highly stretched as compare to neutral chains with the same composition. In case of adding salt in polyelectrolyte solution, salt ion can decrease repulsive interaction leading to form looped of chain and decrease the length of chain. The different of chain structure between presence of salt and absence of salt was presented in figure 2.13.

The repulsion of each monomer can be decreased by adding of salt (NaCl) in the solution which tends to screen the repulsive force and make more flexibility of the polyelectrolyte chain. If a concentration n of salt is added to the solution the columbic interaction between two charges at a distance r is given by the debye-huckel potential $\upsilon(r)$ where l_B is the bjerum length and κ the persistent length.

$$\upsilon(r) = \frac{kTl_B}{r}\exp -\kappa r$$

$$l_B = \frac{q^2}{4\Pi\varepsilon\kappa T}$$

$$\kappa^{-1} = (8\Pi n l_B)^{-1/2}$$

In the absence of added salt, the interaction is long ranged and the chains are highly stretched; their size R is given by

$$R \sim Na(f_B^2 / a)^{1/3}$$

The size of the blob is such that the electrostatic interaction inside a blob is of the order of kT. As salt is added, the local blob structure of the chain is not affected but if the screening length is smaller than the size of the chain, the chain is no longer fully elongated and bends. It is in general characterized by a persistence length l_p which is the length over which it remains stretched. Depending on the theoretical approach, the persistence length is predicted to decrease with the salt concentration as κ^{-1} or κ^{-2}. Experimental results have not allowed us to discriminate between these two results. At very high ionic strength, the electrostatic interaction is short range and is equivalent to an excluded volume interaction, the corresponding excluded volume parameter is υ_{el}.

$$\upsilon_{el} = 4\Pi l_B \frac{f^2}{\kappa^2}$$

2.2.3 The Layer-by-Layer Deposition

The so-call layer-by-layer (LbL) deposition technique (Figure 2.14) also falls into the category of template assisted assembly. Template assisted assembly is faster than self-assembly/chemical modification cycles whose outcome is often uncertain or difficult to predict. For the case of LbL-deposition, it can be tailored to even allow multimaterial assembly of several compounds without special chemical modifications, thus giving access to multilayer films whose complex functionality can fall into the two following categories:

1. Tailoring of surface interaction: Every object interacts with its environment via its surface. Thus all properties depending on this interaction are dictated by surface functionality which can be tailored for many needs (e.g. corrosion protection, antireflective coatings, antistatic coatings, stickiness or non-stickiness, surface induced nucleation, antifouling, hydrophilicity or hydrophobicity, biocompatibility, antibacterial properties, molecular recognition, chemical sensing or biosensor, microchannal flow control).

2. Fabrication of surface based devices: The sequence of deposition of different materials defines the multilayer architecture and thus the device properties. One may call this knowledge based (or programmed, or directed, or controlled, or template

assisted) assembly, in contrast to self-assembly. It leads to property engineering by controlling the mostly one-dimensional spatial arrangement of functionality in multimaterial layered nanocomposites (membrane reactors, photonic devices such as light emitting diodes or complex waveguides, compartmentalized films with barrier layers or separation membranes.

The fabrication of multicomposite films by the LbL procedure means literally the nanoscopic assembly of hundreds of different materials in a single device using environmentally friendly, ultra-low-cost techniques. The materials can be small organic molecules or inorganic compounds, macromolecules, biomacromolecules such as proteins or DNA or even colloids (metallic or oxidic colloids or latex particles). The technique can be applied to solvent accessible surfaces of almost any kind and any shape, the more exotic ones being microcapsules, colloids or biological cells.

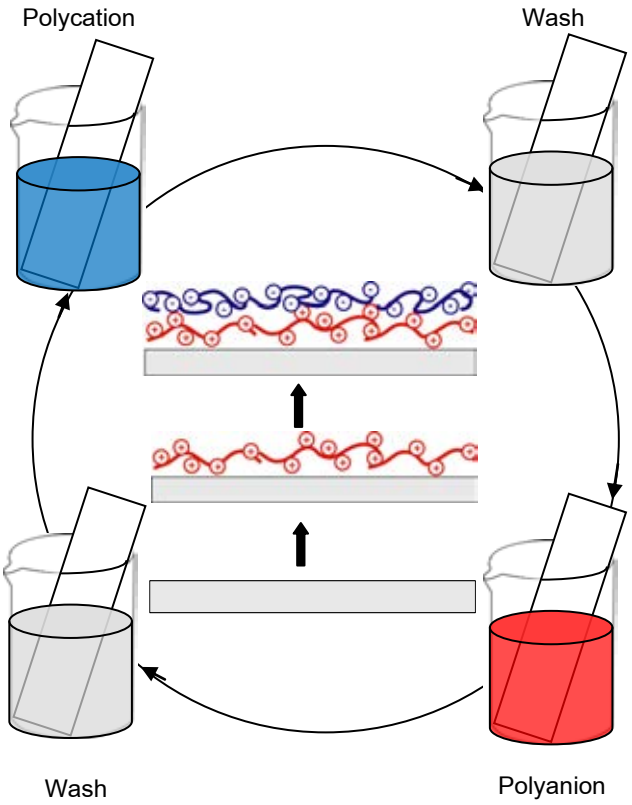

Figure 2.14 Schematic of the electrostatic self-assembly.

For most cases, an LbL film has a unique layer sequence that depends strictly on the deposition sequence. These points to the fact that LbL deposition should be considered as an analogue to a chemical reaction sequence (Figure 2.15). While a chemical reaction takes place between different synthons and typically yields a unique molecule after each synthesis step, layer-by-layer deposition involves the adsorption of a single species in each adsorption step and yields a multilayer film with a defined layer sequence. While molecules are synthesized in several consecutive reaction steps, a multicomposite film is fabricated in several adsorption steps.

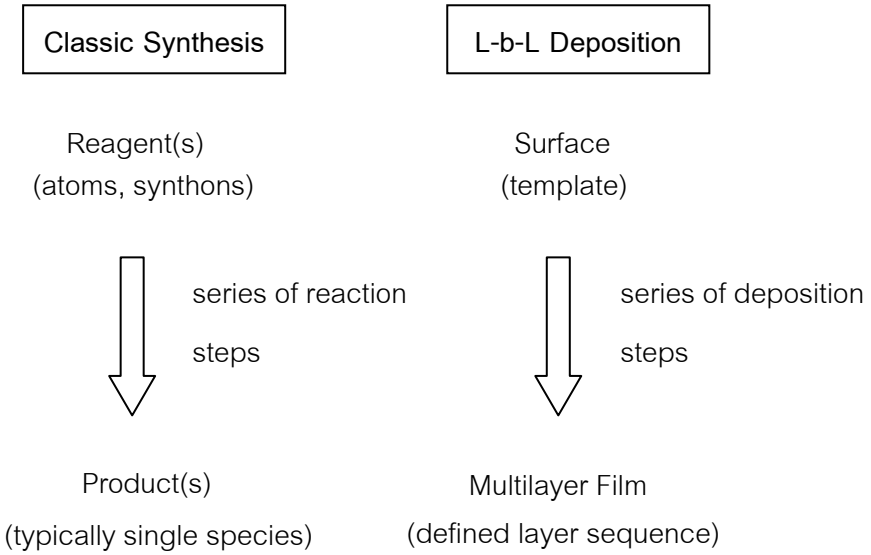

Figure 2.15 Schematic of chemical multistep synthesis and multilayer deposition.

Given the large set of materials which are easily incorporated into multilayer films, layer-by-layer deposition is a rather general approach for the fabrication of complex surface coatings. It combines several advantages as shown in figure 2.16. It is possible to coat almost any solvent-accessible surface starting with sub-micron objects up to the inside of tubings or even objects with a surface of several square meters. Like a chemical reaction, the precise structure of each layer depends on a set of control parameters such as concentration, adsorption times, ionic strength, pH, or temperature, but in general the processing window is rather broad.

Advantages: deposition on surface of almost any kind and any shape

broad processing window

many control parameter: concentration

adsorption times

ionic strength

solvent composition

temperature

Figure 2.16 Schematic of summary of some of the advantages of layer-by layer deposition.

Parameters controlling the growth of PEM

1. Deposition time: Dipping time can be affected the growth of multilayers as shown in figure 2.17 [65].

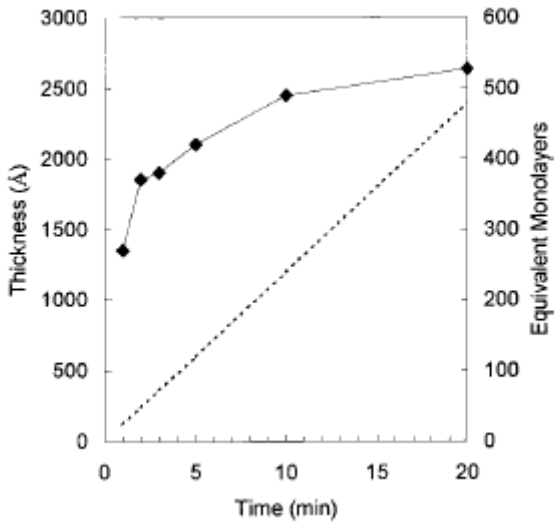

Figure 2.17 Relationship between thickness and dipping timer for a PSS/PDADMAC multilayers[65].

The adsorption of polyelectrolyte as the thin film is controlled by a diffusion process time plays in the formation of the multilayer. The negatively charged substrate is immersed into a positively charged polyelectrolyte. The electrostatic interaction is enough to allow a thin film formation of polyelectrolyte on the surface. The surface

charge becomes less negative and more positive as more polycations adsorb onto surface. When the surface is completely coated with polycations, the adsorption of new polyelectrolyte is stopped because repulsive force. This is a limiting adsorption of one layer process.

2. Ionic strength (salt concentration): Adjustment ionic strength of polyelectrolyte solution can be obtained by adding salt into the solution. The effect of salt concentration related to electrostatic theory [63].

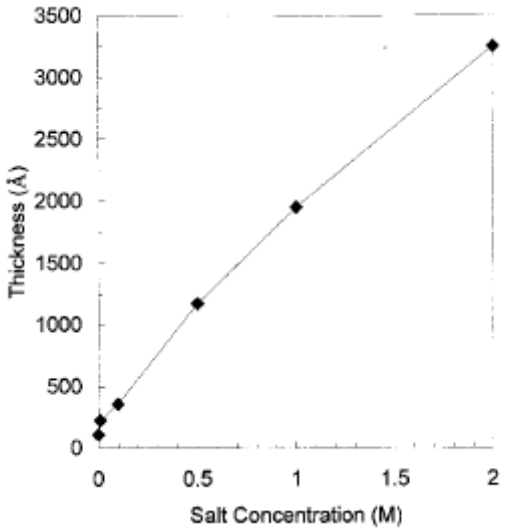

Figure 2.18 Film thickness versus salt concentration for multilayer with 10 layer pairs each [65].

Adding salt into the solution can cause increasing amount of polyelectrolyte adsorption on the surface. This condition has influenced to the thickness of PEMs that shows linear dependence on salt concentration between 10^{-2} M and 2 M like figure 2.18 [65]. The adsorbed amounts depend on scaling with the exponent [63].

3. pH-controlled polyelectrolyte multilayer growth: pH is the factor that concern weak polyelectrolyte adsorption because pH relate to degree of ionization. In case of strong polyelectrolyte as poly(styrene sulfonic acid) and poly(diallyldimethyl ammonium chloride), adjustment of pH is not affected because strong polyelectrolyte present the same ionized form in all pH. In case weak polyelectrolyte, the suitable pH is different in order to ionize polyelectrolyte in solution. Adjustment pH should follow pKa of

polyelectrolyte in order to complete ionization of polyelectrolyte in solution. The example of pH controlled thin film formation is present in figure 2.19. Ammonium groups of Poly(allylamine hydrochloride) (PAH) become deprotonated (cation) when pH higher than pKa.

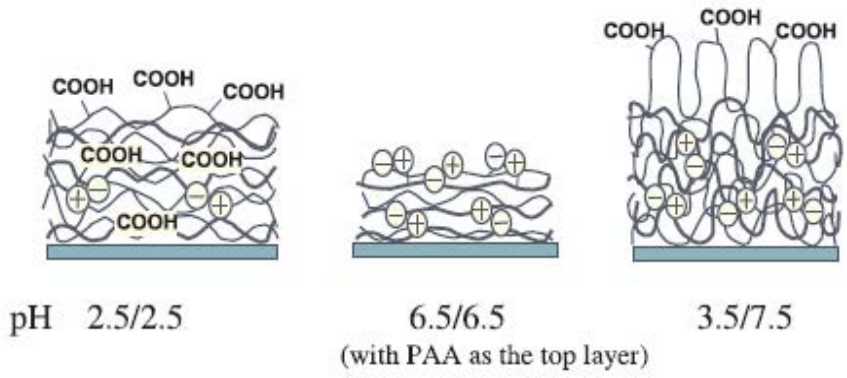

Figure 2.19 Schematic representation of the molecular organization of PAA/PAH multilayer film assembled with the dipping solution at different pH levels [63].

2.3 Introduction to Microfluidic device

Recent advancements in fabrication technology led to the reduction in size of sensor devices by several orders of magnitude. One field of research that benefits in particular from this trend is the area of microfluidic system. Microfluidic device can be identified by the fact that it has one or more channels with dimensions in length of micrometers, which allow the handling and manipulation of minute amount of fluids in nano or even pico liters level [66]. There are many advantages of micro/nano systems such as low consumption of sample volumes [67], high surface to volume ratio [68], fast analysis tine [69], and inexpensive [70]. Microfluidic is a multidisciplinary which encompasses the fields of physics, chemistry, nanotechnology, engineering, and biotechnology. It has been developed extensively for many applications such as handling biological entities such as DNA separation, immunoassay, cell sorting, biosensors, and enzymatic assays due to the potential offered by miniaturizing, high throughput of analysis, low cost of fabrication, multiplex functionality and portability.

Microfluidic concerns the handling and manipulation of minute amounts of fluids in micro liters and nano liters or even pico liters level. Microfluidic device can be identified by the fact that it has one or more channels with dimension in micrometer or nanometer, microfluidic devive is shown in figure 2.20. Microfluidic devices are used as new tools for separating variety of compounds.

The basic principles of capillary electrophoresis (CE) are used in microfluidic systems. In microfluidic devices, the fluid is driven by applying either an electric potential or an external pressure. However, applying voltage is a popular method in driven fluid in separation due to the flat flow profile. When the voltage is applied, the fluid is migrated by the Electrophoretic mobility and electro-osmotic flow.

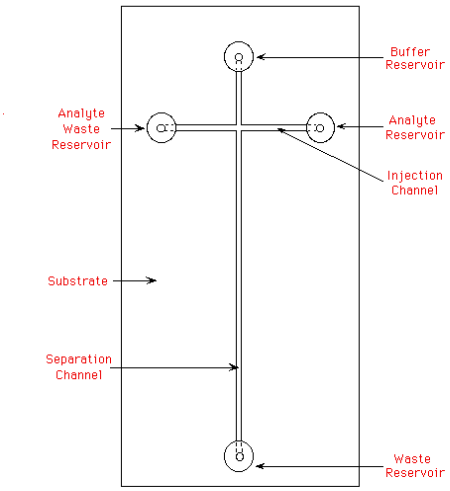

Figure 2.20 Microfluidic devices.

2.3.1 Microchip operation by applying pressure

Applying pressure methods are used to drive fluids through the microfluidic system. Such pumps normally have passive check valves that regulate the flow of fluid into and out of the pump chambers. During a single pump cycle, movement of the diaphragmfirst increases the volume of the pump chamber (during the suction or expansion stroke), thereby drawing fluid into the chamber [71]. In some cases, more than one pumping chamber is connected in series to form a peristaltic pump [71].

Certain micropumps operate by continuously adding momentumor directly imparting Lorentz-type forces in the fluid volumes. They require the conversion of nonmechanical energy to kinetic energy to supply the fluid with momentum. These phenomena are practical only on the microscale.

Flows are governed by the Navier Stockes equations [72], which can be drastically simplified in micro and nanofluidic systems as the ratio of the inertia terms to the viscous term (characterized by the Reynolds number Re) which becomes negligible (Re<<1). These results in applying the so called Stockes equation:

$$0 = -\nabla p + \eta \nabla^2 \vec{\mu}$$

where p is the pressure (in Pa), u is the fluid velocity ($m.s^{-1}$) and μ is the dynamic viscosity of the liquid (dynamic viscosity of water is 8.90×10^{-4} Pa.s). This equation can be solved for various shapes of microchannels. In the case of cylindrical microchannels, a parabolic flow develops and the relation between pressure and flow rate is described by the Hagen-Poiseuille equation [72]:

$$\Delta P = \frac{8\eta L Q}{\Pi r^4} = \frac{8\eta L \upsilon}{r^2}$$

Where ΔP is the pressure drop between the two ends of the channel, L is the total length of channel, Q is the volumetric flow rate, r is the radius of the channel and v is the average flow velocity across the section.

In the case of planar channel with a height h very small as compared to the width w (h<<w,) the solution of the Poiseuille flow gives:

$$\Delta P = \frac{3\eta L}{h^3 w} Q$$

There are three classes of system to control liquid motion in microfluidic and nanofluidic devices. Some systems use a pressure difference to control the flow rate (hydrostatic or pressure generators), whereas other system can directly impose a flow rate (syringe pumps). Finally, liquid pumps and electro-osmotic pumps can be used to generate a liquid flow that will depend on the fluidic resistance of the device.

2.3.2 Electrophoretic Mobility

The principle of electrophoresis refers to the migration of charged electrical species when dissolved, or suspended, in an electrolyte through which an electric current is passed. Cations migrate toward the negatively charged electrode (cathode) and anions are attracted towards the positively charged electrode (anode). Therefore, separation by electrophoresis relies on differences in the speed of migration (migration velocity) of ions or solutes. Ion migration velocity can be expressed as: $\nu = \mu_e E$ Where ν is ion migration velocity (ms^{-1}), μ_e is electrophoretic mobility ($m2v^{-1}s^{-1}$) and E is electric field strength ($V\ m^{-1}$).

The electric field strength is a function of the applied voltage divided by the total capillary length.

$$E = V/L$$

Electrophoretic mobility is a factor that indicates how fast a given ion or solute may move through a given medium (such as a buffer solution). Electrophoretic mobility is given by

$$\mu_e = \frac{q}{6\pi\eta r}$$

Where q is the charge of the ionized solute, η is the buffer viscosity, and r is the ion radius. From μe equation it can see that the migration rates depend on charge-to-size ratio. A smaller ion will migrate faster than a larger ion of the same charge. An ion with a higher charge will migrate faster than one with a lower charge, if they are the same size. Electrophoretic mobility is probably the most important concept to understand in electrophoresis. This is because electrophoretic mobility is characteristic property for any given ion or solute and will always be constant. It is the defining factor that decides migration velocities. Different types of ions or solutes have diverse electrophoretic motilities. So, they also have various migration velocities at the same electric field

strength. From difference in electrophoretic mobility, it is possible to separate mixtures of various ions and solutes by using electrophoresis.

2.3.3 Electroosmotic Flow (EOF)

In capillary electrophoresis, the buffer solution usually also moves through the capillary under the influence of an electric field. This phenomenon is termed electroosmotic flow. Thus a buffer is placed inside a capillary; the inner surface of a capillary acquires a charge. This may be due to ionization of the capillary surface or adsorption of ions from the buffer onto the capillary. An uncoated fused-silica, the surface silanol (Si-OH) groups are ionized to negatively charged silanoate (Si-O-) groups at pH above three. The silanoate groups attract cations from the buffer, which form an inner layer of cations at the capillary wall. These cations are not sufficient density to neutralize all the negative charges, then, outer layer of cations forms. The inner layer is tightly held by the Si-O- group, which is referred to as the rigid layer. The outer layer of cations is not tightly held because it is further away from the silanoate groups, and it is referred to as the diffused layer, as represented in figure 2.21.

When a voltage is applied across the capillary, cations in the diffuse layer are free to migrate towards the cathode, carrying the bulk solution with them. The result is a net flow in the direction of the cathode.

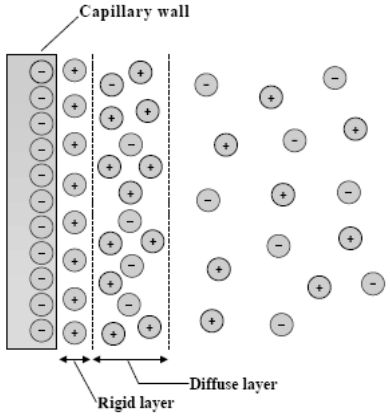

Figure 2.21 Schematic of double electric layer.

Electroosmotic flow has a relatively flat profile, figure 2.22(a), compared to pump or laminar flow, figure 2.22(b). The advantage of flat flow profile is that all of the solute molecules experience the same velocity component caused by electroosmotic flow

regardless of their cross-sectional position in the capillary. They were eluting as narrow bands giving narrow peaks of high efficiency, Figure 2.22(c). On the contrary, the solutes move through a tube under the influence of pump flow, where the solutes in the center of the tube move faster than those nearer the wall. The result of this flow profile is relatively broad peaks, Figure 2.22(d).

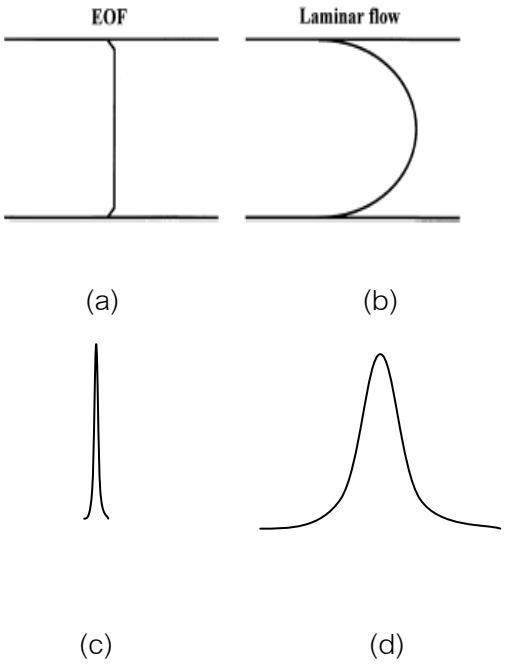

Figure 2.22 (a) Flat profile (b) Laminar profile (c) Peak from flat profile (d) Peak from laminar profile.

2.3.4 Net Flow

In normal mode, the direction of electroosmotic flow is towards the negatively charged cathode, which means the buffer flow from the source vial, through the channel.

Charged solute molecules are separated due to differences in their electrophoretic mobilities, and will tend to migrate toward the electrode that has an opposite charge from the solute, figure 2.23 (a). Negatively charged anions are attracted to the positively charged anode and, with no electroosmotic flow, would simply migrate into the source vial without passing through the capillary and detector. The

electroosmotic flow of buffer is usually greater than the electrophoretic mobilities of negatively charged solutes so they are carried along with the buffer toward the detector. Electroosmotic flow can be strong enough to carry even small triply charged anions toward the negative electrode. Since anionic solutes are pulled back toward the source vial by the positive charge of anode, they move at the rate that is lower than electroosmotic flow. Neutral solutes are not influenced by electrophoretic mobilities, and therefore move through the capillary at the same rate as the electroosmotic flow. Positively charged solutes migrate toward the negative electrode under the influence of both electrophoretic mobilities and electroosmotic flow, and so move faster than the electroosmotic flow. It can be seen in figure 2.23.

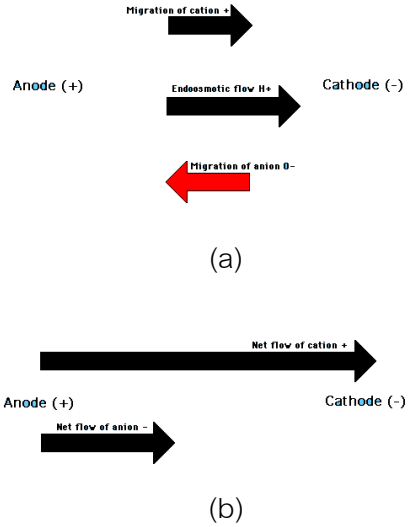

Figure 2.23 (a) Direction of migration ions (b) Net flow

2.4 Electrochemical detection methods for microfluidic device [73]

The most interesting of detection techniques are the optical methods of fluorescence, absorbance and the electrochemical methods of amperometry, conductimetry and potentiometry. Fluorescence detection was employed, presumably because its inherent high sensitivity is a good match for the small detection volumes available. This mode of detection has since been widely used and has been implemented in the early commercial instruments available. Most analyte species do not

fluoresce intrinsically, however, and therefore have to be chemically derivatized. The success of fluorescence detection is partly due to its high sensitivity but also to the facts that the analysis of biochemically relevant species is of high interest and those amino acids and related species can be derivatized readily with a fluorescent tag. However, the technique is not as easily implemented and direct fluorescence detection cannot be considered a universal approach. It is therefore not surprising that in order to extend the use of microfluidic separation devices beyond the now established biochemical applications; much attention is given to the development of other detection techniques.
The electrochemical detection method has been interesting attention. For all electrochemical detection methods the chemical signal is directly converted into the electronic domain via simple electrodes, therefore the overall system can be more compact and the goal of miniaturization can be driven further.

2.4.1 Amperometry

Amperometric detection is based on measuring the oxidation or reduction currents of analytes at a working electrode. It has the advantage of generally good detection limits but is restricted to electroactive species. It is the most widely reported electrochemical method for conventional capillary electrophoresis and a number of research groups have recently reported its implementation for microchannel based separations. One possible approach to eliminating any interference by the applied electrical field on the detection is to use a so-called decoupler in front of the detector. These consist of a porous material through which the solution is in contact with the electrophoretic ground electrode.

2.4.2 Potentiometry

A potentiometric detector based on a miniaturized ion-selective electrode in a micromachined flow-channel has been demonstrated by Manz and co-workers for the detection of Ba^{2+} and proposed for detection in electrophoresis chips. Special membranes have to be used for this purpose in order to achieve detection of a range of ions rather than the usually desired selectivity to just a single ion. This kind of detector has not been widely used in standard capillary electrophoresis. However, they are a

simple alternative, attractive for ions which are not readily detected otherwise, show low conductivity and are not amenable to optical detection.

2.4.3 Conductimetry

Conductimetric detection has also been investigated for chipbased separation and is a good technique in particular for small (inorganic) ions which are otherwise not readily detected. For conventional capillary electrophoresis conductivity detection has recently seen a renaissance.

2.4.3.1 Conductivity Detection on Microchips

Conventional detection of microfluidic device is dominated by optical methods such as ultraviolet (UV) absorption or laser-induced fluorescencence [73-75]. For different reasons, development of conductivity detection on-chip CE has interested. This is due to the fact that the reduction of the dimensions of the separation-channel on microdevices considerably shortens the optical light path [76]. So conductivity detection is an alternative method instead of UV-absorption method. A second reason may be found in difficulty to achieve electrochemical set-up in conventional CE. Now microstructuring technologies and thin film techniques enable totally new approaches to the problem. Few report of conductivity detection has been studied systematically as a detection method for microchips. Nonetheless, the broad range of analytes can be applied with conductivity detection.

The detection principle is based on the electrical properties of ions. A common detector consists of two metal electrodes, which test the conductivity of the analyte solution. An alternating potential is applied across the electrodes. Under the presence of the electric field, the cations migrate during one cycle toward one electrode, and the anions toward the other. The corresponding current is measured and related to the conductivity of the solution through the value of the equivalent measured resistance, R. Metal deposition, and thus microelectrode fabrication, is well known in microfabrication technology. As a result, electrodes can easily be incorporated onto a microdevice along with the fluidic structure (Figure 2.24).

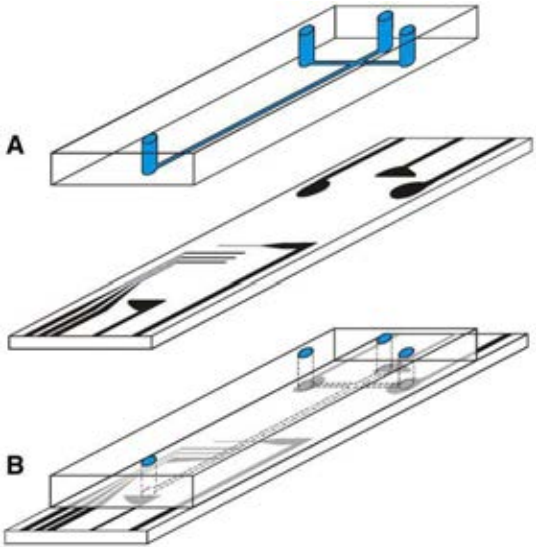

Figure 2.24 A typical electrode and fluidic structure before (A) and after the bonding (B). Besides electrodes for the electrochemical detection, there are also electrodes for separation voltage. After bonding, these electrodes are directly under the reservoirs.

It is clear that the bump an electrode constitutes on the surface causes problems during the sealing process when the cover slip with the electrodes is adjusted to the structured part of the chip that contains the fluidic manifold. Up to now, only polymeric material has been shown to be flexible enough for a tight sealing. For glass chips, either end-on detectors have been constructed or a relatively complicated procedure of embedded electrodes has been developed [76]. The completed electrode substrate has to be bonded to the chip. Here an alignment problem appears. A typical separation channel is approx 50 µm. The electrodes have to be positioned relative to it in a reproducible manner. Two electrode designs are feasible in this situation (Figure 2.25).

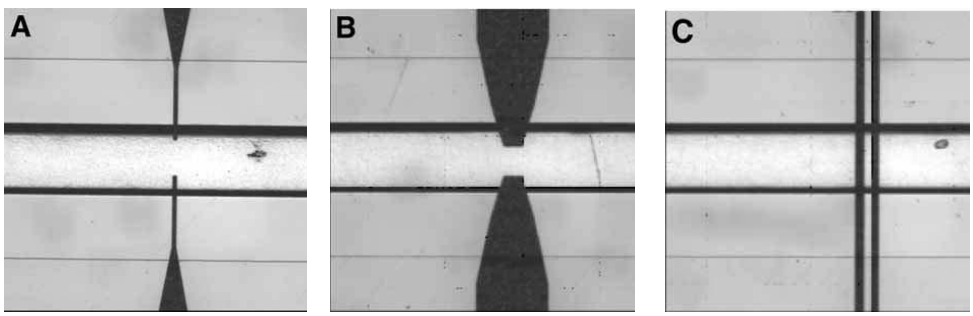

Figure 2.25 Three different electrode designs for conductivity detection. (A) The electrode width is 12 µm and the spacing is 76 µm. Alignment is rather difficult in this

case. Resolution and sensitivity is good. (B) The electrode width is 49 μm and the spacing is 77 μm. Obviously, resolution is lower as in case A. But alignment is much easier and fairly reproducible. (C) Electrode width is 22 μm and spacing between the electrodes is 24 μm. Alignment is no problem, resolution and sensitivity are comparable to case B.

2.4.3.2 Contactless conductivity Detection on Microchips

The conductivity detection technique makes the use of electrodes inside microchannel. The main disadvantage of this technique is that the electrodes are fouling and bubbles can be formed in the microchannel. Contactless conductivity detection can prevent these effects which the analyte and electrodes are electrically insulated.

Conductivity detection can be performed in contactless mode. Simple contactless conductivity detection is based on placing two planer electrodes on the outer side of microchip and measuring the impedance of the solution in the microchannel. Electrodes of contactless conductivity detection are insulated from the channel by thickness of the cover microchip lid. If the electrodes are placed across of the microchannel in the same planar and they are insulated by thin layer of microchip material [77]. At least two electrodes are required which use for applying the AC signal and measuring the signal after passing through the electrode [78]. This is the similar equivalent circuit model between contact and contactless conductivity detection.

2.5 Electrode fabrication [76]

For the development of microfluidic systems toward complete integration, the complete analytical process must fit into one microdevice and includes sample pretreatment, analytical separation, chemical reaction and analytical detection. This has led to the development of miniaturized detection. There are various detection methods used with microfluidic devices such as ultraviolet detection for highly resolved screening of illicit drugs [79], fluorescence detection for microfluidic chip electrophoresis analysis [80], contactless conductivity detection for the determination of major inorganic ions and lithium in serum and urine samples [8]. The electrochemical detection technique is the

most frequently used, which possess excellent detection limit for various analytes and high compatibility with micro-fabrication technologies [81]. The development of miniaturized detection electrodes with high sensitivities and low signal-to-noise ratios, fast response times, multiplex functions for microfluidic systems are attractive issues to integrate complete analytical process into one microdevice. Various techniques have been used to fabricate microelectrode into microfluidic devices such as electroless deposition of nickel for microchip electrophoretic measurement of alcohols and sugars [82], metal sputtering to eliminate the band-broadening characteristic of the end-channel configuration in microchip device [83], screen-printing of carbon thick film as a flexible electrochemical detection for CE chips [84], and micro-molding of carbon ink on polydimethylsiloxane [85]. Among these techniques, micro-molding technique is widely used for preparation of microelectrode because it provides many good properties, simple technique, inexpensive process and ambient temperature operation.

The conductivity detection principle is based on the electrical properties of ions. A common detector consists of two metal electrodes, which test the conductivity of the analyte solution. An alternating potential is applied across the electrodes. Under the presence of the electric field, the cations migrate during one cycle toward one electrode, and the anions toward the other. Metal deposition, and thus microelectrode fabrication, is well known in micro-fabrication technology. As a result, electrodes can easily be incorporated onto a micro-device along with the fluidic structure. A typical standard metal deposition process consists of three different steps. In a first step a photolithographic structure has to be created on a substrate. Therefore, the substrate is coated with a photoresist and exposed with an UV-lamp through a photomask. Typically, this is an e-beam written mask. After exposure and development the metallization starts. Because of the higher kinetic ion energy the adhesion of a sputtered metal film is much higher compared with a vapor-deposited layer. Therefore, sputtering should always be preferred over vapor deposition. After stripping of the photo-resist, the result will be a thin layer electrode on the substrate. But even the adhesion of platinum or gold films, which are usually used because of their electrochemical inertness, on glass or plastic is unsatisfactory and an extra adhesion layer is necessary. A well known and

characterized material for an adhesion layer in thin-film technology is chromium. However, pure chromium is prone to be dissolved in electrolyte solutions especially in addition with high voltages. Under typical separation conditions for CE this can result in severe damage of the electrodes. Away to prevent this is to oxidize the chromium during the sputter process. Under optimized conditions, the adhesion of the dichromium trioxide will be adequate and the damage of the electrodes will be impeded.

The various established methods used to prepare metallic thin film include: Chemical Vapor Deposition (CVD), Electro deposition, Lithography and Magnetron sputtering but preparing conducting thin film by these techniques is a complex procedure involving several stages. The whole procedure is time consuming and involves high cost due to the need for a clean room environment and special apparatus such as vacuum deposition or sputtering.

2.5.1 Screen printing technique

There are many types of printing such as lithography and screen printing. The concept of screen printing, the pattern of electrode is sketched and fixed to the frame. Resist is coated on the screen to fill up the meshes that are not necessary. Conductive ink goes through the unfilled meshes, and then conductive inks are transferred to the substrate. This technology provides thick film materials on alumina and plastic substrates.

Banks AE and co-workers [86] reported the fabrication of disposable and flexible screen printed carbon microelectrodes which had radii between 60 and 100 microns. The carbon–graphite ink and dielectric ink were printed onto a polyester flexible film to obtain the conductive tracks.

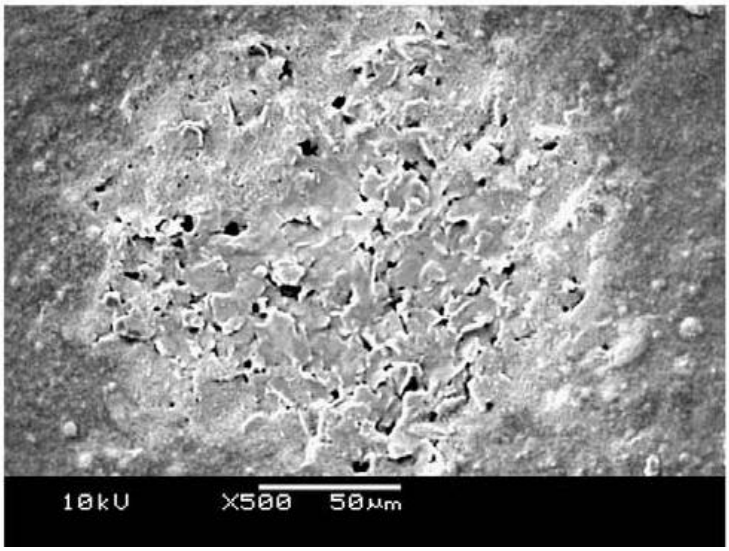

Figure 2.26 Scanning electron micrographs of two screen printed microelectrode.

The SEM images as depicted in figure 2.26 highly suggest that non-recessed graphite electrodes have been successfully fabricated. The microelectrodes were observed to have flake-like graphite particles covered with polymeric binder material which produced a surface with a webbed aspect.

Bachas LV and co-workers [87] reported micro-fabrication of screen-printed nano-liter vials with embedded surface-modified electrodes. It was a combination of screen printing and laser ablation techniques to create nano-liter volume electrochemical cells. Using multi-sweep cyclic voltammetry, the surface of the working carbon electrode was modified with a polypyrrole film, increasing the surface area of the electrode.

2.5.2 The physical vapor deposition technique

The physical vapor deposition technique is based on the formation of vapor of the material to be deposited as a thin film. The material in solid form is either heated until evaporation (thermal evaporation) or sputtered by ions (sputtering). In the last case, ions are generated by a plasma discharge usually within an inert gas (argon). It is also possible to bombard the sample with an ion beam from an external ion source. This allows varying the energy and intensity of ions reaching the target surface.

2.5.3 Electroplating Methods

Electroplating is often also called electrodeposition. Electroplating can be considered to occur by the process of electrodeposition. It's a process using electrical current to reduce cations of a desired material from a solution and coat that material as a thin film onto a conductive substrate surface. This method is an Electrolytic process in which the part to be plated will be submerged in a water solution which contains molecules of an acid, base or salt. These molecules are separated into positively and negatively charged ions and these ions are what carry the charge in the solution. This Ionized solution is known as the electrolyte.

Wenping Hu and co-workers proposed [88] a method for the integration of the synthesis of silver-tetracyanoquinodimethane (AgTCNQ). The method was performed by electroplating Ag between gold coplanar micro-gap electrodes in tetracyanoquinodimethane (TCNQ) solution.

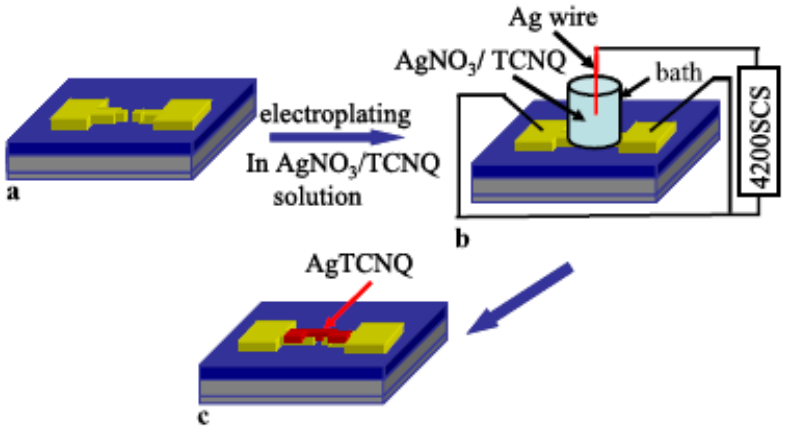

Figure 2.27 Schematic of AgTCNQ in situ synthesis and devices fabrication process. (a) original Au gap electrodes (gap width: 2 μm) prepared by photolithography; (b) AgTCNQ electroplating system; (c) device after electroplating.

The in situ synthesis and devices fabrication of MTCNQ could be depicted as shown in figure 2.27 by using AgTCNQ. The method was performed by electroplating Ag between gold coplanar micro-gap electrodes in tetracyanoquinodimethane (TCNQ) solution. As soon as silver was electrochemical dissolved in TCNQ solution, it would immediately react with TCNQ to form AgTCNQ and then deposited between Au gap

electrodes. With the continuing of the reaction, the Au micro-gap electrodes were connected by AgTCNQ to form Au/AgTCNQ/Au coplanar gab devices.

2.5.4 Micromolding technique

The technique uses poly(dimethylsiloxane) (PDMS)-based microchannels, which are reversibly sealed to a glass substrate, to define the size of the microelectrode. The microchannels are filled with conductive inks that are commonly used in the screen-printing of electrodes. After filling channels with conductive ink, the reservoir where vacuum had been applied is filled with the conductive ink/thinner solution. After this period of time, the PDMS could be removed from the glass, leaving the carbon microelectrode attach to the glass surface.

Martin RS and co-workers [85] reported a technique to pattern carbon microelectrodes for use in microfluidics.

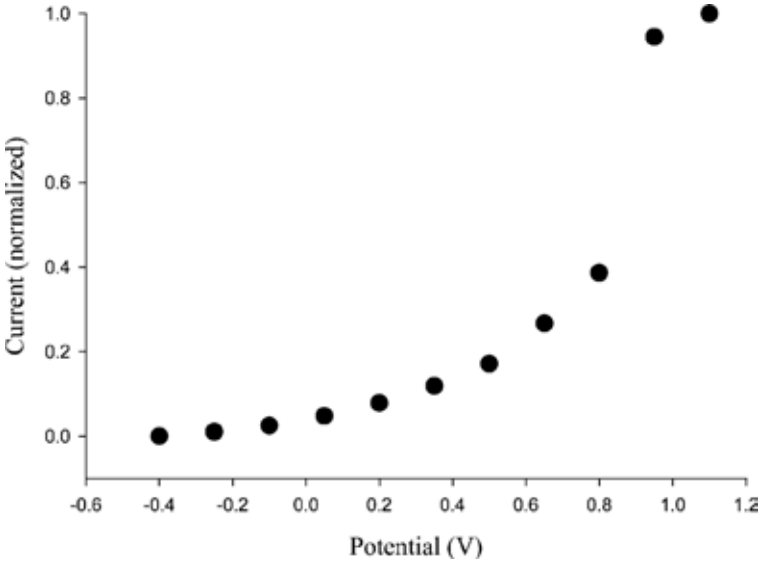

Figure 2.28 Hydrodynamic voltammogram for discrete injections (0.133 mL) of catechol (2 mM) into the microchip-based flow system.

An off-chip injection system was used to discretely inject analyte into the flow channels. A catechol solution (2 mM in HBSS) was injected into the flow system and the peak current monitored as a function of the applied potential (hydrodynamic voltammogram, figure 2.28). A typical sigmoidal response was seen, with a half-wave potential of +0.85 V and diffusion-limited currents occurring at potentials above +1.0 V. As compared to use of a conventional Ag/AgCl reference electrode, these values are

shifted to higher values, 37 due to use of a platinum quasi reference electrode. The electrodes were characterized in terms of both their ability to be used in a microchip-based flow analysis system and their analytical performance. It was also shown that the microelectrode could be modified.

2.6 Thin film surface resistivity [89]

Surface resistivity could be defined as the material's inherent surface resistance to current flow multiplied by that ratio of specimen surface dimensions (width of electrodes divided by the distance between electrodes) which transforms the measured resistance to that obtained if the electrodes had formed the opposite sides of a square. In other words, it is a measure of the material's surface inherent resistance to current flow. Surface resistivity does not depend on the physical dimensions of the material. According to Ohm's law for circuit theory, the resistance of a material is the applied voltage divided by the current drawn across the material across two electrodes [90].

$$R = V/I$$

Where:

R = the resistance (ohms,Ω)

V = Voltage (volts,V)

I = Current (amperes, A)

This electrical resistance is proportional to the sample's length and the resistivity and inversely proportional to the samples cross sectional area.

$$R = \rho l/A$$

Where:

ρ = Resistivity

A = cross- sectional area

l = length

2.6.1 Van der Pauw method

The Van der Pauw technique is widely used in the semiconductor industry to determine the resistivity of uniform samples as shown in figure 2.29. The sample

thickness must be much less than the width and length of the sample for this technique. It is preferable that the sample is symmetrical (Figure 2.29). The Van der Pauw technique also requires that four ohmic contacts be placed on the sample as shown in figure 2.29 [91].

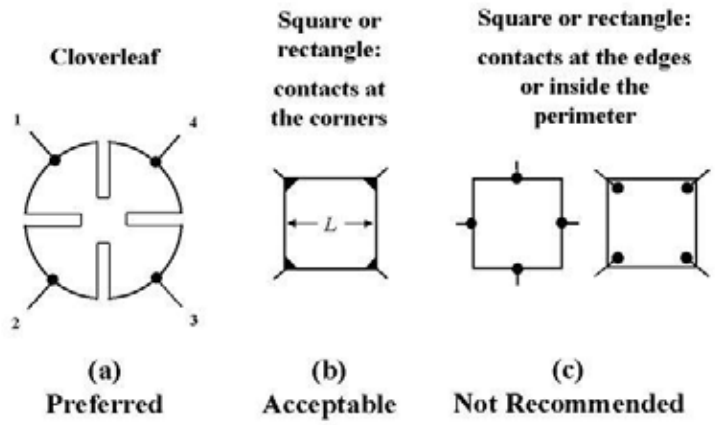

Figure 2.29 Sample geometries for Van der Pauw resistivity.

A schematic of a rectangular Van der Pauw configuration is presented in figure 2.30.

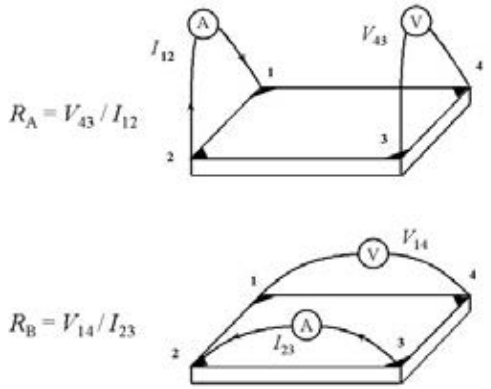

Figure 2.30 Schematic of a Van der Pauw configuration.

The sheet resistance R_S can be determined from the two characteristic resistances

$$R_A = (R_{21,34} + R_{12,43} + R_{43,12} + R_{34,21})/4 \text{ and}$$
$$R_B = (R_{32,41} + R_{23,14} + R_{14,23} + R_{41,32})/4$$

via the Van der Pauw equation $R_A = V_{43/I12}$ and $R_B = V_{14/I23}$. If the conducting layer thickness d is known, the bulk resistivity $\rho = R_S\, d$ can be calculated from R_S.

2.6.2 Linear four point probe method

The four point method uses the two additional probes to measure the voltage potential of the material surface. The theory is a fixed current is injected into the sureface through the two outer probes, and a voltage is measured between the two inner probes as shown in figure 2.31. If probes with uniform spacing s are placed on an infinite slab material, then the resistivity, ρ, is given by:

$$\rho = (2\pi t/\ln 2)V/I = 4.53\ t(V/I) \text{ Ohm-Centimeters for } s>>t,$$

with t representing the thickness of the thin film.

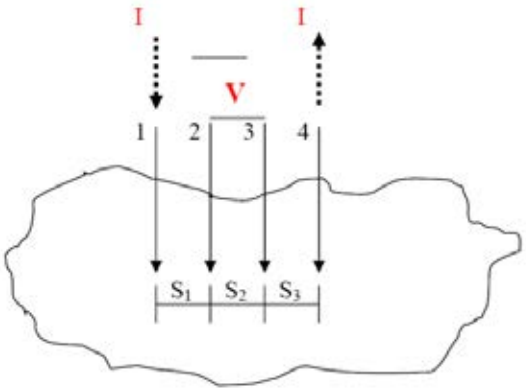

Figure 2.31 Four point probe test setup. Probes 1 and 4 carry current (I), 2 and 3 measure voltage (V).

2.7 Zeta potential measurement

Zeta potential is a measure of the magnitude of the repulsion or attraction between particles. Zeta potential of the particle can obtain by application of the Henry equation. The Henry equation is:

$$U_E = \frac{2\varepsilon Z f(Ka)}{3\eta}$$

Z = Zeta potential

U_E = Electrophoretic mobility

ε = Dielectric constant

η = Viscosity

f(Ka) =Henry's function.

Zeta potential is not only use for measuring colloids, but it is also use to determine the characteristic of PEM formation.

The nanocrystalline materials used in such multilayers include CdS, CdSe, CdTe, ZnS, PbS, TiO_2, ZrO_2, Ag, Au, SiO_2, MoO_2, polyoxometallates, HgTe, Fe_3O_4. Several experimental techniques can be employed to monitor the formation of each polyelectrolyte layer deposited sequentially on colloids. Microelectrophoresis provides a qualitative indication as to whether or not multilayers are deposited. Figure 2.32 shows the ζ-potential as a function of polyelectrolyte layer number for negatively charged polystyrene (PS) particles coated with poly(allylamine hydrochloride) (PAH) and poly(styrenesulfonate) (PSS), or with poly(diallydimethylammonium chloride) (PDADMAC)/PSS. As expected, the negatively charged (uncoated) PS particles show a negative ζ-potential, ca. 65 mV. The presence of a single layer of adsorbed positively charged polyelectrolyte on the PS particles causes a reversal in ζ-potential to positive values, and subsequent deposition of a negatively charged polyelectrolyte reverts the ζ-potential back to negative values.

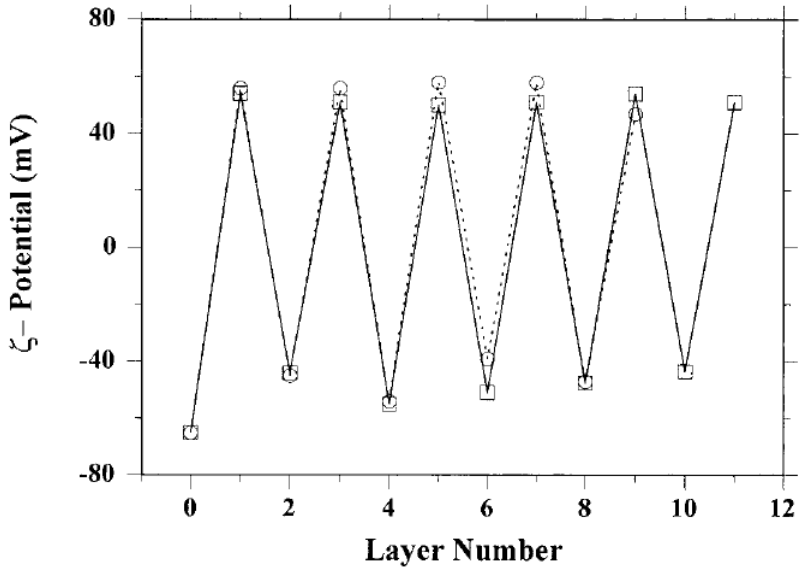

Figure 2.32 ζ-potential of negatively charged 640 nm diameter PS particles as a function of polyelectrolyte layer number for (circles) PAH/PSS- and (squares) PDADMAC/PSS coatings. The odd layer numbers correspond to PAH or PDADMAC deposition and the even layer numbers to PSS adsorption.

Further polyelectrolyte depositions cause the ζ-potential to alternate in sign, depending on whether the outermost layer is positively or negatively charged. This alternation in ζ-potential qualitatively demonstrates a successful recharging of theparticle surface with deposition of each polyelectrolyte layer, suggesting that stepwise layer growth occurs on the particles. Similar data have been observed for a broad range of layer-by-layer assembled polyelectrolyte coatings.

The characteristic of PEM formation is also measured by zeta potential of PAH/PSS on magnetic liposome as a function of number of layer shows reversal of charge when addition new layer as shown in figure 2.33.

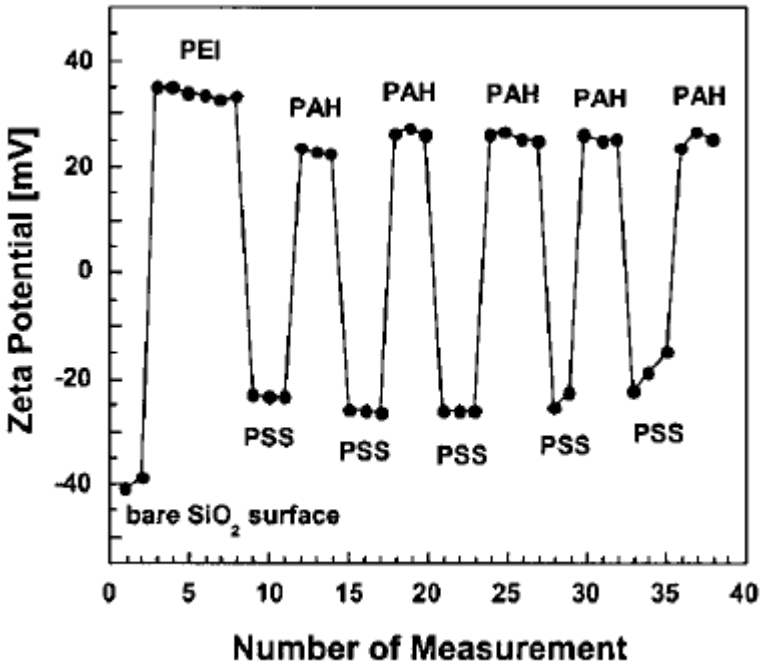

Figure 2.33 Streaming potential measurements showing the surface charge reversal during multilayer buildup in situ. The first layer was poly(ethylene imine) (PEI) followed by 5 deposition cycles PSS and PAH [92].

The diagram in figure 2.34 results from a measurement using a quartz capillary that was carried out in collaboration with the groups of Schaaf and Voegel [92]. It demonstrates nicely that the adsorption of each polyelectrolyte layer leads to an overcompensation of the previous surface charge.

CHAPTER III

METHODOLOGY

3.1 Chemicals and Materials

All the chemicals were used without further purification. Deionized distilled water used for the preparation of chemical and reagent solutions. List of chemicals was summarized as follow:

3.1.1. Poly(4-styrenesulfonic acid-*co*-maleic acid) sodium salt ($C_{12}H_{10}Na_2O_7S$, M_w=20,000) (Aldrich, USA)

3.1.2. Poly(sodium 4-styrenesulfonate) ($(C_8H_7NaO_3S)_n$, average Mw ~70,000) (Aldrich, USA)

3.1.3. Alginic acid, sodium salt ($NaC_6H_7O_6$, M_w =198) (Aldrich, USA)

3.1.4. Humic acid, sodium salt (Aldrich, USA)

3.1.5. Poly(diallyldimethylammonium chloride), medium molecular weight, 20 wt. % in water ($(C_8H_{16}ClN)_n$, average M_w ~200,000-350,000) (Aldrich, USA)

3.1.6. Silver nitrate ($AgNO_3$, M_w = 169.87) (Merck KGaA, Germany)

3.1.7. Gold (III) chloride trihydrate, 99.9+% ($HAuCl_4 \cdot 3H_2O$, M_w =393.83) (Aldrich, USA)

3.1.8. Sodium borohydride ($NaBH_4$, M_w =37.83) (Labchem, Australia)

3.1.9. Sodium citrate dehydrate, 99+% ($Na_3C_6H_5O_7 \cdot 2H_2O$, Mw =294.1) (Aldrich, USA)

3.1.10. Acetic acid (Glacial grad) (CH_3COOH, M_w =60.05) (AnalaR, England)

3.1.11. Potassium chloride (KCl, M_w =74.55) (Carlo Erba, Italy)

3.1.12. Sodium Chloride (NaCl, M_w =58.44) (Carlo Erba, Italy)

3.1.13. Sodium hydroxide (NaOH, =39.997) (Carlo Erba, Italy)

3.1.14. Sodium acetate trihydrate ($C_2H_3NaO_3 \cdot 3H_2O$, M_w =136.08) (Carlo Erba, Italy)

3.1.15. Hydrochloric acid 37% (HCl, M_w =36.48) (Lab-Scan Analytical Science, Ireland)

3.1.16. Sulfuric acid 96% (H_2SO_4, Mw =98.079) (Carlo Erba, Italy)

3.1.17. Hydrogen peroxide 30% (H_2O_2, M_w =34.01) (Merck, Germany)

3.1.18. Carbaryl (1-naphthyl methylcarbamate) ($C_{12}H_{11}NO_2$, M_w =201.22) (Yip In Tsoi&Jacks Ltd., Thailand)

3.1.19. PMMA sheets (1 mm thick, Sumipex Co., Ltd., Thailand)

3.1.20. SYLGARD® 184 Silicone eleastomer kit (Dow Corning, USA)

Remark: Cationic polyelectrolyte is number 5 and anionic polyelectrolytes are number 1-4.

3.2 Instruments and equipments

3.2.1. UV-Vis Spectrophotometer, Analytikjena SPECORD S 100, Japan

3.2.2. JEOL Scanning Electron Microscope, JSM-6400, Japan

3.2.3. JEOL Transmission Electron Microscope, JEM 2100, Japan

3.2.4. Function Generator, GW INSTEK SFG-2110, Taiwan

3.2.5. Field Emission Scanning Electron Microscope, Hitachi S-4700, Japan

3.2.6. Standard Contact Angle Goniometer with DROP image Standard, ramé-hart Model 200, USA

3.2.7. Laboratory Microscope, MICROS AUSTRIA LILY MCX500, Australia

3.2.8. Atomic Force Microscope, Nanoscope IIIa, Japan

3.2.9. DC and AC current source, Keithley Model 6221, USA

3.2.10. Nano voltmeter, Keithley Model 2182A, USA

3.2.11. Particle size and zeta potential Measurement, Zetasizer Nano ZS, UK

3.3 Preparation of solutions

3.3.1 Preparation of 10 mM PDADMAC solution

The 3.88 mL of 20% wt PDADMAC was dissolved into 50.00 mL volumetric flask as a 0.100 M stock solution. The stock solution was then diluted ten times with deionized water using volumetric flask containing 2.922 g of sodium chloride to obtain 1M NaCl concentration.

3.3.2 Preparation of 10 mM PSS solution

The 1.031 g of PSS was weighed and dissolved in 50 mL of deionized water to make 0.100 M stock solution. PSS was then diluted to 10 mM concentration which contained 1 M of sodium chloride.

3.3.3 Preparation of chitosan solution

Chitosan (0.100 g) was dissolved in 0.100 M acetic acid solution and finally adjusted the volume with deionized water into 100 mL volumetric flask. The solution was adjusted to the required pH with 0.1 M sodium hydroxide or 0.1 M hydrochloric acid. The resulting solution was finally diluted in deionized water. The final solution contained 1M of sodium chloride.

3.3.4 Preparation of alginic acid solution

Alginic acid (0.100 g) was dissolved in deionized water into 100 mL volumetric flask. The solution was adjusted to the required pH with 0.1 M sodium hydroxide or 0.1 M hydrochloric acid. The resulting solution was finally diluted in deionized water. The final solution contained 1M of sodium chloride.

3.3.5 Preparation of humic acid solution

The humic acid (0.100 g) was dissolved in 100 mL of deionized water using volumetric flask. The solution was then adjusted to pH 9 with 0.1 M sodium hydroxide.

3.3.6 Preparation of potassium chloride solution

The potassium chloride (0.746 g) was dissolved in 100 mL of deionized water using volumetric flask as a stock solution. The stock solution was then diluted to 2, 4, 6, 8, 10, 12, 14, 16, 18 and 20 mM by deionized water using volumetric flask.

3.3.7 Preparation of carbaryl solution

The carbaryl (0.010 g) was dissolved into 100 mL of deionized water using volumetric flask. The solution was adjusted to the required pH with 0.1 hydrochloric acid.

3.3.8 Preparation of sodium citrate

The sodium citrate was (2.941 g) was dissolved in 100 mL of deionized water using volumetric flask. Then, solution was diluted to 15, 30 and 60 mM by deionized water.

3.4 Preparation of metal nanoparticles.

3.4.1 Silver nanoparticles preparation

Silver nanoparticles were prepared by using anionic polyelectrolytes as stabilizer, sodium borohydride as a reducing agent and silver nitrate. First, 2 mM of silver nitrate was vigorous stirred with an anionic polyelectrolyte. Then, sodium borohydride was added into the solution to reduce silver ions. The solution was kept for 3 h at room temperature.

The effects of types and concentration of stabilizing agents on the size and charges of silver nanoparticles were studied. We chose humic acid, poly(4-styrenesulfonic acid-*co*-maleic acid) and alginic acid as stabilizers which was used to synthesis silver nanoparticles. The obtained silver nanoparticles were used to study in monolayer adsorption and multilayers thin film formation parts.

3.4.2 Gold nanoparticles preparation

The aqueous auric acid ($HAuCl_4$) solution was mixed with sodium citrate solution (Na_3CT) under boiling and stirring condition until observing the red wine color solution. The auric acid was set at 1 mM. The effect of sodium citrate on the characteristic of gold nanoparticles was investigated by varing the ratio of Na_3Ct:$HAuCl_4$ as 15:1, 30:1 and 60:1.

3.4.3 Characterization of nanoparticles

3.4.3.1 Surface plasmon absorption spectrum

Metal nanoparticles were characterized by measuring plasmon band using UV-Vis spectrophotometer. UV plastic cuvette with path length of 10 mm was used for the experiment. For the measurements, the metal nanoparticle solutions in plastic cuvette were measured in the 180 to 800 nm UV-Vis range. The deionized water was first introduced and recorded as a background.

3.4.3.2 Zeta potential measurement

To confirm the synthesis of metal nanoparticles capped with anionic polyelectrolytes, charges on surface of metal nanoparticles were investigated using zeta potential measurement. Zeta values were performed by injection 1 mL of metal nanoparticles solution into a 1 cm quartz cell. Three measurements were done for each sample.

3.4.3.3 Transmission electron microscopy (TEM)

The particles size and morphology of all conditions of metal nanoparticles were studied by JEOL transmission electron microscope. These solutions were prepared by dropping solutions onto Cu grids and dried at ambient temperature over night. TEM images were obtained, using an acceleration voltage of 100 kV. High-magnification images were taken at 100,000 and 300,000 times of specimen size.

3.5 Preparation of coating substrates

Glass slides were used as the substrates for metal nanoparticles deposition in all experiments. First, they were cleaned by dipping into piranha solution (2:1, H_2SO_4/H_2O_2) for 30 min. Then, glass slide substrates were rinsed with DI water several times and dried with air. In order to deposit the nanoparticles on the glass surface, the primer base film was needed to enhance the adhesion between metal nanoparticles and the substrate surface. A primer base film was coated on the surface of slide-glass plate by using the layer-by-layer technique. The clean substrate was immersed into a solution containing 10 mM PDADMAC and NaCl 1 M for 2 minutes followed by 1 minute rinsing with water for three times. The substrate containing positive charge, the first coating layer was then immersed into a solution containing 10 mM PSS and NaCl 1 M for 2 minutes followed by 1 minute rinsing with water for three times. These steps were repeated for 5 layers where the top of the primer thin film contained positively charges.

3.6 Kinetic study of monolayer

The metal nanoparticles prepared in 3.4 were used to study kinetic adsorption. All metal nanoparticles were deposited on the surface of glass slide plate to generate the nanoparticles monolayer thin film and the samples were measured for λ_{max} by UV-visible spectrophotometer every 15 second until the absorbance values were found to be constant. The process for establishment of silver nanoparticles monolayer thin film was shown in figure 3.1.

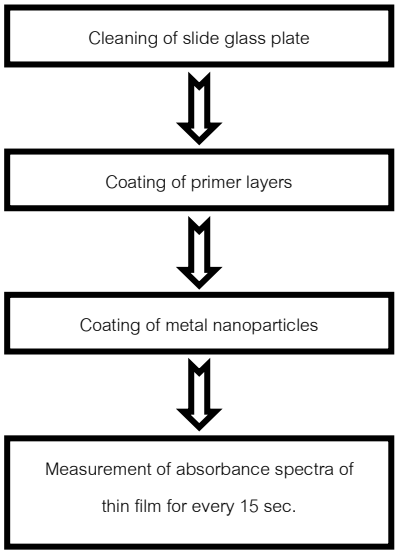

Figure 3.1 The procedure of kinetic adsorption.

To confirm the metal nanoparticles formation, surface roughness of 0.0005 %wt alginic acid stabilized silver nanoparticles monolayer thin film was chosen an example thin film which was monitored every 30 seconds by contact angle measurement.

3.7 Preparation of metal nanoparticles multilayers thin films

3.7.1 Preparation of metal nanoparticles multilayers thin films

The fabrication metal nanoparticles multilayers thin films was carried out as follow. A glass-slide substrate containing primer layer was immersed in 1 mM of the PDADMAC solution and rinsed with water three times to remove excess polymers. Subsequently, the glass-slide was then immersed in solution of metal nanoparticles capped by polyelectrolyte, followed by rinsing with water again for three times. This simple two-step was repeated until the desired number of layers was obtained. The method for preparation of nanoparticles/PDADMAC multilayer thin film was revealed in figure 3.2. The metal nanoparticles multilayers thin films were prepared by using all types and concentration of stabizing agent prepared metal nanoparticles.

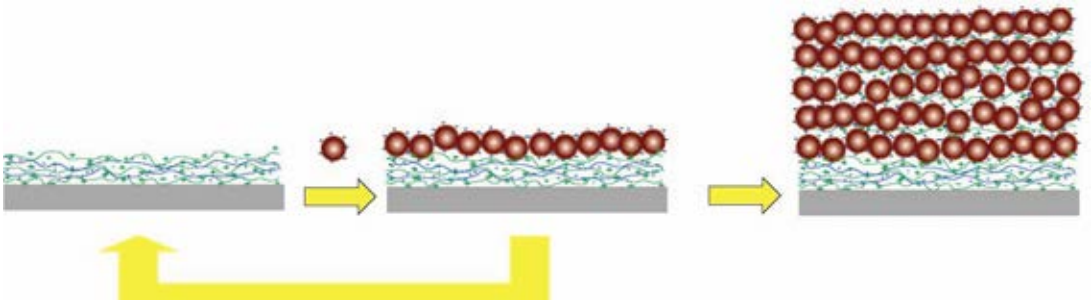

Figure 3.2 The metal nanoparticles-PDADMAC multilayer thin films.

3.7.2 Characterization of metal nanoparticles multilayers thin films

3.7.2.1 UV-Vis Spectroscopy

The glass slides were coated with PDADMAC-metal nanoparticles multilayers thin films and then analyzed using UV-Vis spectrophotometer. Prior to any UV-Vis measurements, a bare clean glass slide was first introduced and recorded as a background. The absorbance of metal nanoparticles multilayers thin films was measured in the 400 to 700 nm visible range as a function of number of layer.

3.7.2.2 Atomic force microscopy (AFM)

The image of an AFM represents data in three dimensions, so that it is possible to measure the height of nanoparticles quantitatively. Moreover, images can be taken in all environments. The layer-by-layer growth of the metal nanoparticles film was probed using AFM. AFM is usually used to measure surface topography; the thickness of a soft thin film can be assessed by gently scratching the film and measuring its step height with regards to the glass slide substrate.

3.7.2.3 Four-point probe measurement

The resistivity of metal nanoparticles multilayers thin films was characterized by four point probe as a function of number of layer. The four point probe test setup was showed in figure 3.3. The four probes were arranged in a line with the two outer electrodes connection connected to a DC source while the inner probes were connected to a nano-voltmeter. The current flows between the outer probes (probe No.1, 4); the voltage drop across the inner probes will be measured (probe No.2, 3). The resistivity can be calculated:

$$\rho = 4.53\ t\ (V/I);$$

ρ is the resistivity (Ω.cm);

T is the thickness of thin film (cm)

V is the voltage drop across the inner two probes (V)

I is the current flow between the outer two probes (A).

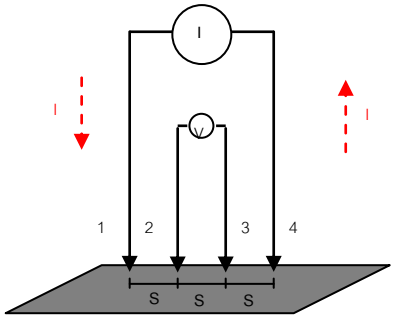

Figure 3.3 Four point probe test setup. Probes 1 and 4 carried current (I), 2 and 3 measured voltages (V).

3.8 The metal nanoparticles microelectrode preparation by flow deposition technique.

3.8.1 Fabrication of poly(dimethyl siloxane) (PDMS) microchip as microelectrode-mold

Sylgard 184 PDMS pre-polymer was mixed with its cross linking agent at ratio 10:1.2 (W/W) and degassed by vacuum pump. The mixture was then poured over the channel pattern master (dual channels). After curing at 65ºC for 2 h and cooling at room temperature, the PDMS was stripped from master to get a pattern of negative relief channel and reservoirs in PDMS. The PDMS pieces, containing pattern, were cut into small size and punched with holes of 4 mm in diameter. The pattern channel was 200 µm in width and depth for both channels, the space between two channels was 200 µm.

3.8.2 Layer-by-layer deposition of gold nanoparticles as micro-electrodes

The PDMS pattern channel was cleaned and sealed on a glass substrate with methanol. The flow in the channel was driven by connecting the outlet to a vacuum pump. In order to improve the growth of the nanoparticles film, a polyelectrolyte multilayer consisting of 5 layers of PDADMAC/PSS was deposited by flow a 10 mM PDADMAC solution through the channel for 2 minute follow by a 10 minute rinse with distilled water. PSS (10mM) was deposited in similar fashion. Both polyelectrolyte solutions had their ionic strength adjusted with 1M NaCl. The purpose of the primer layers was to enhance the adhesion between nanoparticles and the substrate. The microelectrode was then built by flowing either nanoparticles or PDADMAC solution into inlet reservoirs 5 min and then rinse with distilled water. The step was repeated as many times as the desired number of layers. Finally, the PDMS was peeled off from the substrate to reveal the gold nanoparticles microelectrodes. This process was illustrated in figure 3.4.

The type of metallic nanoparticles was chosen to fabricate microelectrode by conductivity property of thin film.

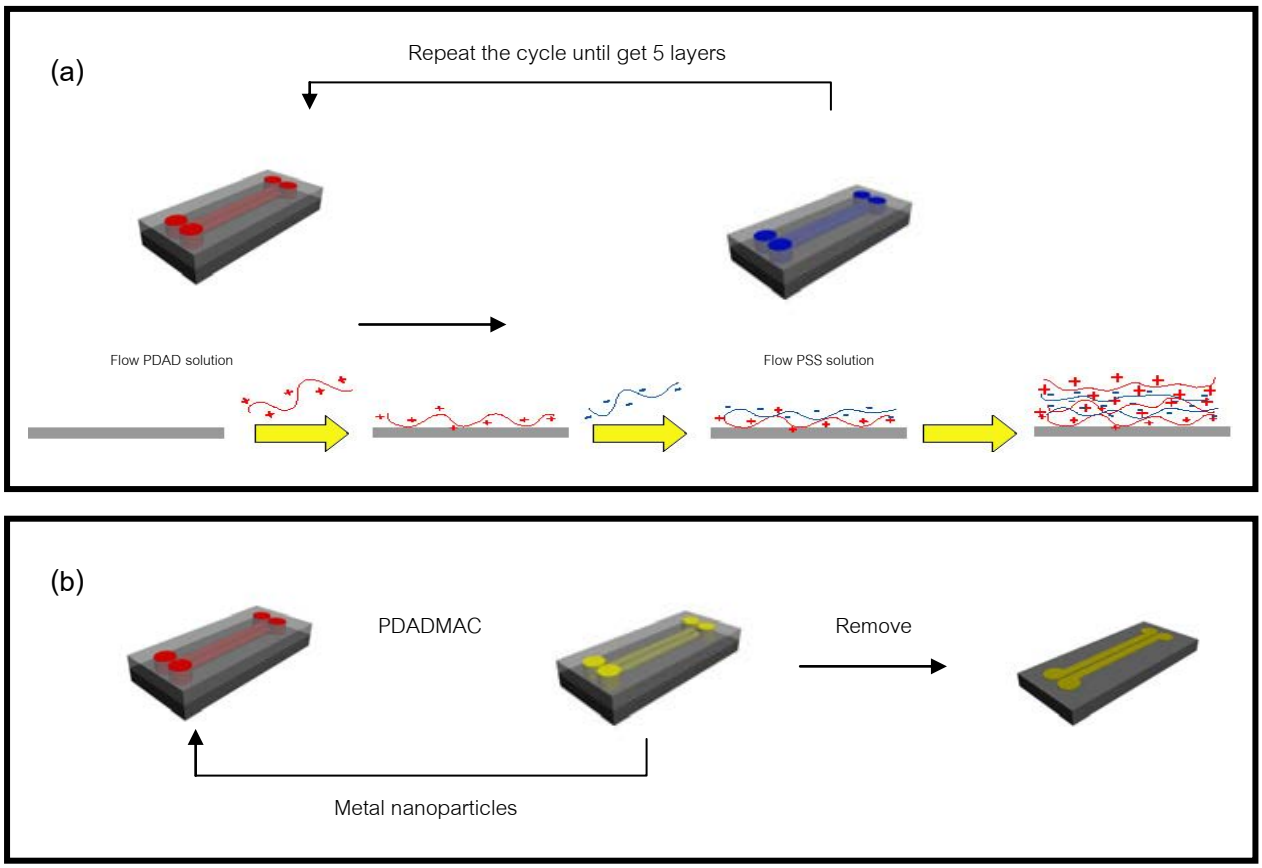

Figure 3.4 Schematic diagram of flow deposition microelectrode process (a) preparation of primer layer steps (b) preparation of modified electrode steps.

3.8.3 Characterization of micro-electrodes

3.8.3.1 Field Emission Scanning Electron Microscopy (FE-SEM)

The surface morphology of sample was monitored by using Field Emission Scanning Electron Microscope (FE-SEM). FE-SEM was also used to confirm the nanoparticles assembly in the microchannel as well as its thickness.

3.8.4 Conductivity measurement of micro-electrodes as detection for lab on a chip device

3.8.4.1 Pressure driven process

The measurement conductivity of microelectrodes was tested to measure the KCl solution ranging from 2 to 20 mM. The flow of KCl in the micro-channel was driven by connecting the outlet to a vacuum pump. In brief, the detection was operated through a straight channel connecting two reservoirs as shown in figure 3.5.

The channel was rinsed with deionized water for 5 minutes. After rinsing step, the inlet reservoir was filled with 2 mM KCl for 1 minute. These steps were repeated by changing KCl concentration from 4 to 20 mM. The repeating process was started from beginning for 3 times.

Sinusoidal current/voltage waveform (AC mode) was used to characterize the detection efficiency of microelectrode as shown in figure 3.5. The voltage sinusoidal waveform (3V) was applied to microelectrodes. A 1kΩ resistor was connected in sequence with electrode to monitor the current passing through the electrode. The voltage value was divided by 1kΩ to obtain the current value.

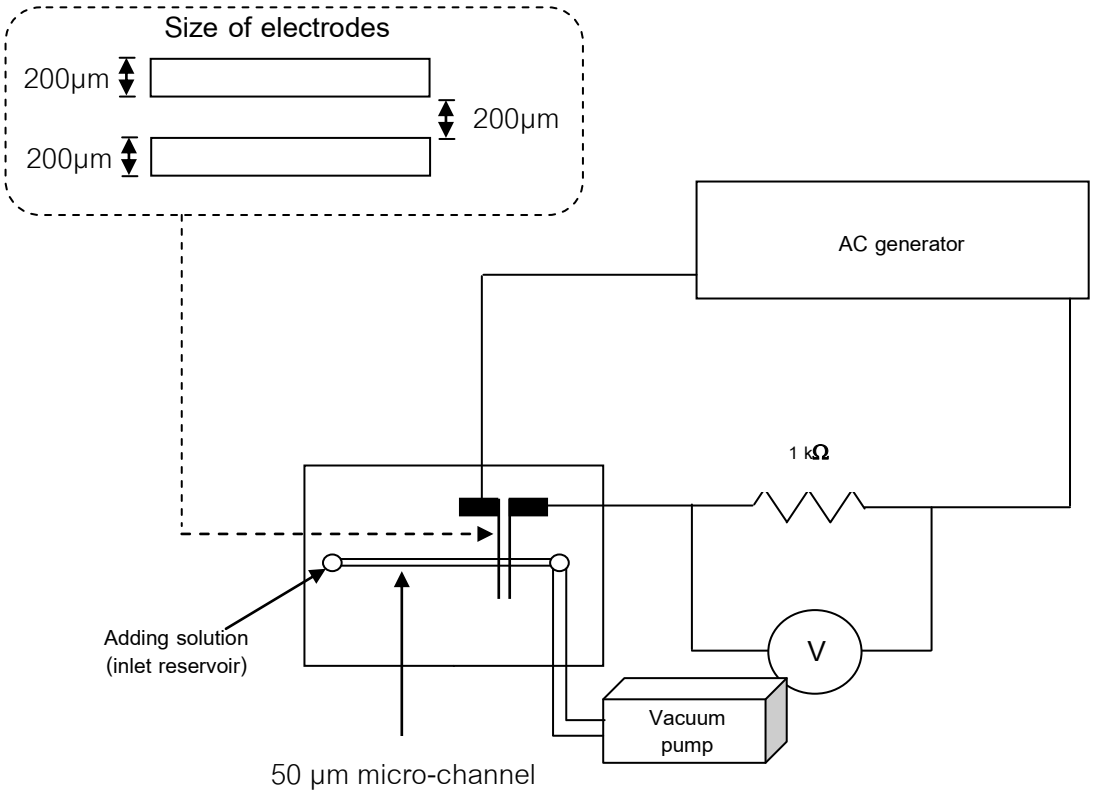

Figure 3.5 AC measurement set up.

3.8.4.2 The operation microfluidic under high voltage

The usage of nanoparticles microelectrodes in microfluidic devices has been done under flow with a vacuum system. So, the integrating gold nanoparticles microelectrodes for electrophoretic operation were then connected with a high voltage power supply. The integrating gold nanoparticles microelectrodes for electrophoretic

operation were then connected with a high voltage power supply. The complete chip was made by reversible sealing the flow channel over the gold nanoparticles microelectrodes. The flow channel length was 4 cm. The channel was 50 μm wide and deep. The 200 μm gold nanoparticles microelectrodes were spaced at 200 μm. The buffer solution was introduced to reservoirs and flowed though the microchannel using vacuum (no bubbles observed with microscope). The operation was only tested with DI water. The high voltage power supply (HV) was operated through a straight channel connecting two reservoirs. The platinum wires were connected to HV via clip wires in order to use as flowing electrodes. The platinum wires were dipping into two reservoirs as shown in figure 3.6. The voltage was then applied to system using 600V for 5 minutes.

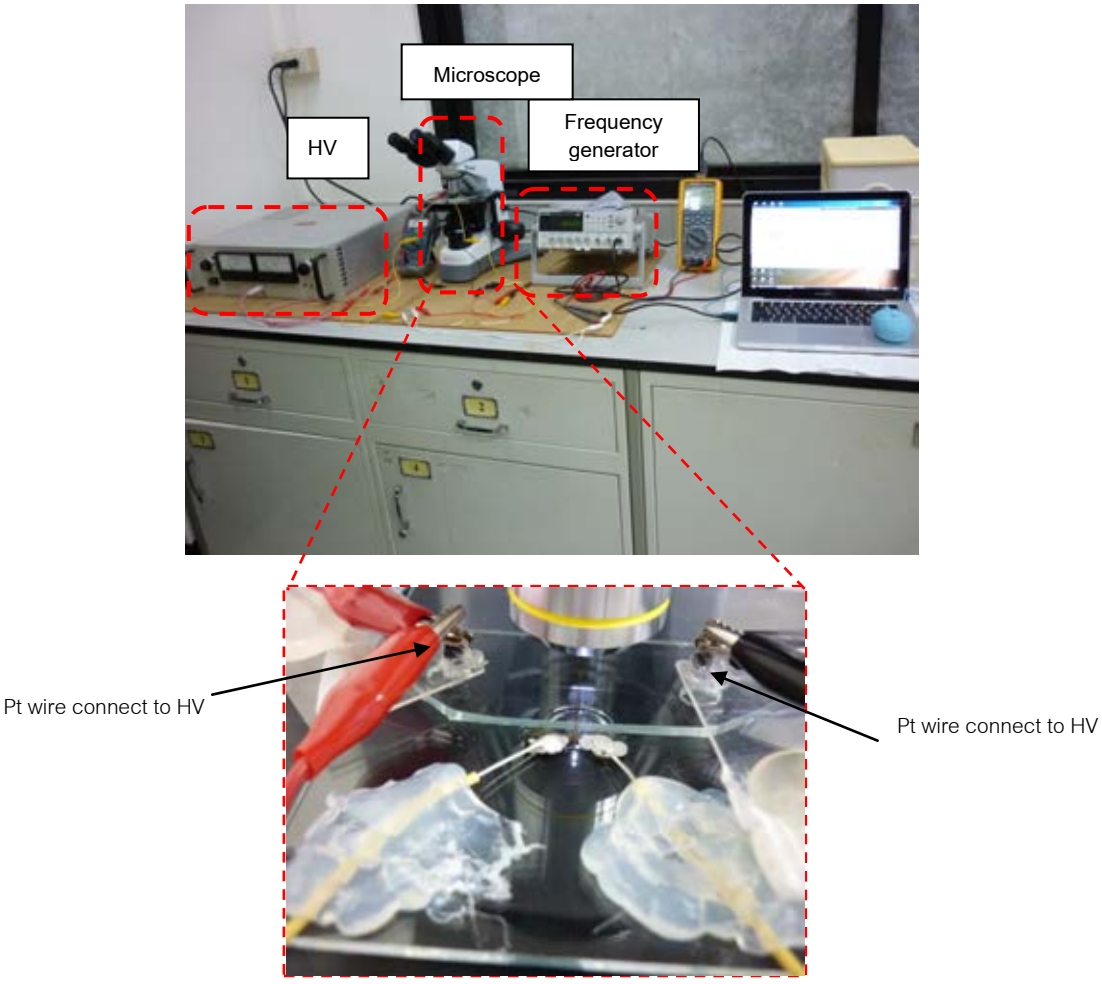

Figure 3.6 The layout of microfluidic device.

The two gold microelectrodes were placed inside a microchannel that were used for conductivity measurement as same as using pressure driven process [93].

3.9 Performance testing of fabricated electrode

3.9.1 Fabrication of gold nanoparticles multilayers thin film electrode

The different sizes of electrodes were fabricated using the method as described in section 3.7.1. The size of electrode was shown in the table 3.1. The electrodes were then tested by measuring the conductivity of KCl solution.

Table 3.1 The relation of cell constant and electrode size

Width (mm)	Length (mm)	A (2electrode) $(mm)^2$	L (mm)	K (mm)
1	2.2	4.4	0.1	0.022727
0.8	2.2	3.52	0.1	0.028409
0.7	2.2	3.08	0.1	0.032468
0.65	2.2	2.86	0.1	0.034965
0.6	2.2	2.64	0.3	0.113636
0.55	2.2	2.42	0.4	0.165289
0.5	2.2	0.55	0.5	0.909091

$K = L/A$

K = cell constant

L = distance between electrode

A = area of electrodes

3.9.2. Contact conductivity measurement of gold nanoparticles electrode

The conductivity measurement of gold electrodes was tested by measuring the conductivity of KCl solution. The measuring method was shown in figure 3.7. Sinusoidal current/voltage waveform (AC mode) was also used to characterize the detection

efficiency of gold nanoparticles electrode. The voltage sinusoidal waveform (3V) was applied to electrodes. A 1kΩ resistor was connected in sequence with electrode to monitor the current passing through the electrode. The voltage value was divided by 1kΩ to obtain the current value.

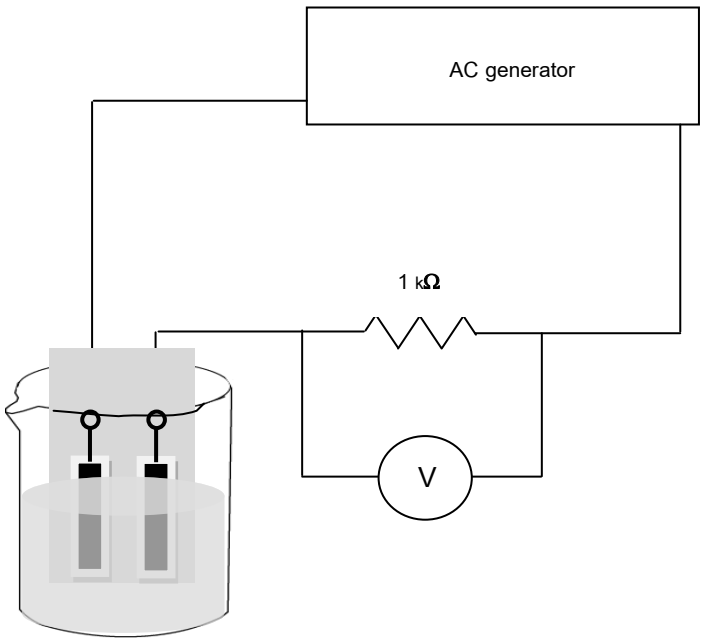

Figure 3.7 AC measurement set up.

The reproducibility of the preformance of the fabricated electrodes was evaluated by testing ten electrodes prepared different days. The current measurement of 1, 10 and 100 mM KCl solutions was performed by observing percent RSD. The reproducibility of run to run of an electrode was also tested by the current detection of KCl solutions for five days.

3.9.3 Adhesion test

The physical contact test was performed in order to evaluate the stability of the electrode surface. Two types of electrodes: the bare gold electrode and PEMs coated electrode were tested. Polyelectrolyte multilayers thin film was coated on top of gold nanoparticles electrode by the same method as described in section 3.5. The number of layer was varied from 1 to 11 layers.

The adhesion test was adapted from ASTM D3359 in order to confirm PEMs protecting surface of electrode[94]. A tape for testing adhesion was applied over our fabricated gold electrodes. The tape was then removed quickly by pulling the tape back off of the test area to reveal the amount of gold nanoparticles lifted off by the test tape. The colors of nanoparticles on transparent tapes were observed to confirm the nanoparticles peeling out. Furthermore, the conductivity measurement of both electrodes with the KCl solution was tested after tape testing.

3.10 Application of gold nanoparticles electrodes and polyelectrolyte multilayers thin film

3.10.1 Carbaryl detection by PEMs with HA

Polyelectrolyte multilayers thin film was coated on top of gold nanoparticles electrode by the same method as described in section 3.5. The numbers of layer were varied as 6, 7, 10, 11, 16, 17, 20, 21 layer in order to test the effect of top layer on HA deposition process. We can find the suitable top layers that can absorb HA. The concentration of HA was fixed at 1 %wt.

After getting suitable number of layers, the effect of dipping time was also studied by fixing the number of layer at 11 layers. The dipping time in HA solution was varied from 10-60 minutes in order to find the dipping time for detection of carbaryl.

The detection of carbaryl was then performed by varying dipping time in 0.01 %wt of carbaryl. The measuring conductivity of 1 mM KCl was done every step which used the method in 3.9.2. The pH of carbaryl solution was also studied at 2.5, 4.3 and 6.

3.10.2 Polyelectrolyte multilayers coating for organic solvent resistant

3.10.2.1 Coating of the PMMA and PDMS with chitosan, alginate and PDADMAC and PSS thin films

The 1 mm thick PMMA sheets were cut into plates with the size of 2.5 cm x 7.5 cm (width x length) as substrates. The two pairs of polyelectrolytes were coated on the PMMA substrates by the method as described in section 3.5. The two pairs of polyelectrolytes consisted of PDADMAC-PSS and chitosan-alginate. The 2 mm thick

PDMS was also cut into plates measuring 3 cm x 3 cm (width x length) to use as substrate. PDMS was only coated with chitosan/alginate pair.

3.10.2.2 Testing of the solvent resistance

To investigate the solvent compatibility of PMMA plates, the percent transmittance of PMMA sample was measured using fiber-optic spectrophotometer. The fiber-optic spectrophotometer was connected to computer with using of spectra-suite software to record spectra. PMMA was immersed into acetonitrile for 60 minute. PMMA was then removed from acetonitrile solution and the percent transmittance of PMMA was recorded at 550 nm every 2 minutes. PDMS samples were exposed to chloroform vapor and their weight recorded as a function of time for various number of chitosan/alginate layers for 120 minutes.

CHAPTER IV
RESULTS AND DISCUSSION

This chapter consists of two parts. The first part presents the simple microelectrodes fabrication procedure from silver and gold nanoparticles using flow deposition technique. The effect of types and concentrations of stabilizers were studied for silver and gold nanoparticles preparations. The silver and gold nanoparticles multilayer thin films were then fabricated as electrodes. Its conductivity property of the electrode was also studied. The electrodes were operated under vacuum system and electric potential system. Finally the potential application of electrode was presented in this part. In the second part, the surface modification of polymeric materials with the layer-by-layer technique was studied to prevent organic solvent.

4.1 Metal nanoparticles preparation

4.1.1 Silver nanoparticles preparation

Stabilizer plays an important role on the preparation of metal nanoparticles. In this section, the types and concentrations of anionic polyelectrolytes as stabilizer were studied. The selection of the type of anionic polyelectrolyte can have a large influence on nanoparticles features, optical properties, conductive properties, and colloid stability of silver nanoparticles [47]. Anionic polyelectrolytes, humic acid (HA), poly(4-styrenesulfonic acid-co-maleic acid) sodium salt (PSS-co-MA), and alginic acid sodium salt were used for preparing silver nanoparticles. The structures of the anionic polylectrolytes were shown in figure 4.1.

The HA contain a lot of functional groups such as –OH, -CONH-, and –COOH groups variously place on aromatic rings. The hypothetical structure of HA was presented in figure 4.1 (a). PSS-co-MA is a synthetic copolymer of poly(sodium 4-styrenesulfonate) (PSS) and maleic acid. The PSS-co-MA was selected as stabilizer because it contains both the strong sulfonate groups in PSS and the weak carboxylic group on the maleic acid segments. Alginic acid is an anionic polysaccharide, which contains only carboxylic groups. As described previously in the section of experimental, the concentrations of anionic polyelectrolytes (%wt) were varied from 0.0005-0.01 %wt.

However at the concentration lower than 0.0001 %wt, the precipitation of silver particles was observed for all anionic polyeletrolytes. This phenomenon occurred due to insufficient stabilizers to cap silver particles result the particle aggregations in the solution.

The preparation of silver nanoparticles were done under un-controlling pH condition because all pH values of silver nanoparticles solution were around 9 after finishing the preparation process.

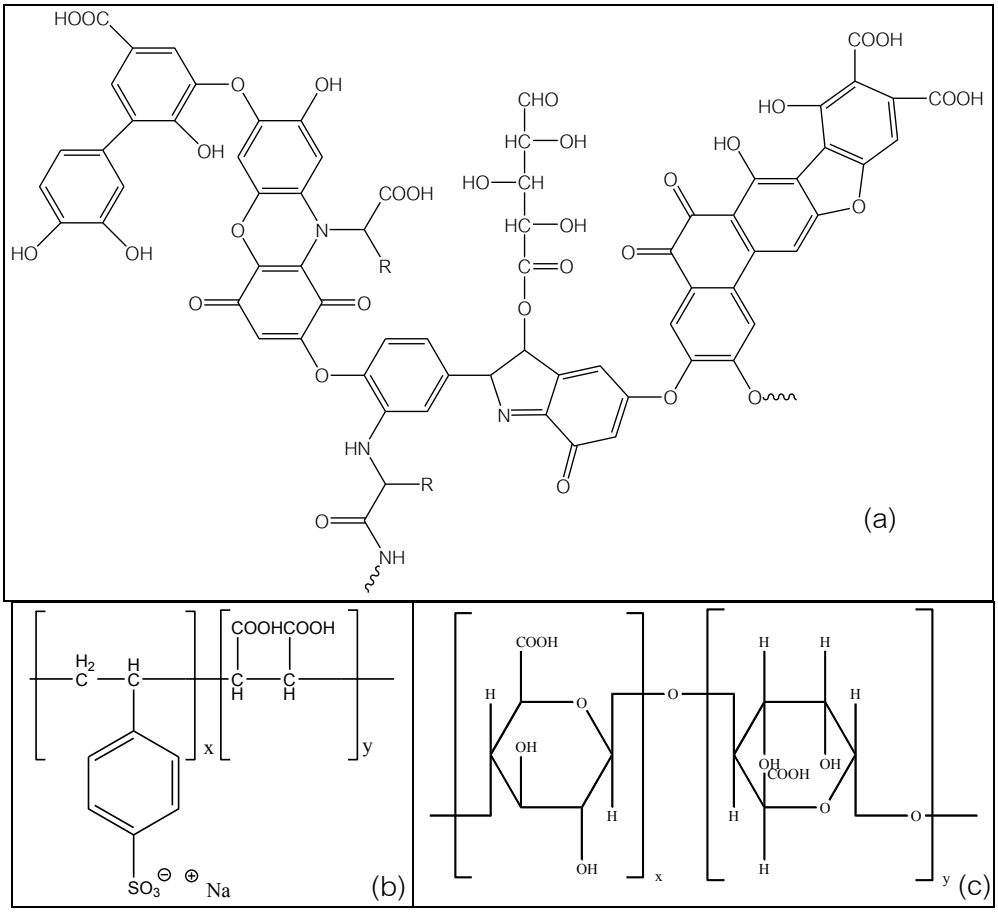

Figure4.1 The structures of humic acid (a), poly(4-styrenesulfonic acid-co-maleic acid) (b) and alginic acid (c).

4.1.1.1 Humic acid (HA)

Humic acid can be used as a capping reagent for synthesis of silver nanoparticles [95]. These silver nanoparticles possess negative charge due to the carboxylic functional group present on HA. Various concentrations of HA were used to prepare silver nanoparticles. The formation of silver nanoparticles from the reduction of silver nitrate with polyelectrolyte can be monitored using UV-Visible spectrophotometer. The UV-vis spectra of silver nanoparticles solutions displays λ_{max} of about 398-425 nm, as shown in figure 4.2. This wavelength is a specific absorbance spectrum of silver nanoparticles [96]. The absorption strongly depends on the particle size, dielectric medium and chemical surroundings [97]. Small spherical nano particles (< 20nm) exhibit a single surface plasmon band [98].

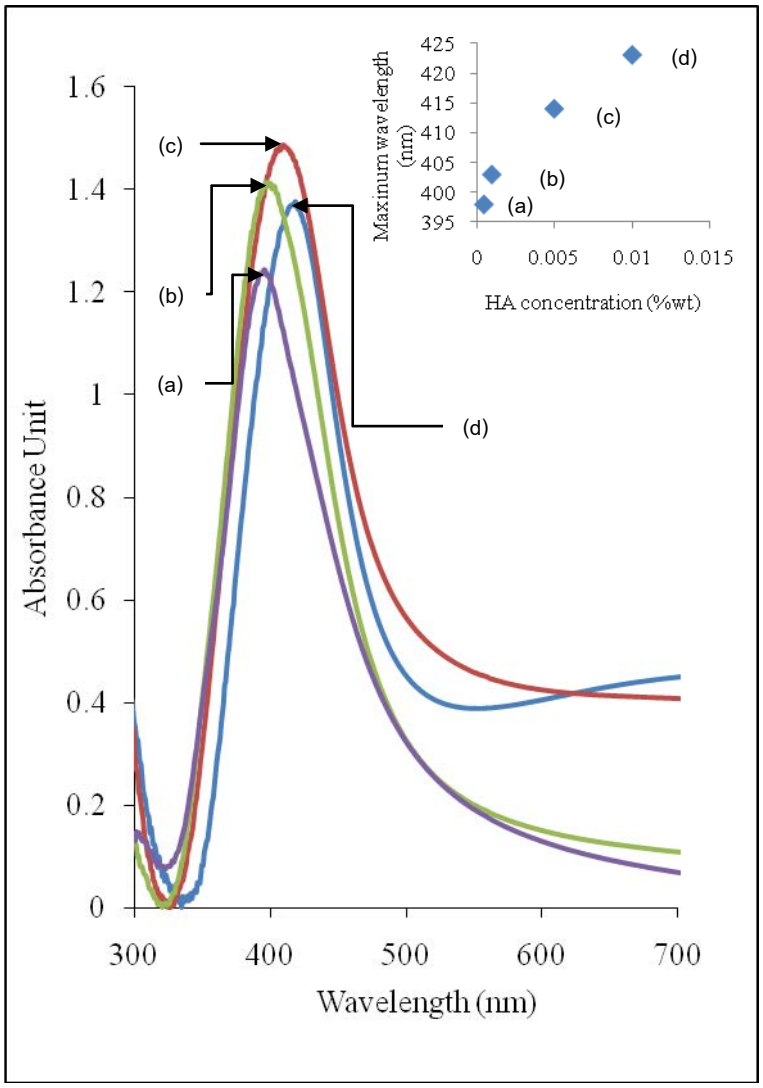

Figure 4.2 Absorption spectra of HA stabilized silver nanoparticles solution with different HA concentrations: 0.0005 (a), 0.001(b), 0.005(c), and 0.01(d) %wt. (inset: plot of absorbance at maximum wavelength with varying amount of HA.).

In this study, the effect of HA concentration on the particle sizes was observed that the red shift of λ_{max} of silver nanoparticles was increased with the increase in the capping agent concentrations. It might be due to the effect of the thicker capping layer on the particles when capping agent concentration increases [95]. The trend of silver nanoparticles size with the capping agent concentration was confirmed by TEM images (Figure4.3). The TEM images also revealed largely spherical particles size for lowest concentration of HA stabilizing silver nanoparticles.

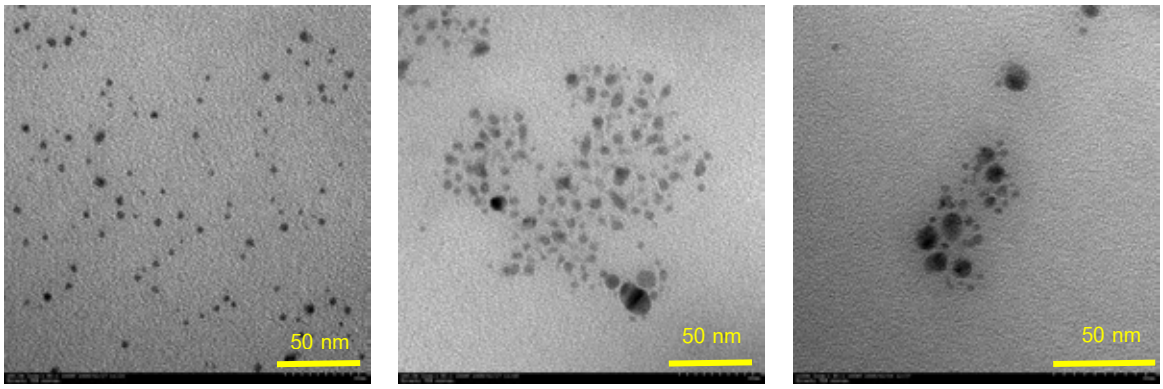

Figure 4.3 TEM images of silver nanoparticle stabilized by different amount of HA: (a) 0.01% wt HA (b) 0.001% wt HA (c) 0.0005% wt HA (scale bar = 50 nm).

The silver nanoparticles prepared by using HA showed a clear affect of high and low concentration of stabilizing agent which high concentration can prepare silver nanoparticles better stabilize particles than low concentration.

4.1.1.2 Poly(4-styrenesulfonic acid-*co*-maleic acid) sodium salt (PSS-co-MA) and alginic acid

Based on the result in the previous section the silver nanoparticles were prepared using the 0.0005 and 0.01 %wt for both PSS-co-MA and alginic acid.

It can be seen that PSS-co-MA and alginic acid stabilized silver nanoparticles showed the same trend as HA stabilized silver nanoparticles that the red shift of of λ_{max} with the increase in the capping agent concentrations. This indicated that silver cations can stabilize with larger amount of anionic polyelectrolytes.

The full band widths at half-maximun (FWHM) could provide the information about the particle size distribution formed in the solution [99].Theoretical model suggested that the FWHM increased with the increase of the particle size [99]. FWHM was increased with the decreasing stabilizing concentration as shown in table 4.1 which indicated that the size of silver nanoparticles were larger. The results are in the agreement with the related theoryl.

Table 4.1 The characteristic of silver nanoparticles with different types and concentrations of stabilizing agent.

Types and concentrations of stabilizers	λ_{max} (nm)	FWHM (nm)[*1]	Mean particles size (nm)[*2]	Zeta potentials (nm)
PSS-co-MA 0.0005 %wt	385	87.68	35	-38.4
PSS-co-MA 0.01%wt	397	79.43	18	-57.9
Alginic acid 0.0005 %wt	388	91.78	50	-36.2
Alginic acid 0.01 %wt	395	81.07	28	-45.4

[*1] Data was calculated by excel,

[*2] Value was obtained from percent are of the majority population.

Figure 4.4 revealed the bimodal size distribution of silver nanoparticles for both PSS-co-MA and aliginic acid with two different concentration levels. The average size of the majority population was shown in table 4.1 which percent peak area of the majority population was 71.9, 78.1, 72.6 and 78.1 for 0.0005, 0.01 %wt of PSS-co-MA and 0.0005, 0.01 %wt of alginic acid, respectively. The smaller distribution was appeared to become more asymmetric which had particles diameter range from few to ten of nanometers. These results indicated that the silver nanoparticles were actually comprised of multiple distributions that changes with stabilizing concentration. The formation of silver nanoparticles through the reduction of silver ions consists of two steps: nucleation and growth whose relative rates determine the size distribution of silver nanoparticle [99-100]. These two processes can affect to find the mixing of two size distribution [99-100].

TEM image results showed that the silver nanoparticles were found to be spherical in shape for all conditions (Figure4.5). The silver nanoparticles have a tendency to aggregate at low concentration of stabilizing agent. A clear trend was

observed by TEM images that 0.0005 %wt concentration of stabilizing agent showed bigger size and some aggregation. It was agreed with the data of particles size.

The particles size of silver nanoparticles using PSS-co-MA was found smaller than silver nanoparticles using alginic acid under the same preparation condition. It might be due to a more dense coating of PSS-co-MA on silver nanopartilce, which was affected by strong sulfonate group of PSS-co-MA.

The zeta potential gives an indication of the potential stability of the colloidal system. Generally, particles size with zeta potential more negative than -30 mV are considered stable[101]. From Table 4.1, all silver nanoparticles prepared under these conditions were stable. The 0.01 %wt concentration showed higher zeta potential compared to the one prepared with 0.0005 %wt for both polyelectrolytes. Furthermore, PSS-co-MA was found to deliver the silver nanoparticels with higher zeta potential compared to the alginic acid at the same concentration. The PSS-co-MA contains both strong acid ($-SO_3^-$) and weak acid (-COOH) while algic acid provides only carboxylic functional group. This is a main reason that PSS-co-MA has a higher zeta potential than alginic acid at the same concentration.

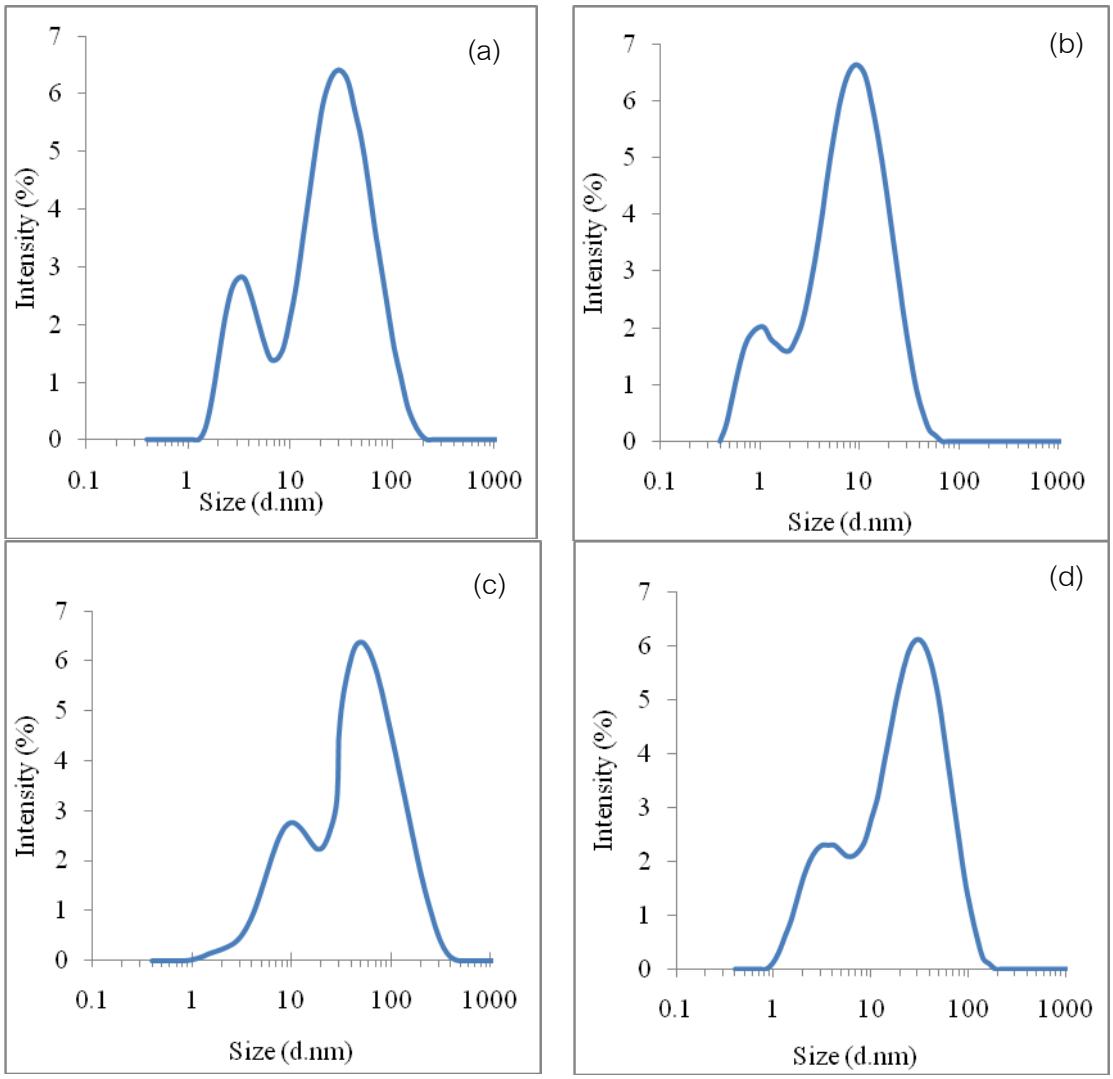

Figure4.4 Particles size distribution of silver nanoparticles stabilized by different amount and type of anionic polyelectrolytes: 0.0005 (a), 0.01 (b) %wt of PSS-co-MA and 0.0005 (c), 0.01 (d) %wt of alginic acid.

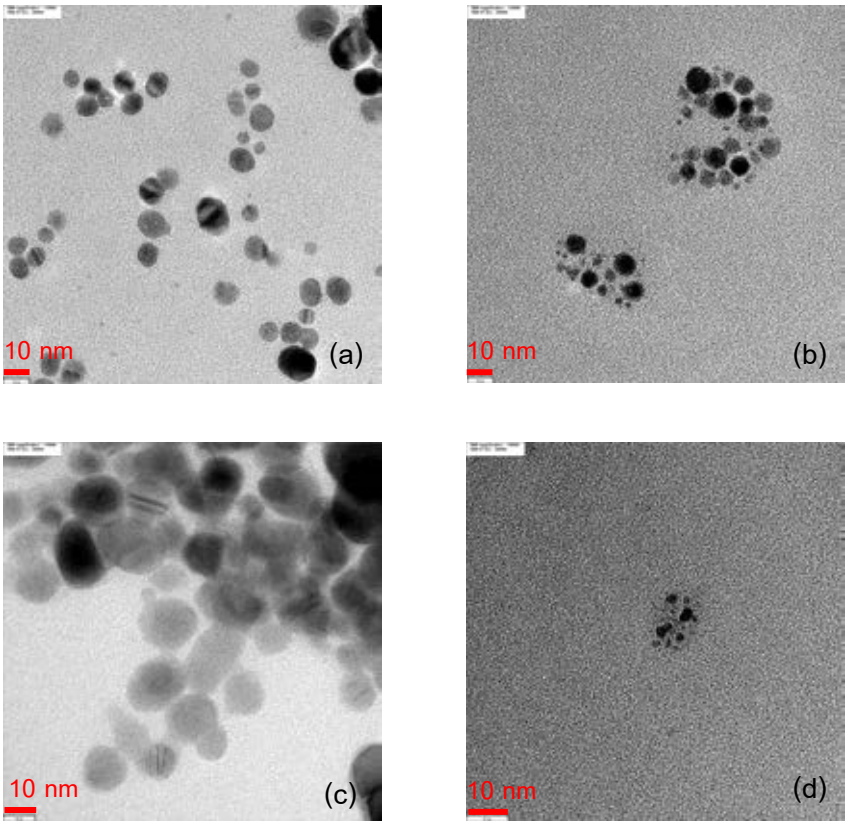

Figure 4.5 TEM images of silver nanoparticles stabilized by different amounts and types of anionic polyelectrolytes: 0.0005 (a), 0.01 (b) %wt of PSS-co-MA and 0.0005 (c), 0.01 (d) %wt of alginic acid (scale bar = 10 nm).

The silver nanoparticles could be prepared using all three types of polyelectrolytes including HA, PSS-co-MA and alginic acid and will be used to prepare thin film in further section.

4.1.2 Gold nanoparticles synthesis

Gold nanoparticles were also used in this study due to their long term stability, high surface to volume ratio, easy synthesis, biological compatibility and easy surface functionalization. In this research, the nanoparticles were prepared by the reduction of chloroauric acid ($HAuCl_4$), in the presence of sodium citrate, where sodium citrates act as both a reducing agent and a capping agent [50]. Ability of sodium citrate to stabilize gold nanoparticles was studied by varying the sodium citrate concentration as 15, 30 and 60 mM with fixing $HAuCl_4$ at 1 mM. The pH of gold nanoparticles solution was found in the range of 6.5-6.8 for all three conditions which was above pKa of sodium citrate. The sodium citrate stabilized gold nanoparticles were negatively charged. The presence of gold nanoparticles can be monitored by UV-Visible spectrophotometer. The plasmon absorption spectra were found at 520-535 nm as shown in figure 4.6 which are usually taken as the indication of gold nanoparticles. The data of gold nanoparticles characteristic was presented in table 4.2. There was a shift in the maximum absorption wavelength of gold plasmon band from 520 nm to 535 nm with the decreasing in the sodium citrate concentrationindicating that the sizes of gold nanoparticles were obtained. This observation was in contrast with the trend obtained in the preparation of silver nanoparticles section. It might be because the polyelectrolytes have long chain molecule that could form a thin layer around nanoparticles. Meanwhile, sodium citrate is a small molecule that forms cluster around nanoparticles.

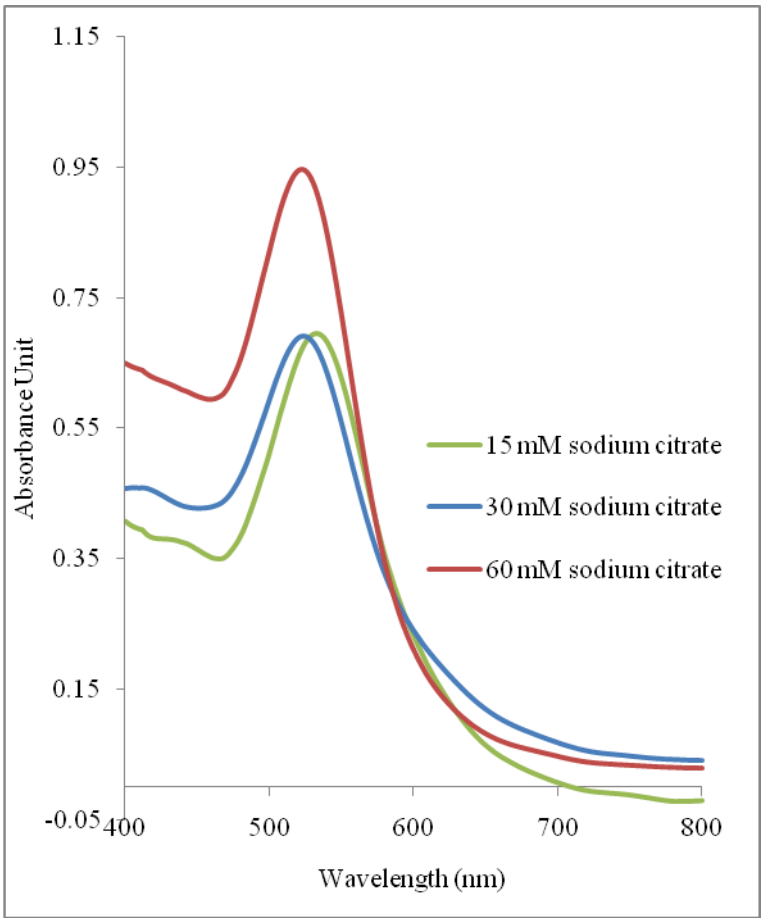

Figure 4.6 Absorption spectra of prepared gold nanoparticles using different concentrations of sodium citrate. (Inset: plot of absorbance at maximum wavelength with varying amount of sodium citrate.)

Based on the FWHM values which were presented in table 4.2, the size of gold nanoparticles were smaller with increasing sodium citrate concentration. It was in agreement with the shift of maximum wavelength (blue or red shift).

To confirm the particles size, TEM images and measurement of particles size with Nanosizer were performed. Particle size determined in TEM images (Figure 4.7) decrease with increasing amount of sodium citrate and absorbance maxima change in a nearly parallel fashion. The effect of particles size can be observed by TEM images because all images were recorded in the same scale.

Table 4.2 The characteristic of gold nanoparticles with different concentrations of sodium citrate.

concentrations of sodium citrate (mM)	λ_{max} (nm)	FWHM (nm) [*1]	Mean particles size (nm) [*2]	Zeta potentials (nm)
15	535	63	42.77	-32.8
30	525	58	42.53	-36.9
60	516	52	26.35	-43.4

[*1] Data was calculated by excel,

[*2] Value was obtained from percent are of the majority population.

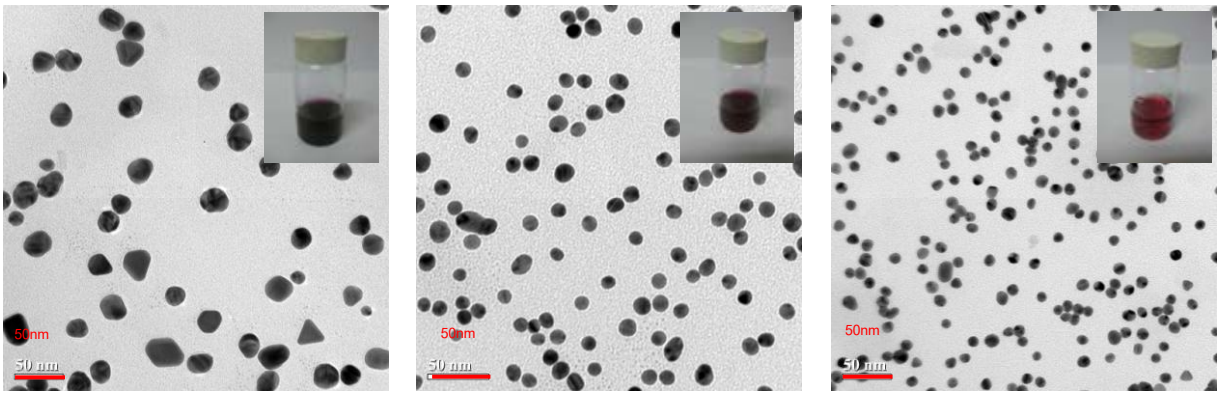

Figure 4.7 TEM images of gold nanoparticles with 15:1 (a), 30:1 (b) and 60:1 (c) Na_3Ct:$HAuCl_4$ ratios (inset: Picture of gold nanoparticles solution).

From TEM images, the effect of sodium citrate concentration on the nanoparticle shape was also observed. Although, the size averages of 15 and 30 mM sodium citrate stabilized gold nanoparticles were found similar size,TEM images revealed that the gold nanoparticles prepared with 30 mM delivered more uniform size and shape comparing to the one prepared with 15 mM sodium citrate. Gold nanoparticles using 15 mM sodium citrate was found the shape of triangles and others as a result of imperfect stabilized gold nanoparticles. Particles have a tendency to gather in the area where the area

covered is not perfect. The spherical nanoparticles were found when using 30 and 60 mM sodium citrate.

The zeta potentials of gold nanoparticles containing 1 mM of $HAuCl_4$ and 15, 30, 60 mM of sodium citrate were also measured and found to be negative for all cases because of the charge of sodium citrate (Table 4.2). Increasing the concentration of sodium citrate led to a significant increasing in zeta potential. When sodium citrate concentration was increased, the number of citrate anions in system increased due to dissociate and acting as stabilizer.

Gold nanoparticles were used to prepare nanoparticles thin film as same as silver nanoparticles in the further section.

4.2 Kinetic study of monolayer adsorption

4.2.1 Silver nanoparticles monolayer adsorption

The effect of dipping time was investigated due to its relation with the quantity of deposited silver nanoparticles on the surface of glass slides. To study the dipping time, kinetic monolayer adsorption is a key controlling the thickness of the multilayers. The kinetic monolayer adsorption was also studied for all silver nanoparticles prepared in the earlier part.

4.2.1.1 Humic acid

In figure 4.8, the kinetic adsorption of silver nanoparticles stabilized by 0.0005 %wt of HA as a function of time was monitored by plot of changing absorbance at the wavelength of maximum adsorption with time. The red shift absorption was observed due to the effect of characteristic surface plasmon on resonance of metal nanoparticles that were sensitive with size, shape and surrounding medium of metal particles as shown in figure 4.8 (a). Moreover, it can be seen that as the time increased, the new peak located at 600 nm was found. This is due to a decreasing distance between particles which caused by aggregation of particles. The distance between particles decreased that mean more adsorption of particles on the substrate. Meanwhile, the peak of isolate nanoparticles was located at 400 nm.

The dramatically changes in absorbance at 600 nm with time was observed at early time indicating that the particles adsorption on substrate was fast (figure 4.8 (b)). The absorption intensity at 600 nm was increased with increasing dipping time. After initial step of time, the adsorption intensity was found constant after seven minutes which suggested the saturated monolayer absorption of nanoparticles.

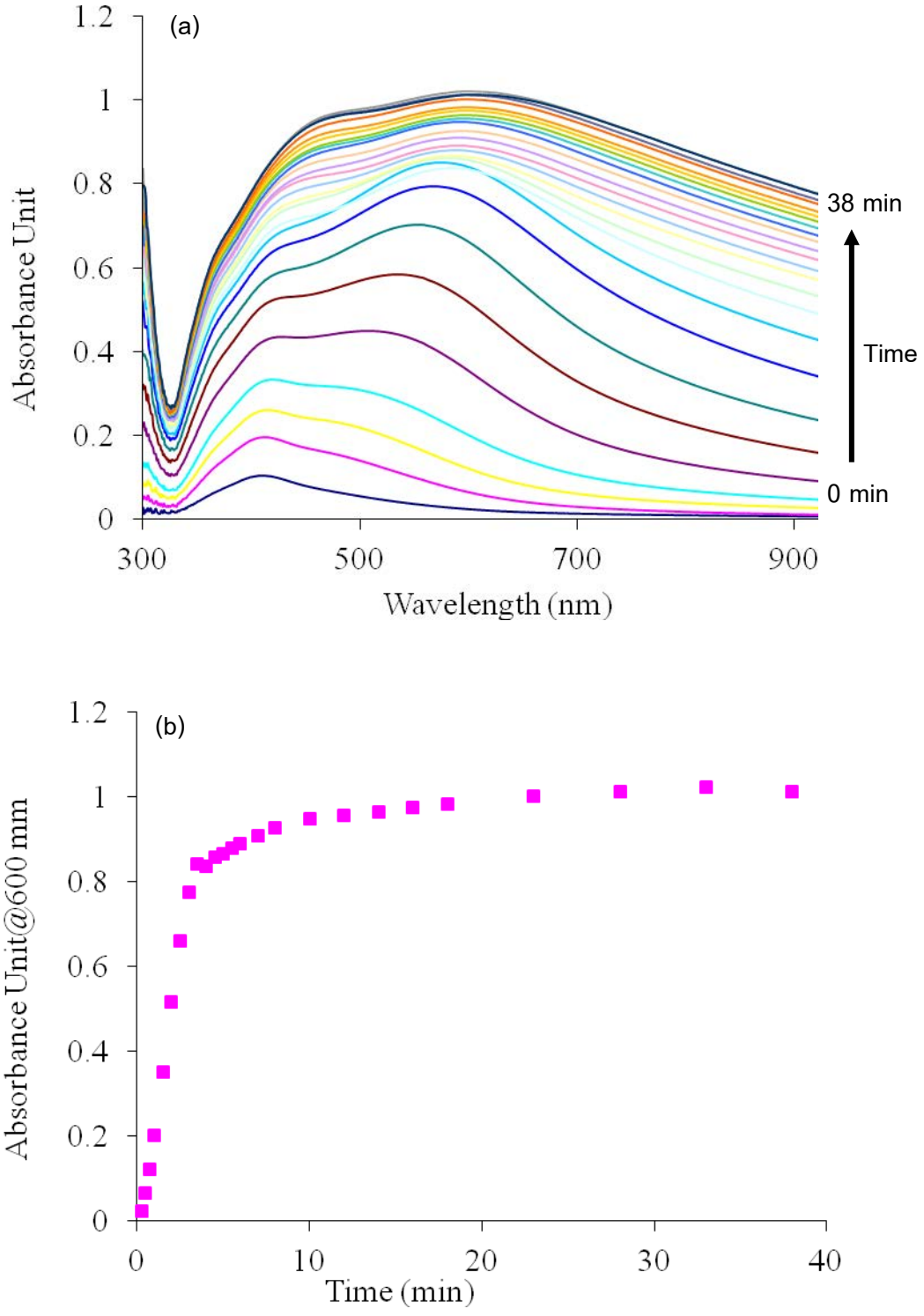

Figure4.8 Absorption spectra of monolayer of silver nanoparticles stabilized by 0.0005 %wt of HA as a function of time (a), plot of changing absorbance at 600 nm as a function of time (b).

The similar absorption spectra obtained from the 0.001 % wt of HA stabilized silver nanoparticles. However, for 0.01 and 0.005 %wt of HA stabilized silver nanoparticles, the single peak of absorption spectra at 440 and 445 nm was revealed because particles repelled each other that can prevent aggregation of particles.

From figure 4.9 (a), the similar trends of absorption isotherm for all concentrations were observed, which appeared steep slope at early time and became constant.

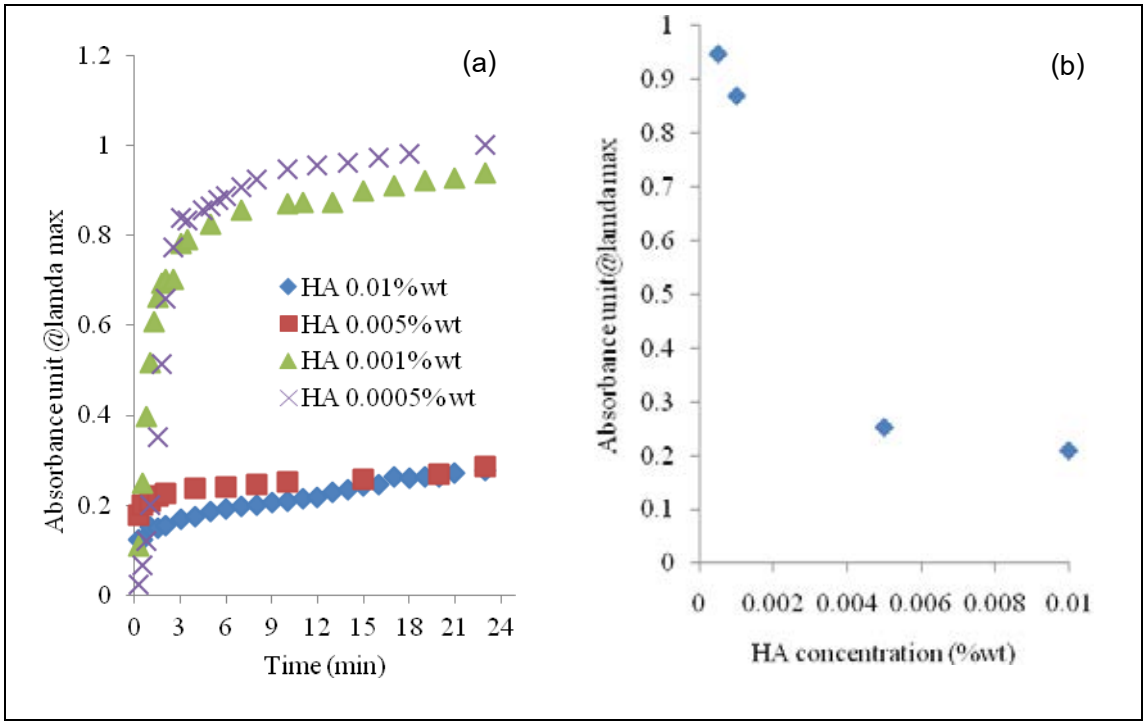

Figure 4.9 Plot of the change in absorption intensity at 440, 445, 480 and 600 nm for 0.01, 0.005, 0.001 and 0.0005 %wt of HA stabilized silver nanoparticles as a function of time, respectively (a); plot of absorbance of the monolayer film fabricated in left hand side after 10 min as a function of the HA concentration (b).

Although, all concentrations of HA stabilized silver nanoparticles was saturated at about seventh minutes, but ten minutes dipping time was used in subsequent experiment to ensure that silver nanoaprticles was completely deposited in each layers.

However, the plot between the change in absorbance with time was found similar for all concentrations of HA but the intensity was increased with decreasing HA

concentration as shown in figure 4.9 (b). Monolayer film prepared by silver nanoparticles using high concentration of humic acid should possess high number of negative charges resulting in large repulsive force between each particle. Therefore, the lower packing density of the particles on the substrate was obtained. On the other hand, the absorption of silver nanoparticles using low HA concentration was higher compared to the higher one because of the smaller repulsive force among particles. The denser monolayer film was observed as show in AFM image (Figure 4.10).

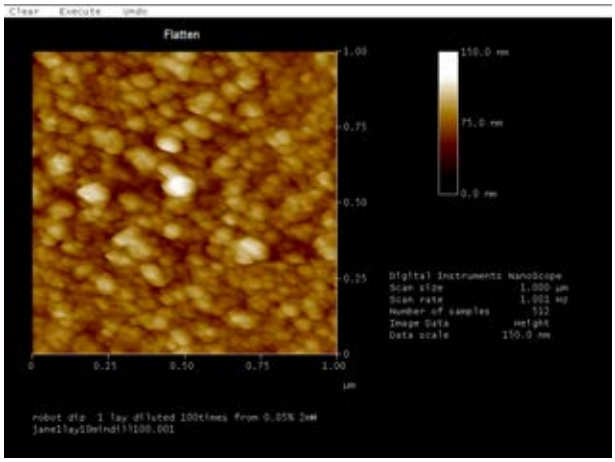

Figure 4.10 AFM image of 0.0005% wt HA-stabilized-Ag nanoparticle monolayer thin film using 10 min dipping time.

4.2.1.2 PSS-co-MA and alginic acid

In the kinetic characterization of silver nanoparticle monolayer formation, the change in absorbance with time was also studied for both PSS-co-MA and alginic acid stabilized silver nanoparticles as presented in figure 4.11. The data displayed similar trend with HA stabilized silver nanoparticles which was discussed above. The saturated point of both PSS-co-MA and alginic acid was about twelve minutes which could be seen from the slope of each plot. However, the fifteen minutes dipping was used in further experiment in order to ensure that the adsorption of silver nanoparticles has been completely formed.

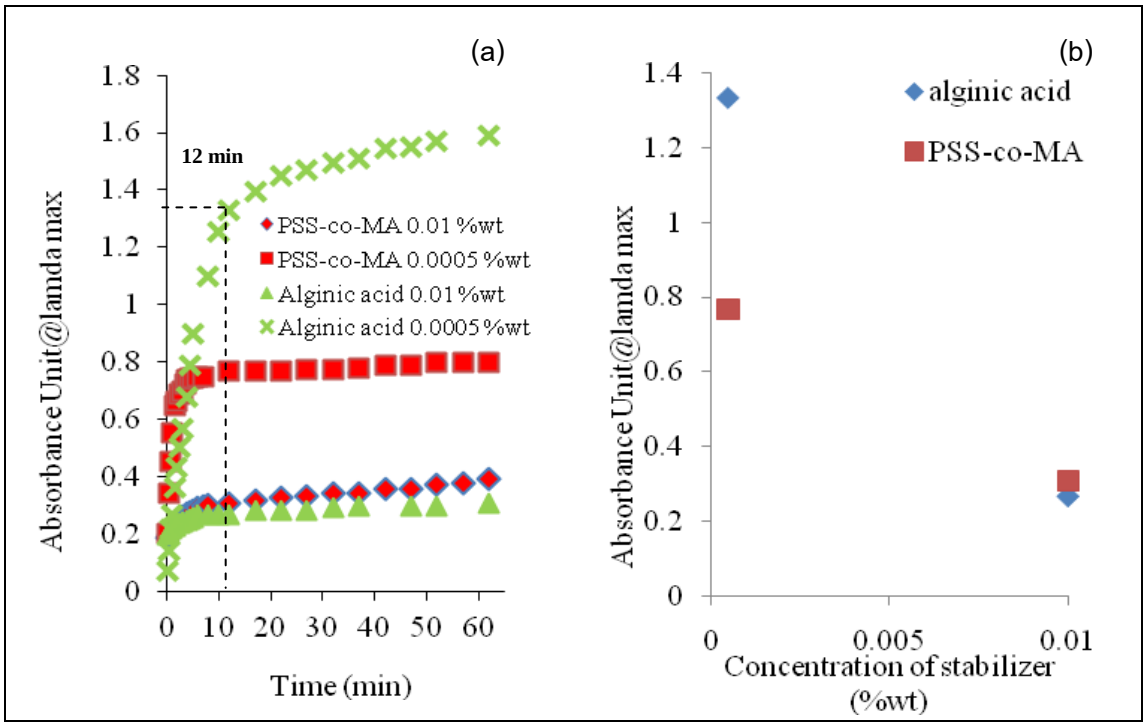

Figure 4.11 The change in absorption intensity at 440, 485 nm for 0.01, 0.0005 %wt of PSS-co-MA and 440, 625 nm for 0.01, 0.0005 %wt of alginic acid as a function of time (a), plot of absorbance of the monolayer film fabricated in left hand side after 15 min as a function of the alginic acid and PSS-co-MA concentrations (b).

When comparing the differences in concentration of stabilizing agent, the low concentration was found to deposit on substrate at higher amount compared to the higher concentration for three types of stabilizing agents (HA, PSS-co-MA, alginic acid). The 0.0005 %wt stabilizer concentration showed higher intensity adsorption than 0.01wt% stabilizer concentration as shown in figure 4.11 (b) for both PSS-co-MA and alginic acid stabilized silver nanoparticles. This may be due to the fact that high concentration shows high charge density. It was confirmed by the results of zeta potential as described previously in which zeta potential was increased with PSS-co-MA and alginic acid concentration. Then, the strong electrostatic repulsion force might prevent the closely deposition of nanoparticles on the substrate.Moreover, the excess of stabilizer could also deposit on to the substrate. Hence, at 0.01 %wt stabilizer concentration showed nearly same intensity adsorption for all types of stabilizing agent.

At the same concentration, the deposition of the silver nanoparticles stabilized with alginic acid higher adsorption intensities were larger comparing to the deposition of silver nanoparticles using PSS-co-MA as stabilizer. This might be due to the effect of different electrostatic repulsion force which was confirmed by zeta potential values, where silver nanoparticles stabilized with PSS-co-MA revealed higher zeta-potential values. It means that PSS-co-MA was found to have stronger electrostatic repulsive force than alginic acid. Therefore, alginate-stabilized silver nanoparticles can be deposited more than PSS-co-MA-stabilized silver nanoparticles.

Only in case of 0.0005 %wt alginic acid, highest intensity absorption was seen. The morphology of silver nanoparticles this thin film was characterized by AFM (Figure 4.12) The AFM image revealed the dense packing of particles as showed in figure 4.12 (a). The average thickness of thin film was 36.103 nm which measured at 15 minutes dipping time as shown in figure 4.12 (b).

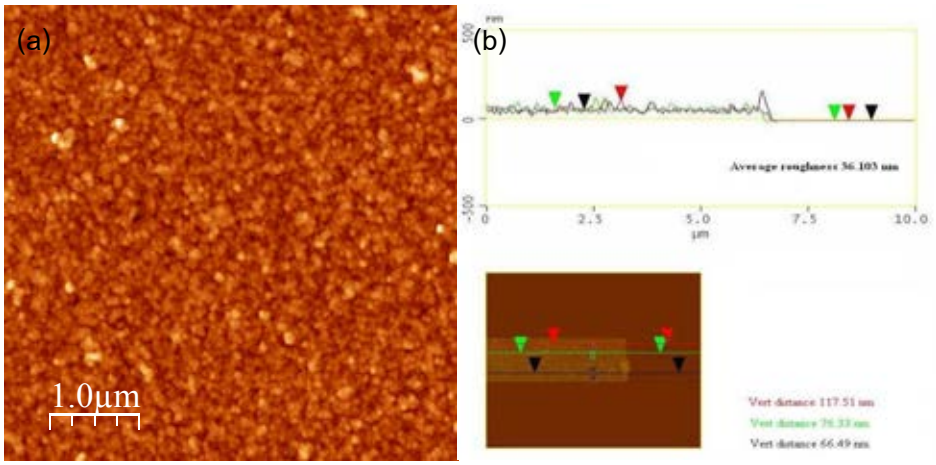

Figure 4.12 AFM image of 0.0005% wt alginic acid-stabilized-silver nanoparticle monolayer thin film (a) surface (b) thickness.

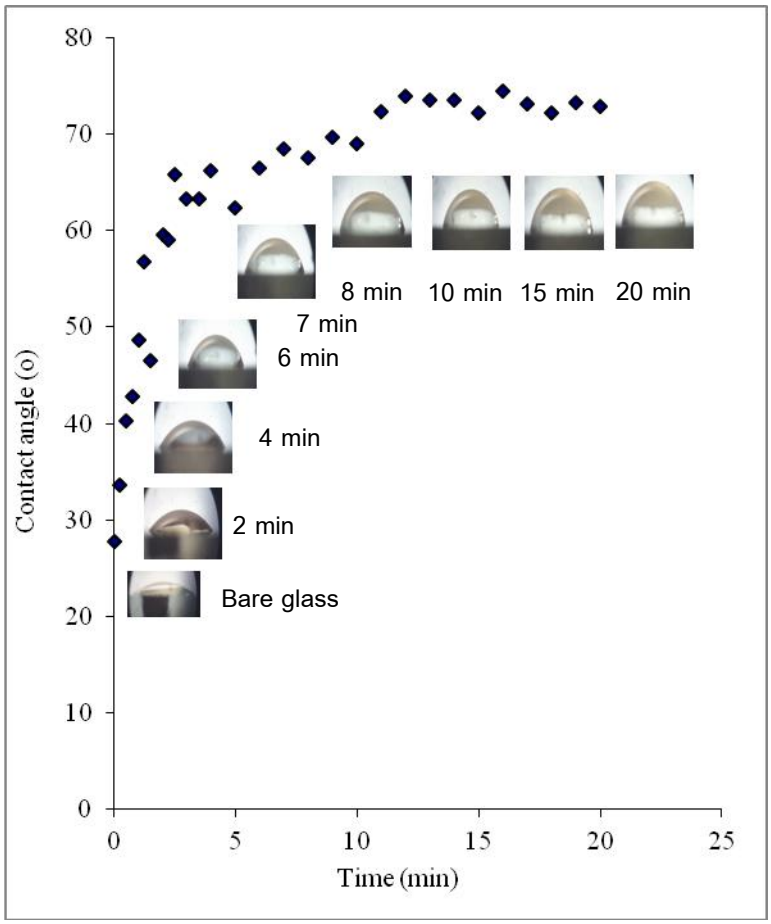

Figure 4.13 Plot of contact angle of monolayer of the 0.0005 % wt alginic acid stabilized silver nanoparticles absorbed on primer layer as a function of time (inset: images of water droplet).

The kinetic absorption was also investigated using contact angle measurement. The bare surface composed of a glass slide has an initial contact angle value of 27°. Upon adsorption of the nanoparticle, the surface provides more roughness and saturated at a value of 73° after 10 minute. The result found similar trend with kinetic adsorption study. The 0-3 minute range tended to increase the contact angle at faster rate, in other words, improved roughness was achieved during the initial time. This was as expected from negative charges on the surface of silver nanoparticles dramatically adsorbed on freely positive charges surface area. Then, it had no more positive charge on the surface that can absorb silver nanoparticles. After it was saturated by silver nanoparticles covered on the surface the contact angle value became constant. The data confirmed the adsorption of silver nanoparticles on the substrate.

4.2.2 Gold nanoparticles monolayer adsorption

Gold nanoparticles preparing in section 3.4.2 were used to study the monolayer adsorption as same as silver nanoparticles.

In figure 4.14, the kinetic monolayer adsorption of gold nanoparticles stabilized by 30 mM of sodium citrate as a function of time was monitored by plotting the changing absorbance at 750 nm. The red shift was similarly observed as in the study of kinetic adsorption of silver nanoparticles. The similar mechanism of adsorption was found but the adsorption peak located at 530 nm which was characteristic of gold nanoparticles. Moreover, the new peak adsorption was appeared at 750 nm. This is due to the aggregation of particles on the substrate [102].

The similar absorption spectra obtained from the 15 mM of sodium citrate stabilized gold nanoparticles. However, for the 60 mM of sodium citrate stabilized gold nanoparticles, the single peak of absorption spectra at 525 nm was revealed because particles repelled each other that can prevent aggregation of particles.

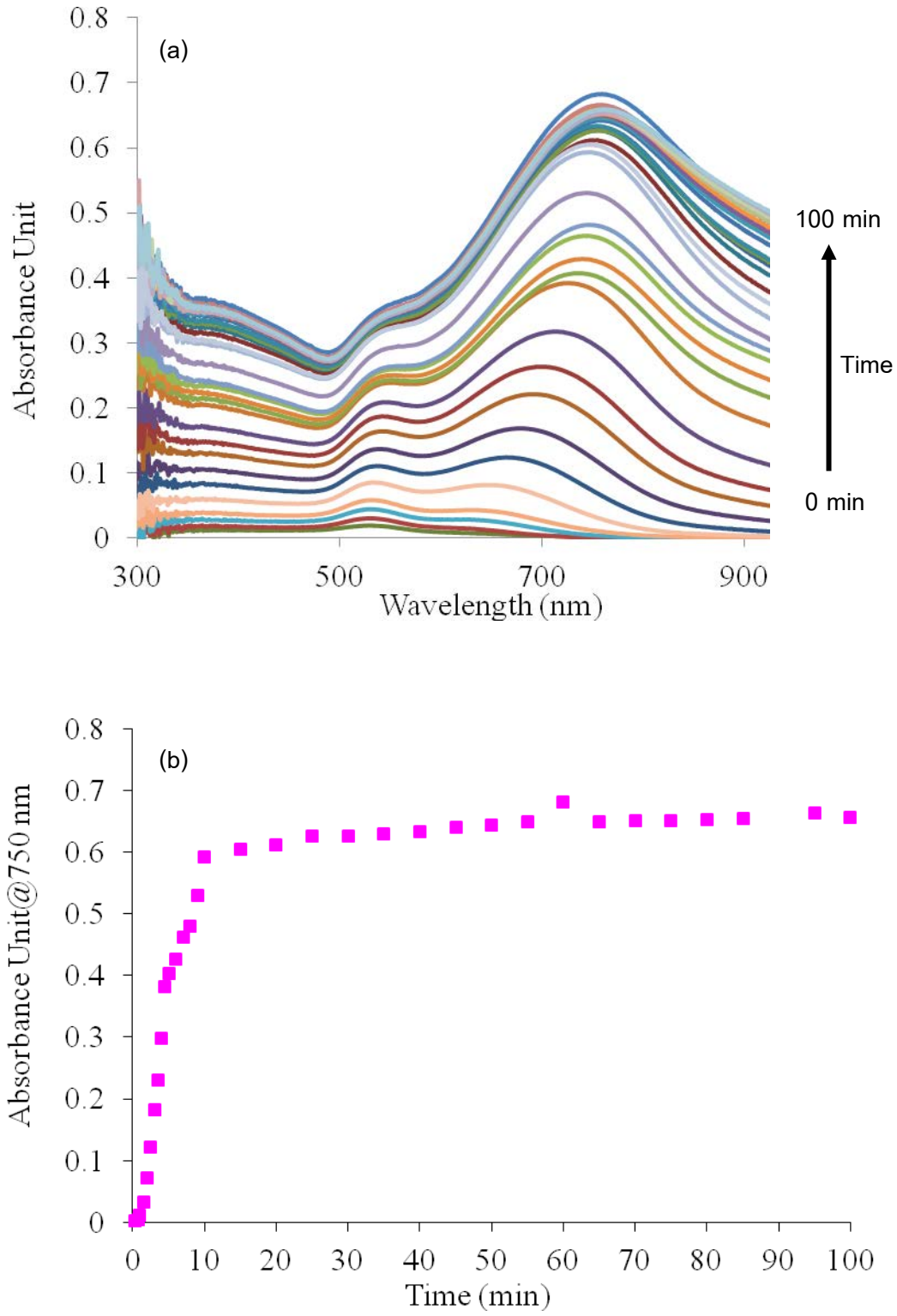

Figure 4.14 Absorption spectra of monolayer of gold nanoparticles stabilized by 30 mM of sodium citrate as a function of time (a), plot of changing absorbance at maximum wavelength as a function of time (b).

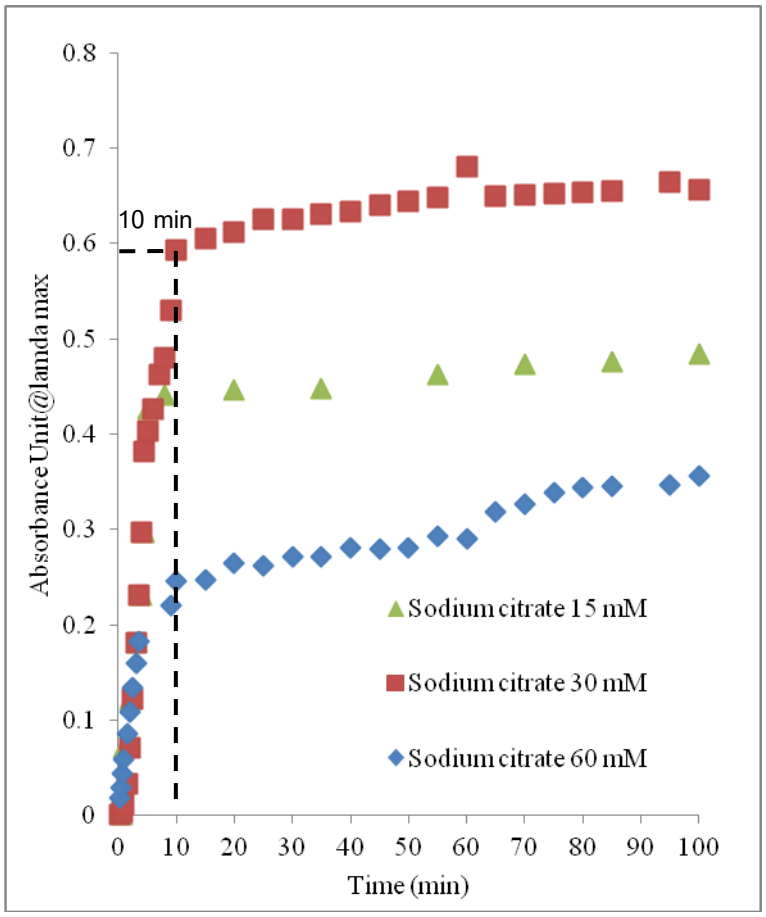

Figure 4.15 The changing absorption intensity at 525, 730 and 750 nm of 60, 30 and 15 mM of sodium citrate stabilized gold nanoparticles as a function of time.

The three curves of sodium citrate stabilized gold nanoparticles monolayer adsorption was presented in figure 4.15. The slopes revealed fast adsorption during the early period as same as the result reported in the section 4.2.1-2. To gain the maximum adsorption of gold nanoparticles on the surface, the dipping time of ten minutes is required and it will be used for further study.

The adsorption data showed that depending on the concentration of the sodium citrate concentration preparing gold nanoparticles solution. From figure 4.15 the less amount of gold nanoparticles prepared with 60 mM sodium citrate could be adsorbed on the substrate. This might be the result of the high repulsive force, which prevents them from coming into close contact as confirmed with zeta potential in table 4.2. Furthermore, the competition between the excess of free sodium citrate in gold nanoparticles solution and the gold nanoparticles to be adsorbed on the surface. At 15

and 30 mM sodium citrate concentration, presented lowed electrostatic charges which was proved by zeta potential results. So the 15 and 30 mM of sodium citrate concentration, of the particles could be adsorbed to the surface, resulting in the formation of thicker layer, as evinced by the increasing absorbance values. However, at 30 mM of sodium citrate showed higher adsorption intensity comparing to the 15 mM of sodium citrate stabilized gold nanoparticles which contradicted with the results in section of kinetic adsorption of silver nanoparticles. The reason was due to the gold nanoparticles preparation which found aggregation of 15 mM of sodium citrate stabilized gold nanoparticles. It consisted with zeta potential that showed the lowest zeta potential of 15 mM of sodium citrate stabilized gold nanoparticles. The low zeta potential can cause aggregation of particles.

Therefore, the suitable dipping time for silver and gold nanoaparticles are 10, minute of HA stabilized silver nanoparticles, 15 minute of PSS-co-MA and alginic acied stabilized silver nanoparticles, 10 minute of sodium citrate stabilized gold nanoparticles and will be used for fabrication metal nanoparticles multilayers thin film in further section.

4.3 Multilayers thin film preparation

4.3.1 Silver nanoparticles-PDAD thin film

The Layer-by-Layer self assembly technique was introduced to fabricate metal nanoparticles multilayers thin films in order to enhance the conductivity properties of thin film. The the effect of types and concentration of capping agent on conducting property of thin film was evaluated. The main driving force in construction of metal nanoparticles multilayer thin film is electrostatic interaction between anionic polyelectrolytes stabilizeded metal nanoparticles and cationic polelectrolyte. Franzen et al demonstrated the construction of conductive thin film containing gold nanoparticles using cross linker but this study focused on construction of metal nanoparticles multilayer thin flim via electrostatic interaction with Layer-by-Layer self assembly technique[18]. The resistivity of matal nanoparticles thin films were monitored by four point probe measurement.

4.3.1.1 The fabrication of multilayer thin film of silver nanoparticles capped with HA and PDADMAC

The growth of the PDADMAC-matal nanoparticles multilayer thin film was monitored using UV-visible spectrophotometer and the abosorption spectrum shown in figure 4.16.

The wavelengths of maximum absorbance were found at 430-465 nm for silver nanoparticles preparing with 0.01 and 0.005 %wt of HA which is due to the plasmon chracteristic of silver nanoparticles. This shift to longer wavelength is the result of the interaction between silver nanoparticles and PDADMAC. The larger absorbance spectra of 0.001 and 0.0005 %wt of HA preparing silver nanoparticles was monitored. The uniform absorbance from 400 to 700 nm have correspondingly high conductivity of the films[18]. The characteristic spectra of 0.01 and 0.005 %wt of HA clearly revealed a single peak of each layer because the high concentration o HA which can prevent the aggregation of particles by presenting high repulsive force between particles. In case of 0.001 and 0.0005 %wt of HA presented two peak of each spectrum which suggested aggregation of particles on the substrate.

The similar characteristic spectra f 0.01 %wt of HA stabilized silver nanoparticles was similar to 0.005 %wt of HA stabilized silver nanoparticles and 0.001 %wt of HA stabilized silver nanoparticles was found similar character of spectra from UV-Vis data. In case of 0.001 and 0.0005 %wt of HA stabilized silver nanoparticles were presented the character of particles aggregation [102-103].

From the result, the growth of thin films were the function of HA concentration used to prepare silver nanoparticles. For every adsorption layer, the adsorption of silver nanoparticles preparing with 0.0005 %wt of HA was higher than other three concentrations

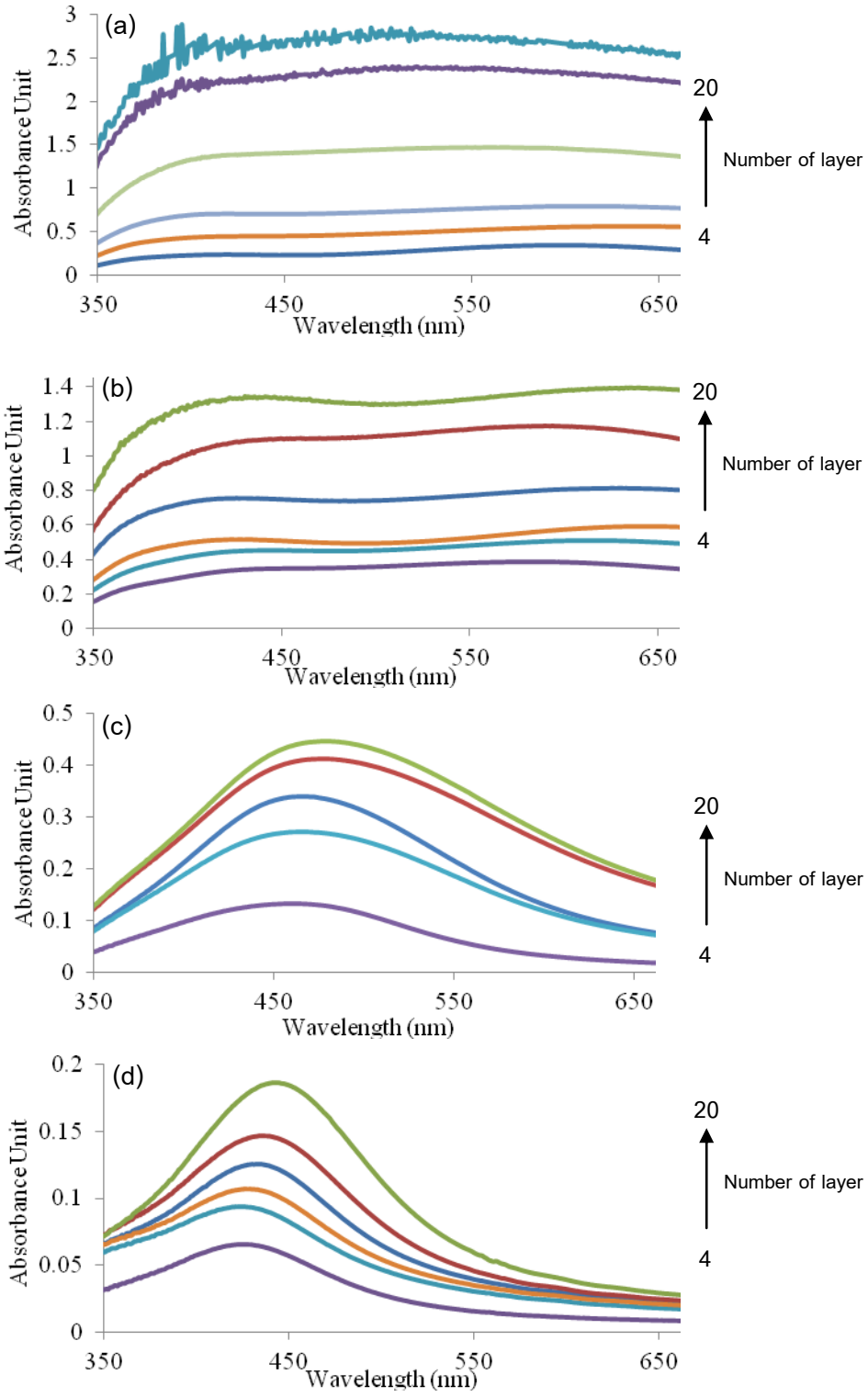

Figure 4.16 Absorbance spectra of silver nanoparticles multilayers thin film with different HA concentration prepared silver nanoparticles: 0.0005 (a), 0.001 (b), 0.005 (c) and 0.01 (d) %wt of HA.

Thus, 0.001 and 0.0005 %wt of HA stabilized silver nanoparticles were chosen to compare the growth of thin film thickness in order to find best conductivity of the film. The film thickness of PEMs was also monitored during the fabrication process (Figure 4.17).

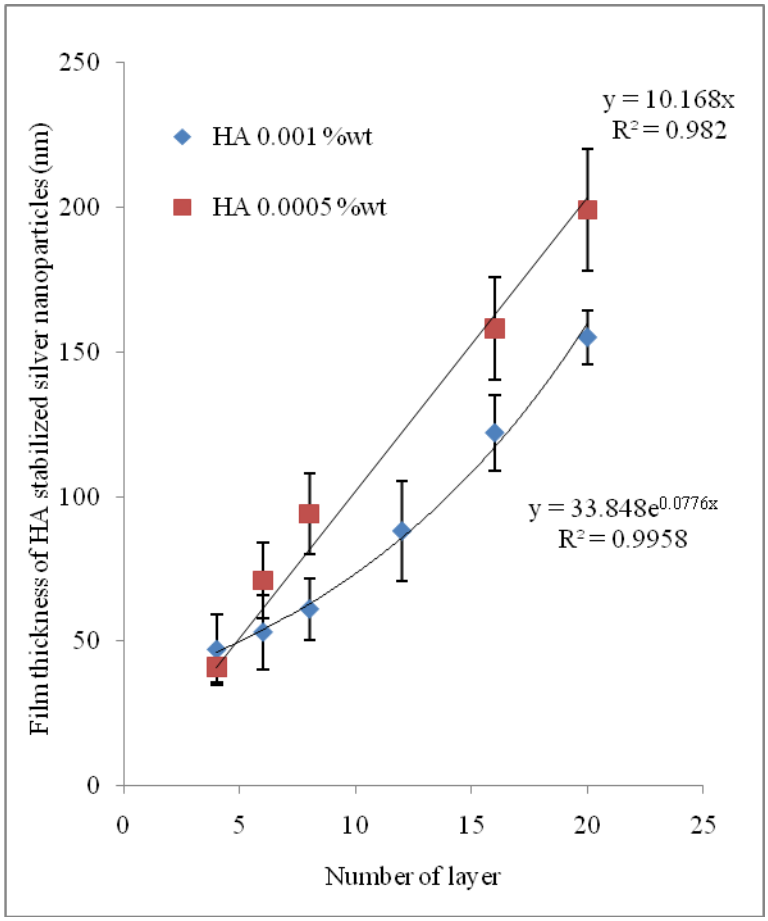

Figure 4.17 Plot of the thickness of silver nanoparticles using different HA concentration/PDADMAC multilayer thin films as a function of the number of deposited layers.

The measurement of the thickness of thin film by scratching the film and measuring its step height revealed that the average thin film thickness increased lineraly with the number of deposition cycles in line as shown in figure 4.17.

In case of 0.001 %wt of HA stabilized silver nanoparticles it can be seen that after depositing few layers (6 layers) the increment in thickness was constant for each deposition step because the amount of particles being deposited for each dipping cycle

was constant. The first few layers were thinner than the third layer containing lower amount of adsorbed particles due to the lower electrical charge of the surface leading to low adsorbed polyelectrolyte in the first couple layers. After the first few layers, it is independence from the surface leading to higher in adsorbed charge and increase the thickness of the film [104]. The stable growth of PDADMAC-silver nanoparticles multilayers was observed for 20 deposition layers. The number of layers was enough to predict that it will continue further in the same fashion. The greater slope of the film prepared from 0.0005 %wt HA stabilized silver nanoparticles compared to 0.001 %wt HA stabilized silver nanoparticles indicated better growth in each deposition layer.

The AFM images of silver nanoparticles capped with 0.0005% HA-PDADMAC thin film as a function of number of layers was shown in figure 4.18.

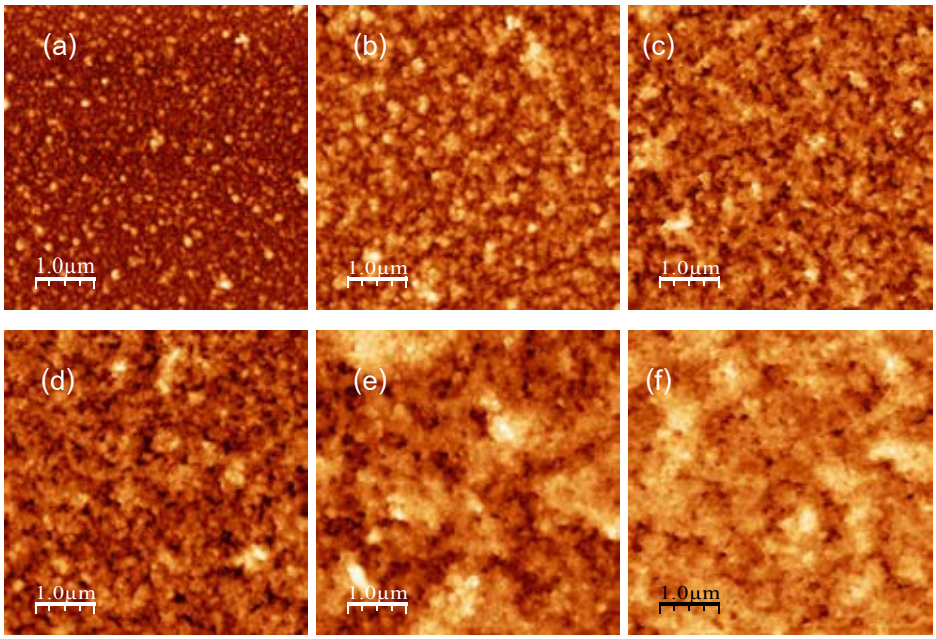

Figure 4.18 AFM images of silver nanoparticles multilayer thin film from HA 0.0005wt% and $AgNO_3$ 2 mM at (a) 4, (b) 6, (c) 8, (d) 12, (e) 16 and (f) 20 layers.

The amount of silver nanoparticles was increased by increasing number of layers. Moreover, the silver nanoparticles were densly packed when increasing number of layers. Compared AFM morphology of the film with varying number of layer revealed the less porous of higher number of layer. The AFM images of layers 12-20 showed increasing homogeneity as each successive layer.

The resistivity of 0.001 and 0.0005 %wt of HA stabilized silver nanoparticles multilayers thin films as a function of number of layers were measuredby four point probe measurement.

The resistivity value was given by:

$$\rho = 4.53\ t\ (V/I)$$

ρ is resistivity (Ω.cm), t is thickness of thin film (cm), V is the voltage drop across the inner two probes (V), I is the current flow between the outer two probes. The thickness of sample was estimated by AFM. The resistivities of thin films with various numbers of layers were measured and were plot as shown in figure 4.19. The resistivity was clearly decreased with increase in the numbers of coating layer especially for 0.0005 %wt of HA stabilized silver nanoparticles.

The enhancement in the conductivity of metal nanoparticles might be due to the low electrostatic repulsion and low charge density of stabilizer. The low concentration of HA could generate the densely packing because of the low repulsive force between each particles.

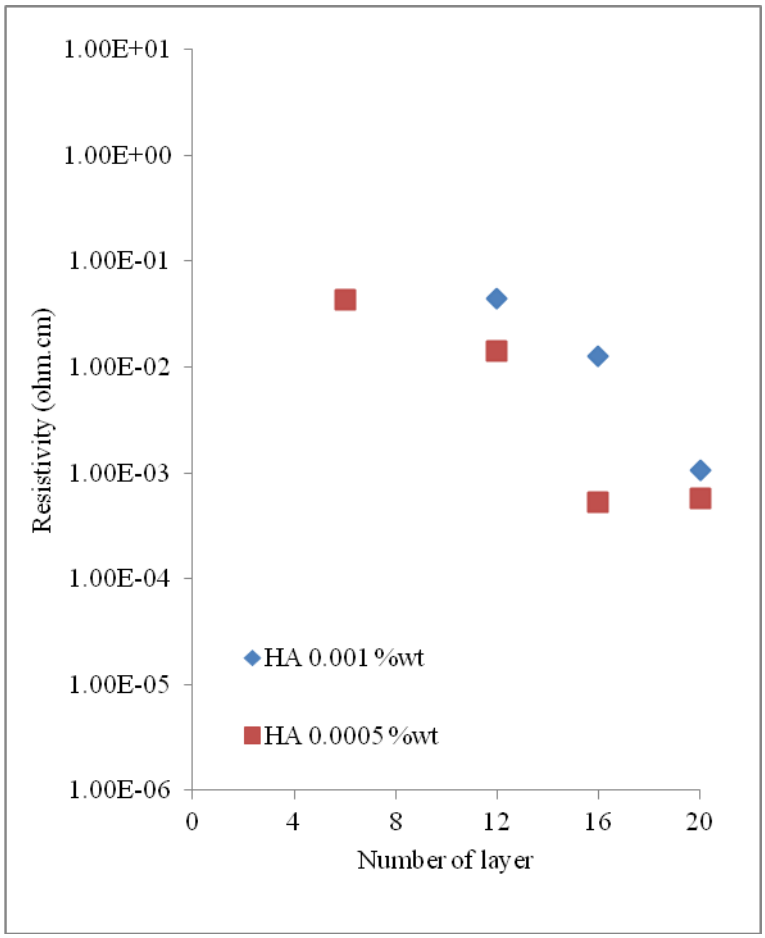

Figure4.19 Resistivity of the multilayer thin films prepared from the layer-by-layer deposition of PDADMAC/silver nanoparticles prepared with 0.001 (diamonds) and 0.0005 %wt of HA (squares).

Both 0.001 and 0.0005 %wt of HA stabilized silver nanoparticles multilayers thin films showed that the conductivity increased with increasing number of layer. For the same layer, the 0.0005 %wt of HA stabilized silver nanoparticles revealed higher conductivity than 0.001 %wt of HA stabilized silver nanoparticles because of the effect of closely packed particles. However, at first few layers of thin film from 0.001 %wt of HA stabilized silver nanoparticles were not conductive enough to be measured.

4.3.1.2 The fabrication of multilayer thin film of silver nanoparticles capped with PSS-co-MA and aliginic acid

To investigate the multilayers thin film fabrication, UV-Vis spectra of the PDADMAC-matal nanoparticles multilayers thin films on glass substrate were performed as shown in figure 4.20.

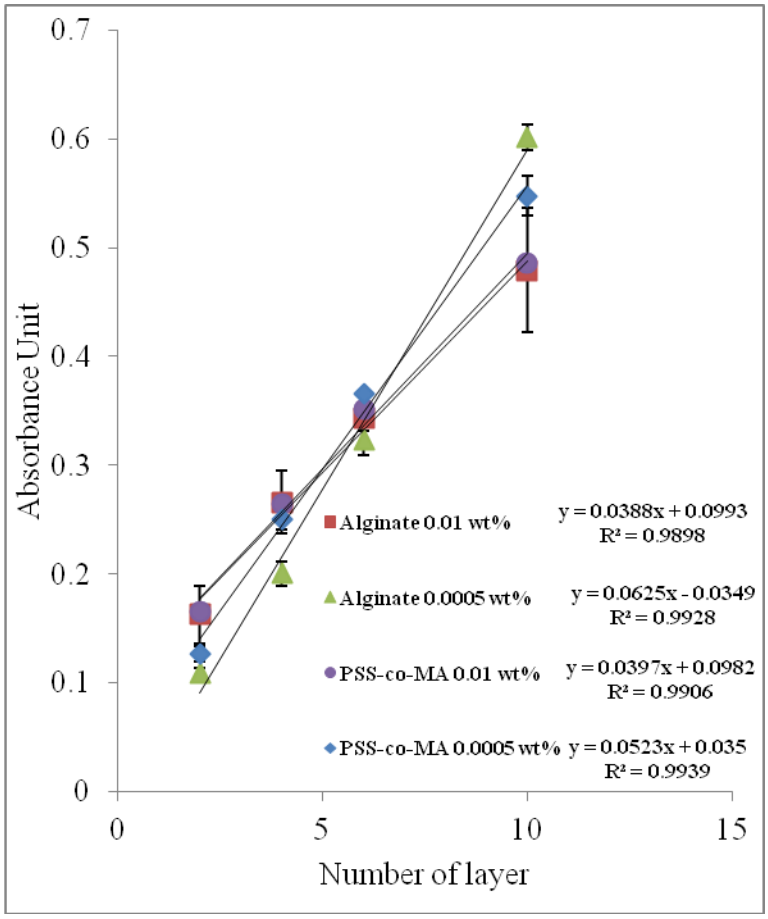

Figure 4.20 Relationship of absorbance at 430, 530, 515 and 530 nm for 0.01, 0.0005%wt PSS-co-MA and 0.01, 0.0005 %wt alginic acid stabilized silver nanoparticles, respectively, vs. number of layers of PDADMAC and silver nanoparticles.

Figure 4.20 showed the layer by layer growth of the silver nanoparticles thin films as a function of the concentrations and types of polyelectrolyte used to prepare the silver nanoparticles. The absorbance of four conditions was found to increase with increasing numbers of layers. The growth of multilayers thin film of PSS-co-MA was found to be slower than alginic acid on the same concentration. As mentioned

previously, PSS-co-MA is a copolymer of PSS and maleic acid. It contains both the strong sulfonate group in PSS and the weak carboxylic pendent group from maleic acid segments. This copolymer can generate high repulsive force between each particle that allows lower adsorption of silver nanoparticles into the thin film. Meanwhile, alginic acid provides only the weak carboxylic pendent group.

The 0.0005% wt of stabilizer concentration showed higher intensity adsorption than 0.01% wt of stabilizer concentration as shown in figure 4.20 for both PSS-co-MA and alginic acid stabilizer. From the slope, it can be seen that silver nanoparticles deposited from 0.0005 %wt concentration of stabilizing agent grow faster than 0.001 %wt concentration of stabilizing agent which were seen from slope of each plot. As described in the section 4.3.1.1, this phenomenon might be due to the lower repulsive force among silver nanoparticles capped with 0.0005% wt and less amount of free stabilizing agents in the solution. These resulted in the higher amount of silver nanoparticles deposition at the same number of layer. The nearly same intensity adsorptions for both types of stabilizers were found at 0.01% wt of stabilizer concentration.

From our observation, the preparation of the conductive multilayer thin film silver nanoparticles electrode is quite tedious work. Therefore, the decrease in the number of layer was considered to eliminate this problem and the conducting property was still considered as well.

The result of this process was confirmed by four-point probe measurement. The resistivity acquired from this instrument was shown in table 4.3. Unfortunately, the multilayer thin film electrodes composed of silver nanoparticles capped with the PSS-co-MA at any concentration have not revealed a conductive property due to the resistivity values over the detection limit of instrument (10^{-1}-10^{-5} ohms.cm.). The result from table 4.3 demonstrated that only the multilayer thin film electrode fabricated with nanopartilces capped with 0.0005% wt of alginic acid possessed the resistivity of 4.39×10^{-2} ohms.cm. This might be due to the densely packed nanoparticles thin film. However, the resistivity value obtaining from the lowest concentration of alginate demonstrated high resistivity when compared with bulk of silver (1.59×10^{-6}ohms.cm.)

because of the stabilizer that affects the interference of the delocalized electron in some direction.

Table4.3 Resistivity value of silver nanoparticles monolayer thin film with different types and concentrations of stabilizer.

Type of stabilizer	Resistivity (ohms.cm.)
Alginic acid 0.0005 % wt	4.39×10^{-2}
Alginic acid 0.01 % wt	$>10^{-1}$
PSS-co-MA 0.0005 % wt	$>10^{-1}$
PSS-co-MA 0.01 % wt	$>10^{-1}$

4.3.2 Gold nanoparticles multilayers thin films

Polyelectrolyte multilayers thin film containing gold nanoparticles can be easily prepared using the layer-by-layer self assembly technique as same as silver nanoparticles. The layer-by-layer self-assembly technique was presented as one of the best technique to prepare nanoparticles array.

The spectra of gold nanoparticles multilayers thin film with different sodium citrate concentration (used in the synthesis of the gold nanoparticles) was presented in figure 4.21. The spectra of gold nanoparticles multilayers thin film were different from gold nanoparticles solution which gold nanoparticles multilayers thin film presented the broad adsorption bands. A feature of these spectra was caused by plasmon adsorption of ensemble of individual gold nanoparticles. The broad peak characteristic was observed for all three gold nanoparticles, indicating that the films were composed mostly of close packing gold nanoparticles that have been reported in literatures [18, 105]. However, the plasmon band of film from gold nanoparticles using 60 mM sodium citrate was less presented a broad band that was composed of isolated gold nanoparticles. The broad band spectrum refers to the long range of light adsorption.

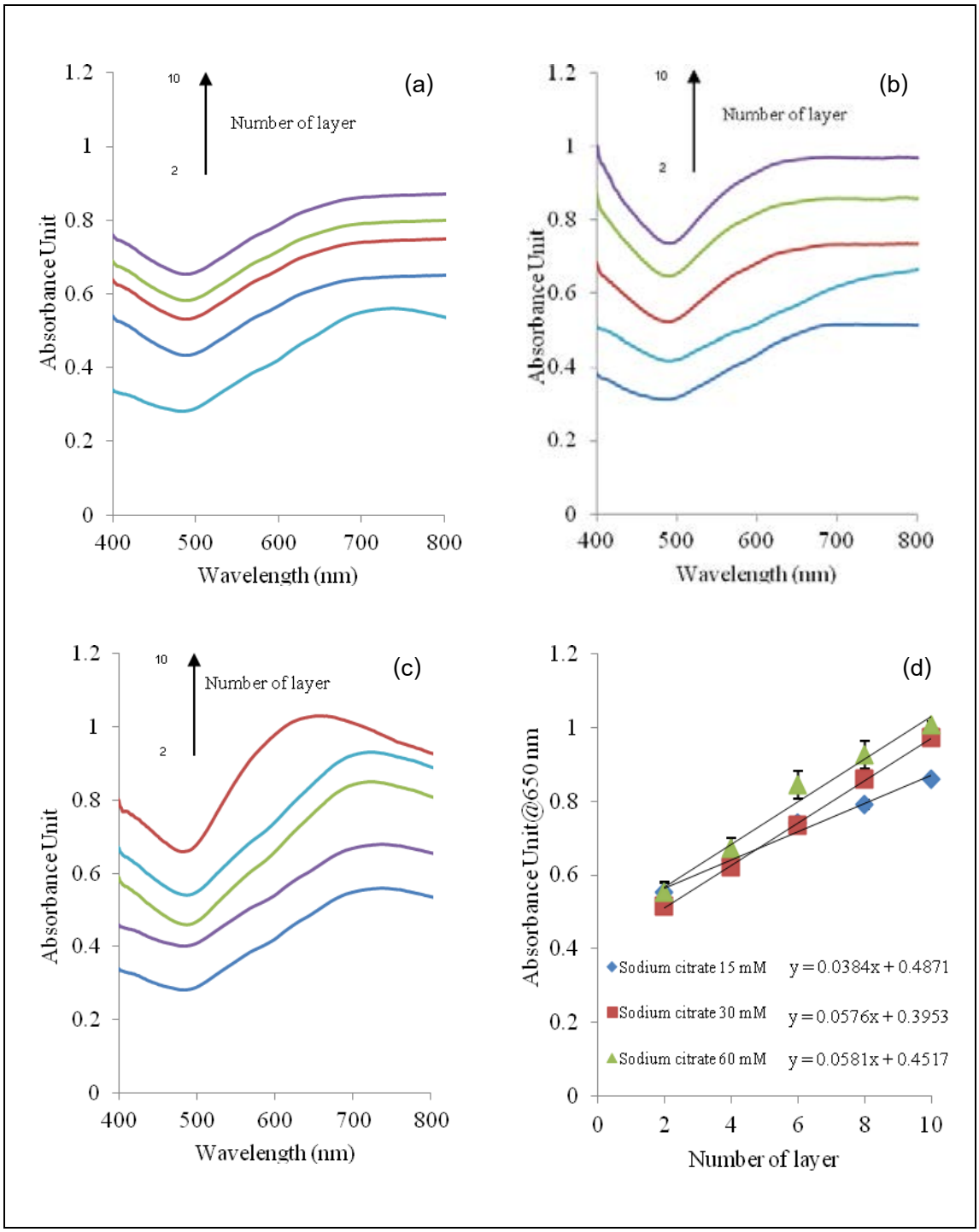

Figure 4.21 The absorption spectra of PDADMAC and gold nanoparticles multilayer thin films using different sodium citrate concentrations: 15 (a), 30 (b), 60 mM (c),and change inabsorbance of PDADMAC and gold nanoparticles multilayer thin films as a function of number of coating layers at different sodium citrate concentrations (d).

For all sodium citrate concentrations, absorbance was found to increase linearly with the number of layers, indicating that in each deposition cycle the same amount of gold nanoparticles was deposited (Figure4.21 (d)). The difference in the slope indicated the different growth deposition rate of thin film where the steeper slope indicating thehigher growth deposition rate of thin film.

The layer-by-layer growth of the gold film was probed using atomic force microscopy and the relationship between dipping cycles and thickness was shown in figure 4.22.The different concentration of sodium citrate affected the particle sizes of gold nanoparticles [103]. The low concentration of sodium citrate presented a large size of gold nanoparticles. The sizes of particles have the impact on the thickness of thin film, because the thickness of each cycle is the size of particles. Moreover, the high sodium citrates concentration prepared gold nanopaticles should obtain less deposition of particle because it is protected by electric charges preventing aggregation. This was related to zeta potential which presented more negatively charged gold nanoparticles at high sodium citrates concentration.

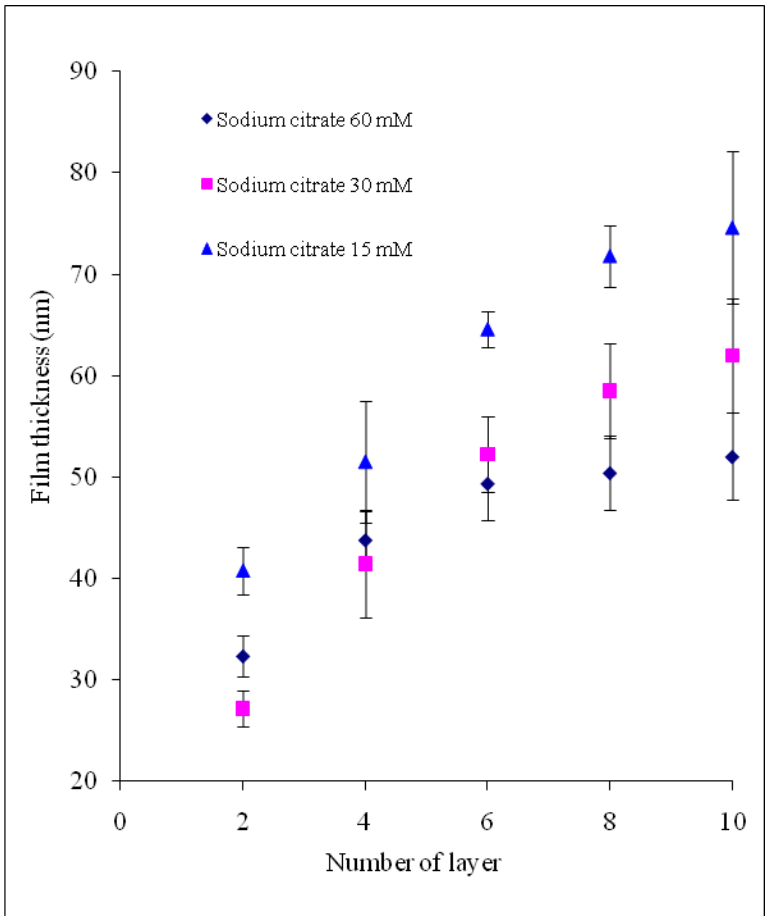

Figure 4.22 Plot of the thickness of gold nanoparticles using different sodium citrate concentration/PDADMAC multilayer thin films as a function of the number of deposited layers.

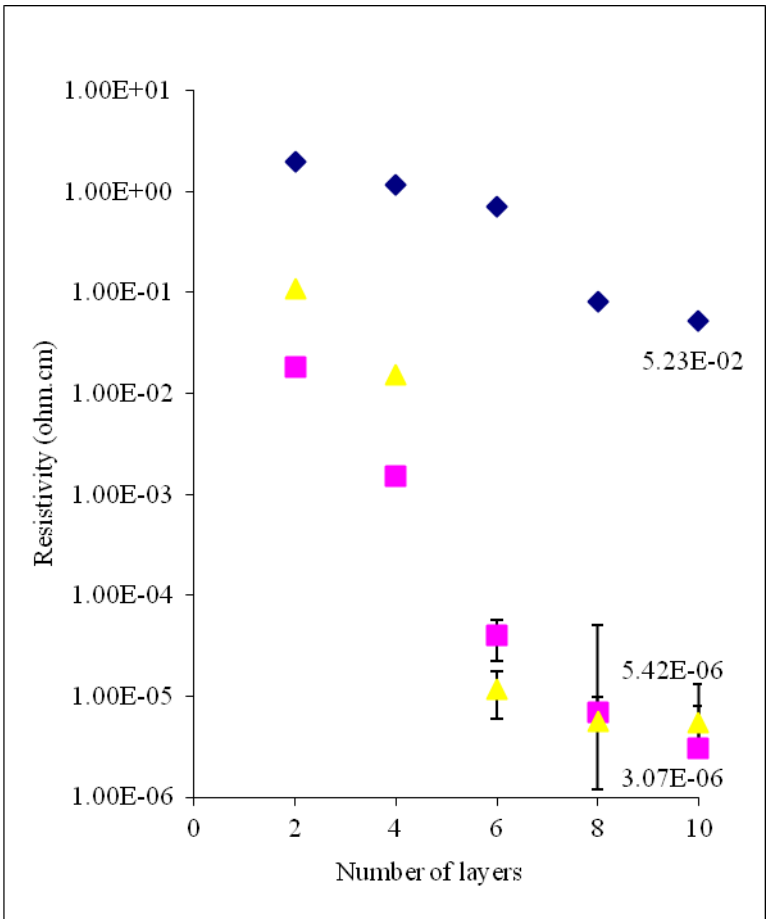

Figure 4.23 Resistivities of the multilayer thin films prepared from the layer-by-layer deposition of gold nanoparticles prepared with 60 mM (diamonds, ◆), 30 mM (squares, ■) and 15 mM (triangles, ▲).

The resistivity of the film was measured as a function of the number of deposited layers for each citrate capping and was shown in figure 4.23. High resistivity of the film when prepared with high citrate (60mM) content is probably due to an insulating effect of the citrate at the surface of the nanoparticles which tends to repel other charged nanoparticles. Almost bulk gold resistivity ($2.44*10^{-6}$ ohm.cm) [106] was achieved after the deposition of 6 layers of gold nanoparticles when using 30 and 15 mM citrate. A lower capping concentration of sodium citrate provided a high conductivity asthe gold. Although conductivity of film prepared from nanoparticles capped with either 15 or 30 mM were sufficiently enough to be used as electrode, the 15mM citrate leads to films which could be easily scratched after testing with ASTM D3359 technique. The poor

adhesion of 15 mM sodium citrate might be the effect of a low binding of gold nanoparticles with PDADMAC in the layer-by-layer process. For this reason the 30mM sodium citrate was used in all further experiments for the development of the electrode.

4.4 Gold nanoparticles microelectrodes fabrication and testing

4.4.1 Morphology and thickness characteristics by FE-SEM images

The objective of this research was to develop micro-electrode, the resistivity of the prepared films was evaluated using a 4 points probe setup as same as silver nanoparticles prepared films. The resistivity as a function of the number of deposited layers for each sodium citrate capping is shown in previous part.

For the design of patterned microelectrode using metallic nanoparticles, the adsorption of closely packed nanoparticles was desired. To this end, our strategy has been to prepare gold nanoparticles capped with a decreasing concentration of stabilizing agent. While particles become larger and less stable, conductivity of the nanoparticle thin film was found to increase with decreasing capping concentration.

This research presents a method for the fabrication of micro-electrode using predesigned microfluidics template. The channels of the microfluidic template represent the branches of the future electrode and can be developed into intricate network in order to improve the detection and function of the electrode. The flow of gold nanoparticles into the microfluidic channels leads to the adsorption of the nanoparticles onto the lower substrate which is in the end the electrode itself. The substrate need to be coated with cationic polyelectrolyte for the gold nanoparticles to adsorb via electrostatic interaction. The method of microelectrode fabrication was called flow deposition technique as shown in figure 4.24.

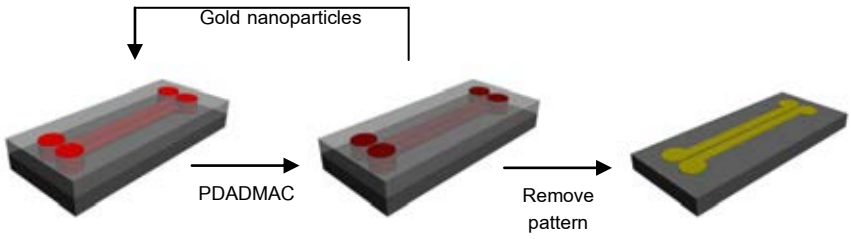

Figure 4.24 Diagram depicting the micro-channel fabrication

The fabrication of gold film on glass slide was adapted to microelectrode by flowing successively either gold nanoparticles or PDADMAC solutions in the microchannel. At each flowing cycles the coating on the lower glass substrate increase in thickness and after 10 cycles, a micro-electrode was obtained. Field emission scanning electron microscopy was used confirm the nanoparticle assembly in the microchanel as well as its thickness.

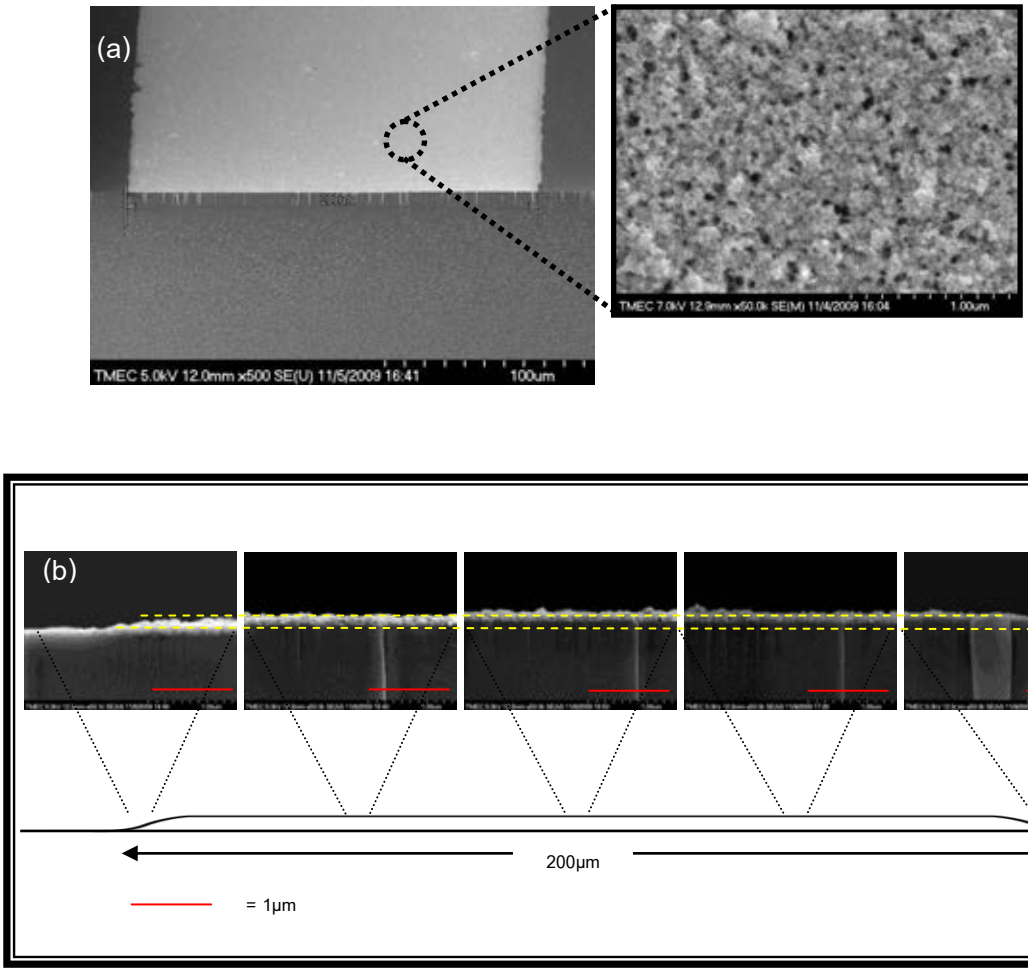

Figure 4.25 FE-SEM surface (a) and thickness (b) images profile of sodium citrate-stabilized-gold nanoparticle microelectrode.

A PDMS master was fabricated with contained channels that were 200 µm wide and 200 µm in deep. The resulted microelectrode was smaller (~200 µm wide and ~120 nm in height) than the original microchannel dimensions as shown in figure 4.25. The height of microelectrode was controlled by number of layers which agreed with thickness from AFM. The cross section of microelectrode was found to be flat profile of electrode as shown in figure 4.25 (b). However, the edge of electrode was smaller because of friction between the channel wall and solution. FE-SEM image showed that the resulting gold nanoparticles microelectrode adhered to the glass substrate because of the electrostatic force between anion of sodium citrate around gold nanoparticles and cationic polyelectrolyte of primer base layer. It was found that if primer base layer step was excluded, the next step of filling the channels with gold nanoparticles were not

successful. Figure 4.25 (a) showed the well packed nanoparticles at the surface of the film which cross section is shown in figure 4.25 (b). The film thickness appeared constant along the cross section with a thickness of 120 nm for the 10 bi-layers gold nanoparticles film. The multilayer films growth in the micro-channel is comparable to the growth at the surface of larger glass slide sample as they present similar final thicknesses. Yet it is necessary to stress the importance of the rinse step in the microchannel, which, if not done properly, leads to the formation of polyelectrolyte complex and block the channel.

4.4.2 Conductivity measurement of micro-electrodes as detection for lab on a chip device

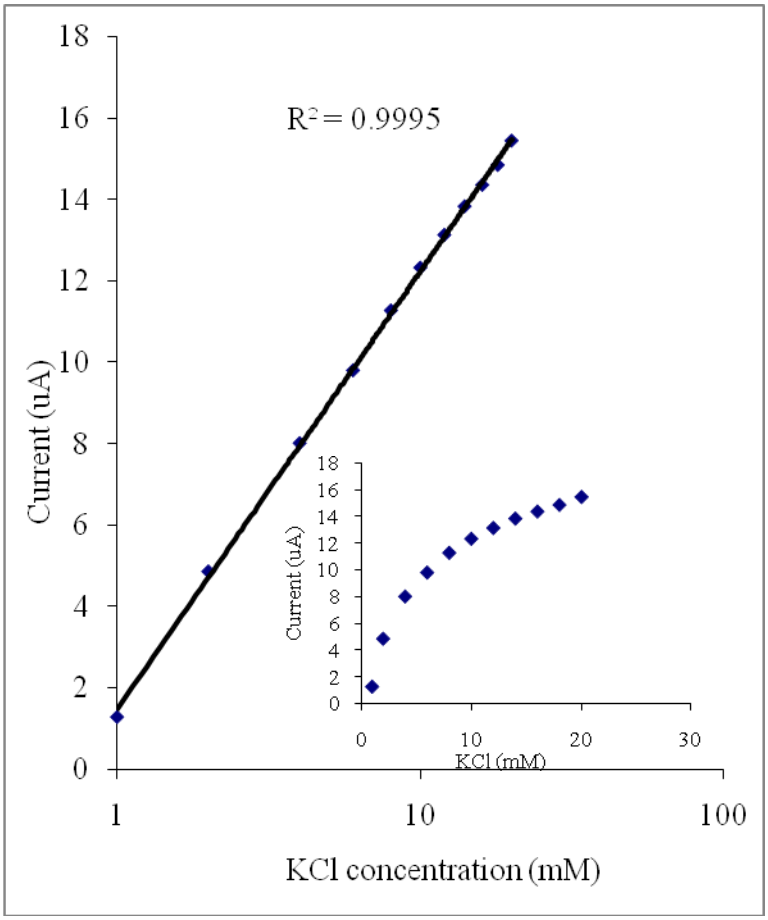

Figure 4.26 Plot of the measured current across the microelectrode when exposed to various KCl concentrations (1-20 mM).

As the micro-electrode was used as detection tool in microfluidic devices, its performance was characterized by current detection using solutions of KCl having concentrations ranging from 1 to 20 mM. The current detection method is commonly used in microfluidic to quantify compound as they travel along the micro-channels. In this method, an alternating current of 1 KHz produced by a function generator is allowed to pass between two electrodes which are position across the microfluidic channel. As an ionic or cationic compound passes in between the two electrodes, the local conductivity in the channel changes as a function of its concentration. In this experiment, various concentration of KCl where detected by measuring the changes in conductivity between the two electrodes. The change in current was found to be proportional to the log scale concentration of KCl (figure 4.26) and based on our instrument setup the limit of detection was 1mM of KCl.

4.4.3 The operation microfluidic under high voltage

The complete chip was made by reversible sealing. the flow channel over the gold nanoparticles microelectrodes.

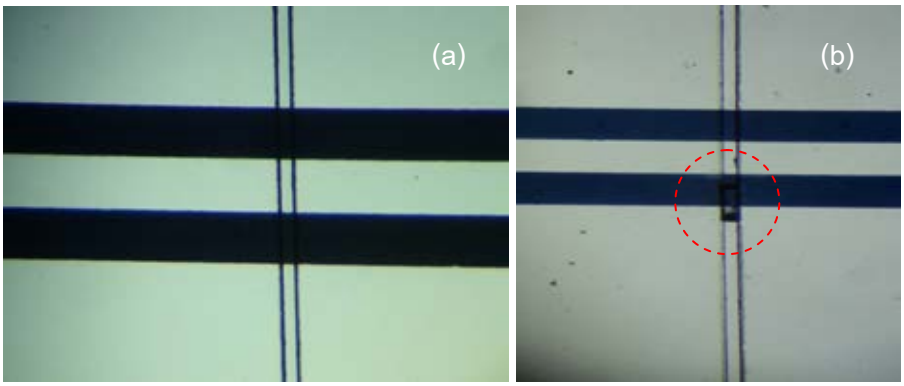

Figure 4.27 The two electrode conductivity with full fill of buffer in micro channel (a) and after run under HV condition (b).

The applied voltages of 150 V cm^{-1} produced 3 V drop across a 200 μm wide electrodes. The voltage drop caused opposite edges of electrode to act as cathodes and anodes. A voltage bias can be occurred in the solution between the two electrodes. As the potential inside the electrode occurs, this means that the potential difference between solution and electrode can become sufficient on parts of electrode. The

reaction was then found on the surface of electrode which the bubbles were caused in the flow channel [107]. The reduction or oxidation of water occurs as equation [108]:

Reduction at cathode: $2\,H^{+}(aq) + 2e^{-} \longrightarrow H_2(g)$

Anode (oxidation): $2\,H_2O(l) \longrightarrow O_2(g) + 4\,H^{+}(aq) + 4e^{-}$

The hydrogen and oxygen gas were produced in reaction which can cause the bubble [109]. So, the electric field induces the voltage drop between electrodes which lead to bubbles formation as showed in figure 4.27(b). If the gradient across the surface of electrode is 1.23V, reduction and oxidation can happen at opposite ends of electrode [110]. In previous work, decouplers have been used to allow placing the ground electrode and thus electrically separate the systems. So, the decoupler is suggested for use in the future work to minimize bubbles formation. A decoupler will be placed prior to working electrode which decoupler is used to separate the electrochemical detection. Metals of the platinum group, and especially palladium, are known for their ability to absorb and pass hydrogen and can therefore be suitable as decoupler electrode material [109].

The problems with electric field system, the gold nanoparticles conductive thin films were applied to detect a specific sample as batch detection in order to eliminate the electrical problem.

4.5 Testing performance by developing method

4.5.1 Contact conductivity measurement

Although, both silver and gold nanoparticles have been prepared in the first part, but only the gold nanoparticles were prepared as electrodes. This was due to gold nanoparticles multilayers thin film was more stable than silver nanoparticles multilayers thin film after preliminary study by KCl solution detection (data were not shown here).

The method for fabrication of the gold nanoparticles electrodes is described in chapter III. The conductivity measurement of the two electrodes was shown in figure 4.28. Normally, the sine voltages generating from function generator will be used to electrode stimulation. For electrodes in contact with the solution, the operating frequency is normally about 1 kHz. The typical frequency behavior of conductivity measurement is shown in figure 4.29 [110]. In this test, sine voltage and 1 kHz was applied to this experiment.

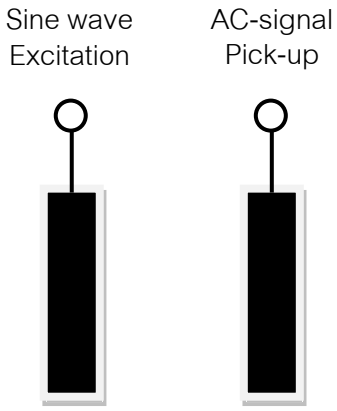

Figure 4.28 Dual electrode detection of conductivity by applying an AC-voltage and measuring the result current.

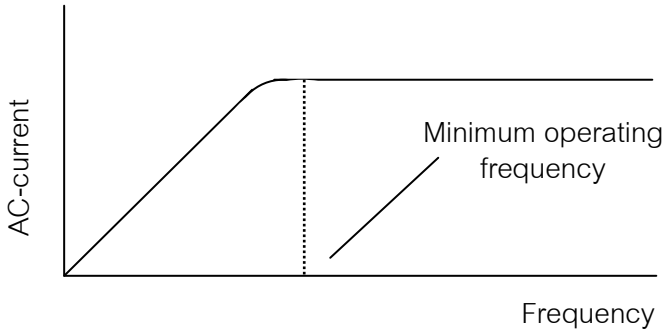

Figure 4.29 Frequency dependence of the current flowing though a conductivity measurement.

The conductivity detection can be used for the analysis of variety of species. In this study, the high dissociate solution of KCl was chosen for testing the conductivity of electrode. The performance of electrodes was studied by testing the influence of the size with varying the size of electrodes. The analytical conductivity (G) is described by [111]:

$$G = \frac{(\lambda_+ + \lambda_-)C}{1000K}$$

Here λ_+ and λ_- (mS m^2 mol^{-1}) are molar conductivity of cations and anions in solution, respectively. C is the concentration (M), and K is the cell constant (K=L/A, where L is the distance between the electrode pair and A is the area of electrodes).

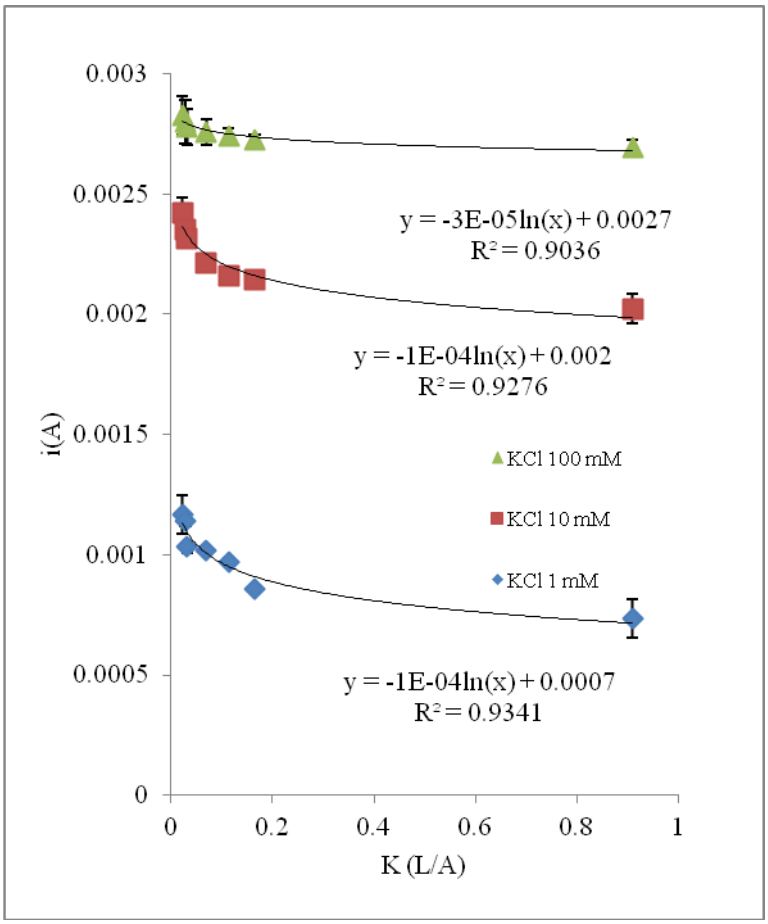

Figure 4.30 The plot of current detection of different KCl concentration with varying cell constant.

The influence of the electrodes size was tested by studying the relationship between the cell constant and current detection of three KCl concentrations. It clearly showed that increasing the area of the electrodes or reducing the spacing between the electrodes can improve the detection limits of the conductivity measurement. In other words, the conductivity of analyte can be improved by decreasing cell constant. The usage of gold nanoparticles electrodes can detect the KCl solutions as showed in figure 4.30. The results were confirmed by the theory of conductivity detection for all of KCl concentration.

For the future work, the 0.91 cell constant (K) value was used as controlling size of electrodes.

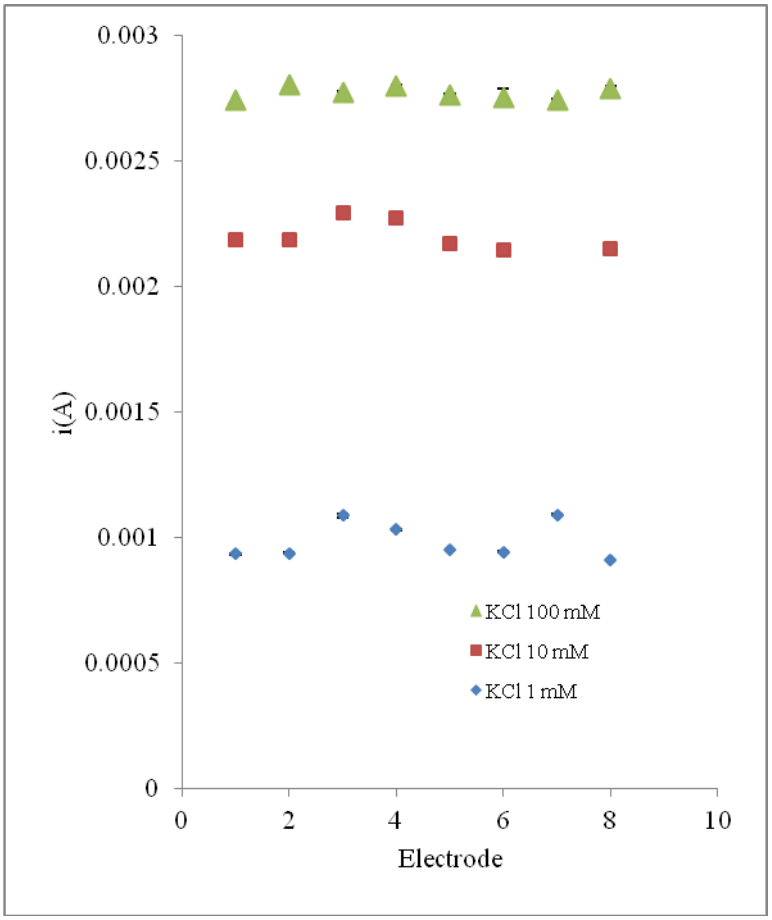

Figure 4.31 The plot of current detection of different KCl concentration with electrode.

The reproducibility of electrode fabrication was evaluated by testing ten electrodes, and the reproducibility was tested because of the handmade electrode fabrication process. The detection of eight electrodes was shown in figure 4.31. The detection of KCl solutions was measured three identical times of each electrode. In order to control the test, the electrodes that presented the maximum and minimum detection value were eliminated. The reproducibility values of electrode fabrication were presented in terms of the percent residual standard deviation (%RSD). The reproducibility of gold nanoparticles electrodes were found 0.29, 0.13 and 0.28 % for

detection of 1, 10 and 100 mM KCl concentration, respectively. The reproducibility of electrode with all three concentrations of KCl was in acceptable value

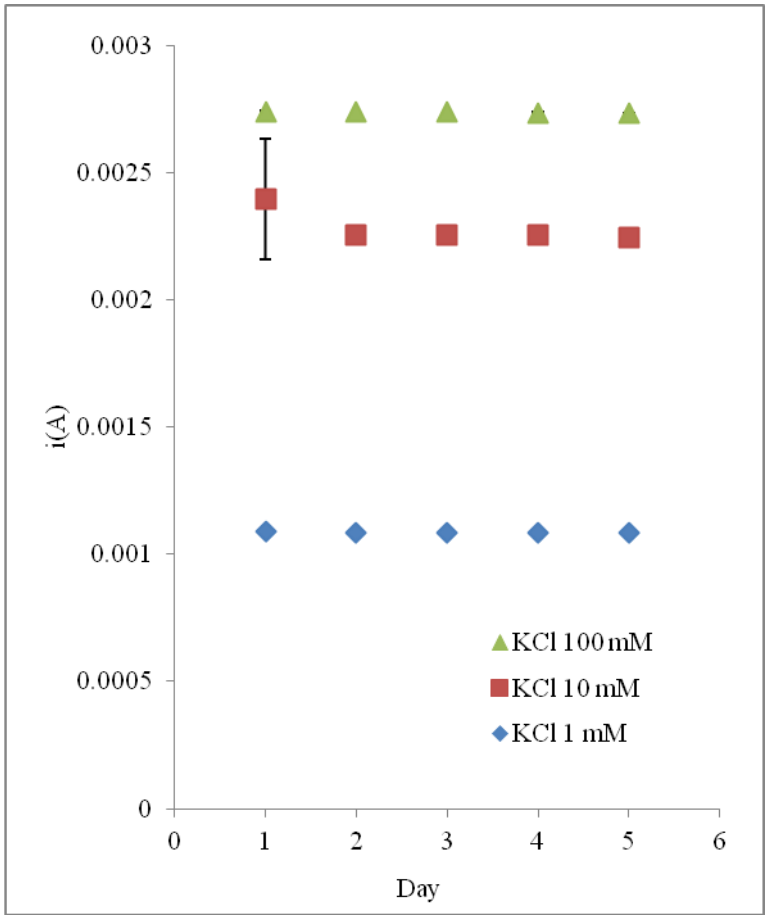

Figure 4.32 The plot of current detection of an electrode as a function of day of oneon different KCl concentrations.

Moreover, the reproducibility of run to run of an electrode was evaluated by detection of KCl solutions (in each day) for 5 days. The detection was measured three times. The detection of KCl with gold nanoparticles electrode was found constant for 5 days as shown in figure 4.32. The % RSD of 1, 10 and 100 mM KCl concentrations were 0.21, 2.18 and 0.08 %, respectively. The results mean that these fabricated gold nanoparticles electrode has a good long term stability under ambient conditions.

4.5.2 Physical contact testing

For gold conductive thin film, the increasing conductivity of the film might be the result of the increase in the number of contacting particles and the contacting area

(closely packed). The increasing contact between particles was done by increasing amount nanoparticles. At low concentration of stabilizing agent can lead to conductive thin film by decreasing repulsion between particles. The low repulsion between particles resulted from low electrostatic charges of low stabilizing concentration. However, the low stabilizing concentration was not only possessed the high conductive thin film but it was also decreased the hardness of thin film. The low hardness of thin film led to an easily scratch of thin film. It was clearly shown when integrated microelectrode as a microdevice. The steps of combine and separate between substrate contained microelectrode and cover plate were found that the microelectrode on substrate plate was peeled off with cover plate. Here, the PEMs coating electrodes was presented as protecting layer on electrodes in order to protect electrode from scratching of electrode.

In order to protect the gold nanoparticles electrodes, the strong polyelectrolytes, PDADMAC and PSS, multilayers thin film was used as a barrier. The PEMs coating on gold nanoparticles electrodes to prevent scratching of electrodes, should not affect the detection of electrodes. To study effect of detection, electrodes were used to measure KCl solution every layer of PEMs coating electrodes.

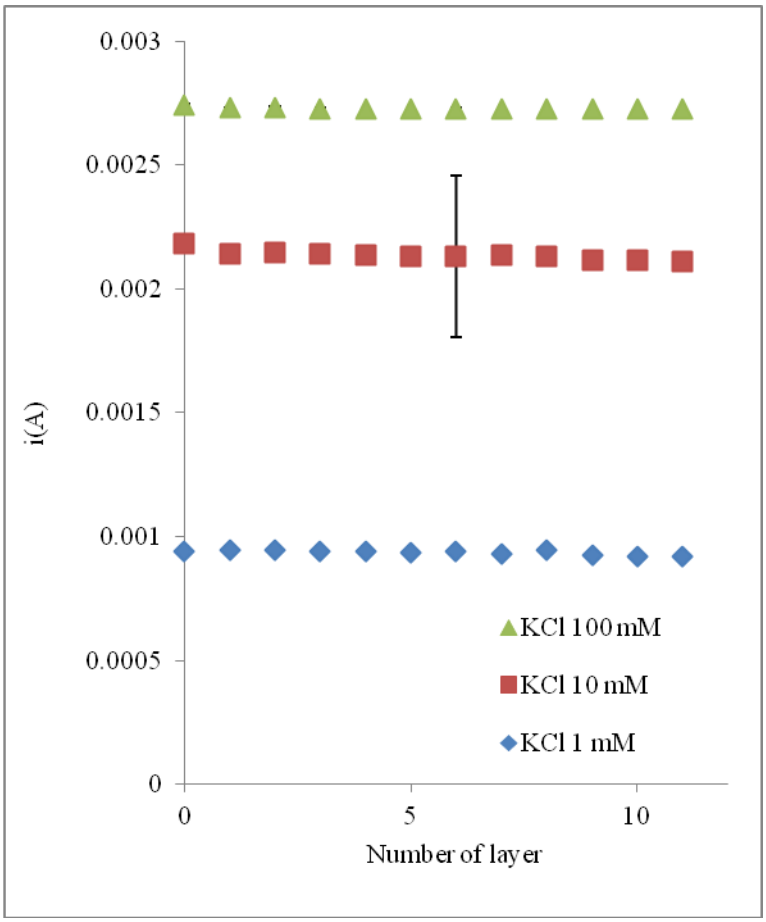

Figure 4.33 The current detection of 1 mM KCl with varying number of PEMs coated electrodes.

Figure 4.33 showed the constant of current detection of KCl solution after coating 11 layers of PEMs on surface of electrode. The result can be implied that the PEMs coated electrodes do not block the ions. The PEMs are porous materials, the ions of KCl can pass through the films [81, 112]. So, it does not affect the detection of electrodes. Moreover, in the previous work it had been found that PEMs can be swelled by water. The swelling thin film allow the permeability of ions [113].

An AC signal is applied to one of the electrode. Current will be generated through the solution, and measured at another electrode. This current is used to relate the impedance (Z) using Ohm's law. Ohm's law in AC, the equation can use as $I=V_{source}/Z$.

In this study, a two electrode contact conducticity can be represented by a simple equivalent circuit, as shown in figure 4.34.

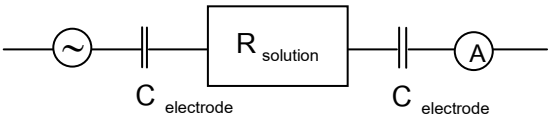

Figure 4.34 equivalent circuit models for contact conductivity detetction.

The impedance measured during conductivity detection in a two electrodes system depends on the resistance of the solution and the two double layer capacitors.

$$Z = \sqrt{R^2 + X_D{}^2}$$

The impedance of capacitor depends on the applied frequency. For contact conductivity electrodes, the capacitive reactance (X_D) is presented by a capacitor.

$$X_D = \frac{1}{2\Pi \cdot f \cdot C_D}$$

Where, f is the AC frequency applied over the electrodes

C_D is double layer capacitance ($C_D \cong 20\ \mu F/cm^2 \cdot A$ where A is the electrode area in cm^2).

In order to study frequency effecting on electrode, the detection of KCl with varying frequencies were tested for 1, 5, 7 and 11 layer of PEMs coating electrodes.

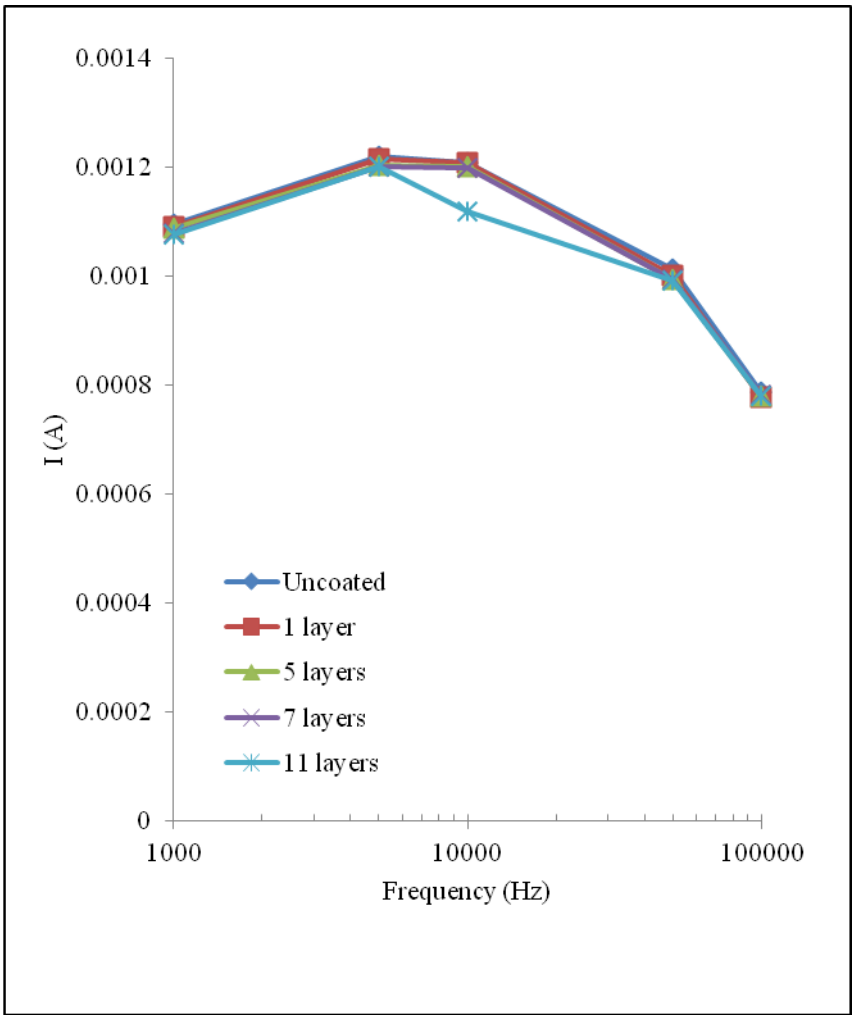

Figure 4.35 The plot of current detection of 1 mM KCl with varying frequency and number of PEMs coated electrodes.

From figure 4.35 showed the relation between frequency applying over the electrodes and current detections. The result presented that the current detection increases with frequency from 1 to 5 kHz which is in agreement with the Ohm's law as $I=V_{source}/Z$ (I is current (A), V_{source} is generated voltage from function generator, Z is impedance). As frequency higher than 5 kHz, the current detection decreased because the ions of analyte do not have sufficient time to move to detection zone of electrodes. In addition, the effect of current detection was shown the same for all layers of PEMs coating electrodes. This means that the PEMs coating electrodes do not affect the detection.

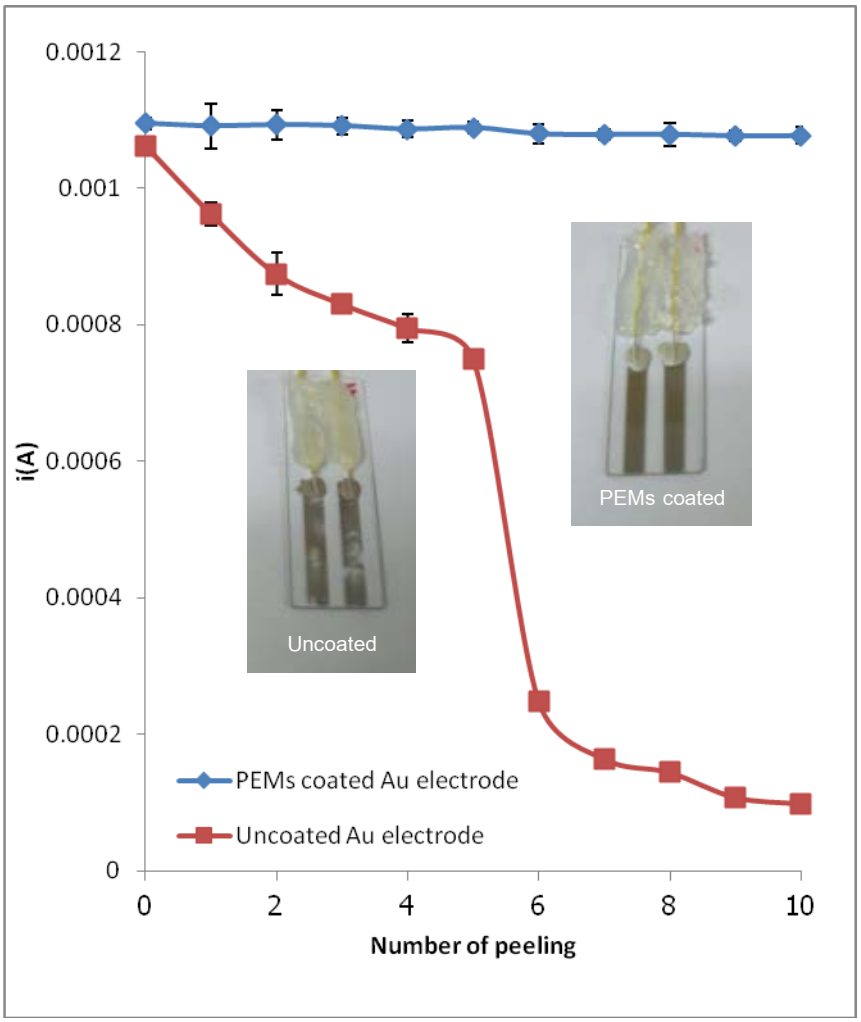

Figure 4.36 the comparison of PEMs coated and uncoated gold electrode to number of pelling test by detection of 1 mM KCl (inset: the picture of PEMs coated and uncoated electrode after 10 time of peeling with tape test).

After the eleventh number of layer coated the electrodes, the protecting of electrode was tested by tape testing process. The results showed that PEMs coating electrodes presented the same detection for all times test while the uncoating electrodes as shown in figure 4.36. The signal was dramatically dropped after testing five times. It can be concluded that the PEMs coating electrodes can prevent scratching of the electrodes without affecting the conductivity detection of KCl ions. So, it was applied to use in the last part of this chapter.

4.6 Application of gold nanoparticles electrodes and polyelectrolyte multilayers thin film

4.6.1 Carbaryl detection by gold nanoparticles electrodes

From the previous section, the PEMs coating the electrodes do not affect the conductivity detection of KCl solution. The PEMs coating electrodes do not only protect the electrodes from scratch, but can still be applied to bind with specific substance by electrostatic interaction. Humic substances are macromolecules that refer to the natural organic polyelectrolytes. So, HA can be formed complexes with wide range of metal ions and pesticides such as Cu, Pd, Cd, Zn, Ca, carbofuran, carbaryl and aldicarb [114-118]. HA could be applied to use as pesticides detector for environmental application. In this study, HA layer has been constructed on the PEMs coating electrodes in order to detect pesticide with conducticivity detection.

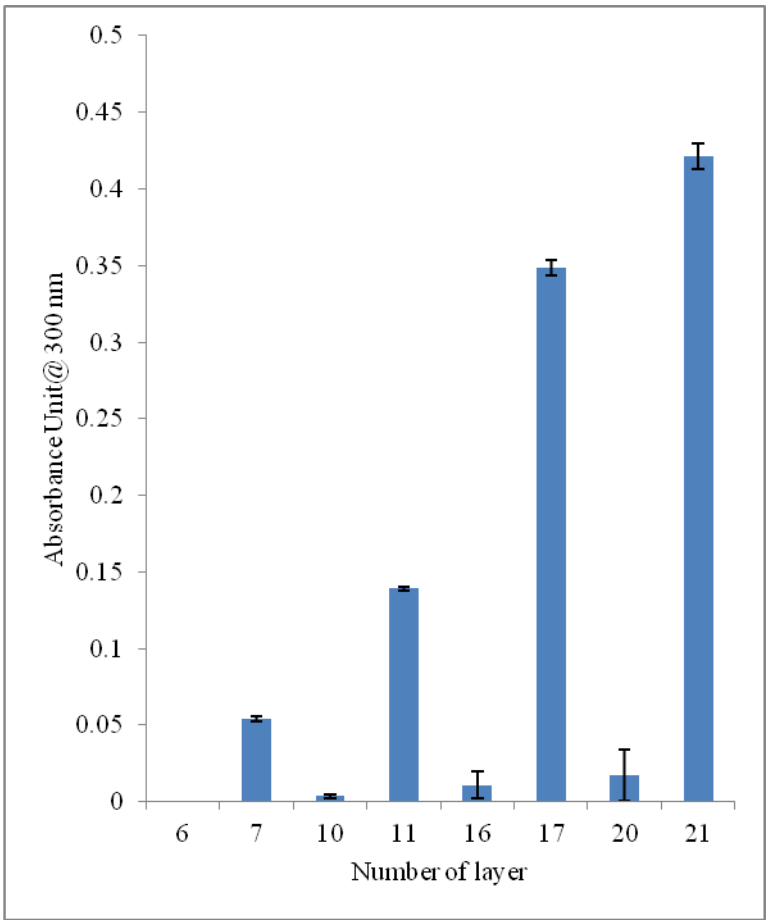

Figure 4.37 The plot of absorbance after dipping into HA solution with varying numbers of layer.

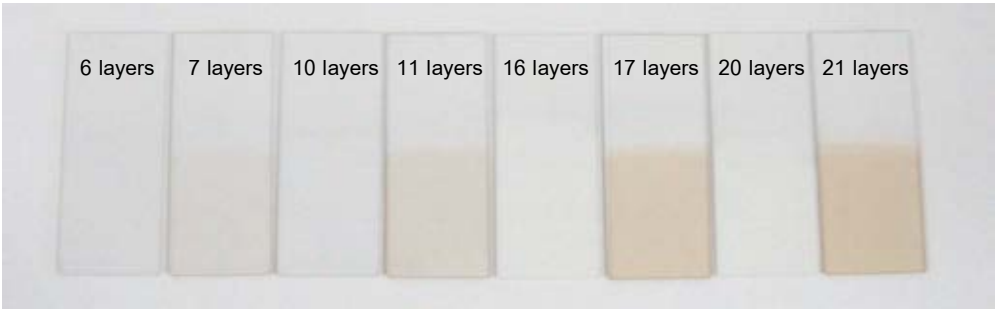

Figure 4.38 The pictures of thin film dip in HA solution samples with varying numbers of layer.

Figure 4.37 showed the increase in absorbance in case of the top layer of adsorption is positive charges. Figure 4.38 showed the varying number of layer PEMs coating electrodes and dipped into HA solution. 1 %wt concentration and pH 9.0 was

used to complete dissolution of HA. At this pH, most carboxylic groups are ionized. HA provide negative sites for the positively charged PDADMAC adsorption through electrostatic driven interaction. To study the kinetic adsorption of HA on PEMs, the 11 layers of PDADMAC-PSS coated glass slide was dipped in to HA solution with varying dipping times. The results of absorbance intensity at 320 nm showed the constant adsorption of HA with time from 10 to 60 minutes (Figure 4.39). To test carbaryl detection, the 11 layers of PDADMAC-PSS coated glass slide with 10 minutes dipping in HA was used.

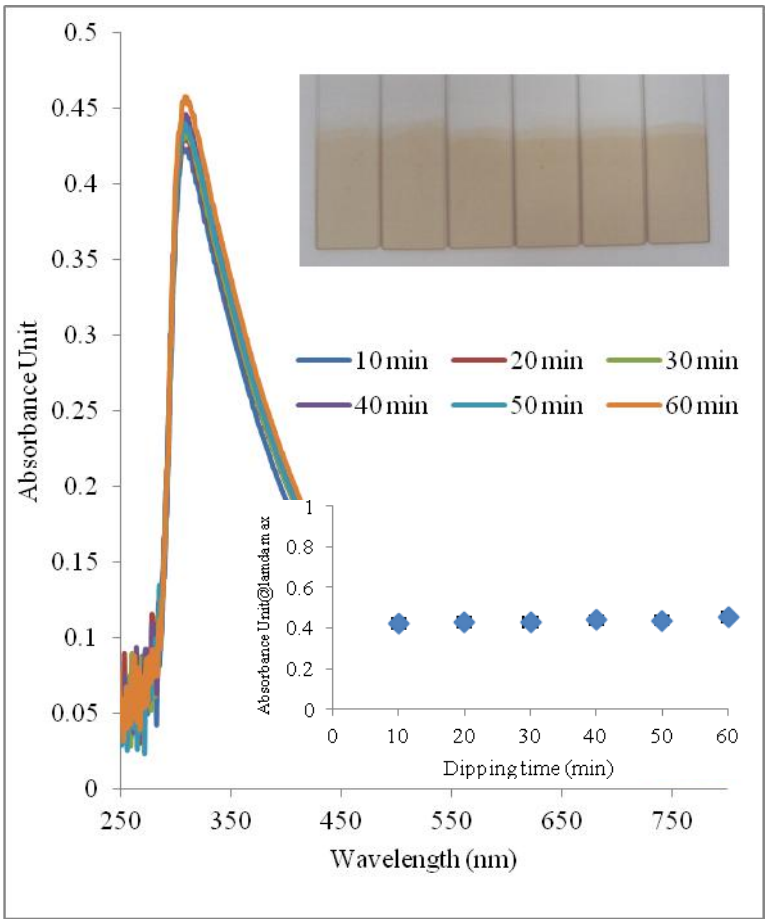

Figure 4.39 The 11 layers of PEMs coated electrode dip in HA solution with varying dipping times.

Pesticides are the organic contaminants in the environment. Carbaryl is a chemical in carbamate family. Carbaryl is used in insecticide for home, and agriculture.

Carbaryl is toxic to humans by skin contact, inhalation, and/or ingestion [119]. The chemical structure of carbaryl is presented as shown in figure 3.40.

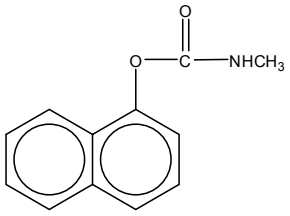

Figure 4.40 The structure of carbaryl.

In previous report, it was found that the carbaryl and dissolve organic matter (including HA) can interact to each other[118]. In this study, HA modified the PEMs coating electrode will be used to detect carbaryl. The result showed that the current detection dropped after dipping in to HA (Figure 3.41).

The 4.75% drop of current after dipping in HA for 10 minutes might be due to the binding between HA and PEMs coated electrodes blocked the ions of KCl. After 10 minutes dipping in HA solution, the current was relatively constant,which may be implied the saturated adsorption on HA on PEMs. After HA was coated on top of PEMs coating electrodes, then, the electrodes were immersed in to 0.01%wt of carbaryl solution with varying dipping times. The current was decreased around 7.28% from the initial value. One hypothesis to describe this phenomenon is that the adsorbed cabaryl could block the transfer of ions either cabaryl bound with PEMs or humic acid. Therefore, the separate experiment was performed to elucidate this observation. The PEMs coated gold electrode was dipped into the cabaryl solution. There was no any drop in the current was observed (data not shown here). The binding between HA and carbaryl is caused by hydrophobic interaction [118].

The effect of pH on the binding between cabaryl and HA was also investigated. The similar changes in observed current values were observed for all three pH values.

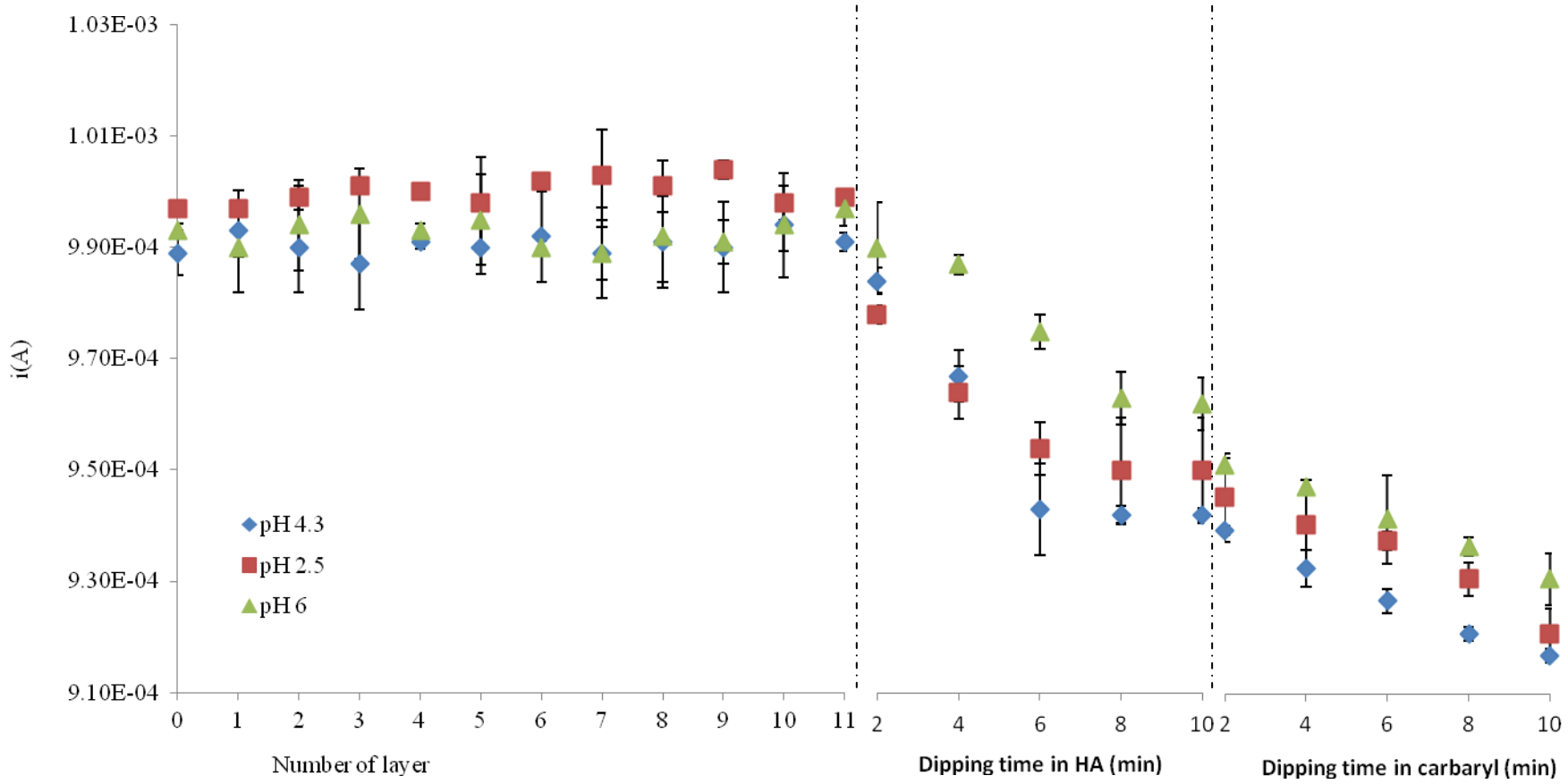

Figure4.41 The plots of current detection of 1 mM KCl with vary number of coating and pH of carbaryl solution.

4.6.2 PEM coating of PMMA surface for organic solvent resistant microfluidic chips

Typically, these devices are fabricated using various materials such as glass/silica, silicon, polymeric materials, elastomers, or a combination of these materials [120-122]. A wide variety of polymeric materials can be used to fabricate microchips with tunable optical, mechanical and surface properties [123-124]. Among all systems used, there is a growing interest in using microfluidic devices for bioanalysis under organic solvent condition [125-128]. However, solvents can cause the loss of transparency of poly(methyl methacrylate) (PMMA) by diffusion and swelling of PDMS based microchip. Transparency is necessary in optical detection of compound by fluorescence. Substrate swelling is also detrimental to the usage of the microchip with organic solvent as it leads to leakage and loss of contact between the sandwiched PMMA component [125, 129]. Limiting the PMMA chip swelling when exposed to acetonitrile is of interest as this solvent is commonly used as organic phase in bioanalysis as well as organic synthesis.

The layer-by-layer (LbL) deposition technique was used to protect Poly(methyl methacrylate), (PMMA) and PDMS substrate from acetonitrile, acetone and vapor of chloroform which used as the organic solvents.

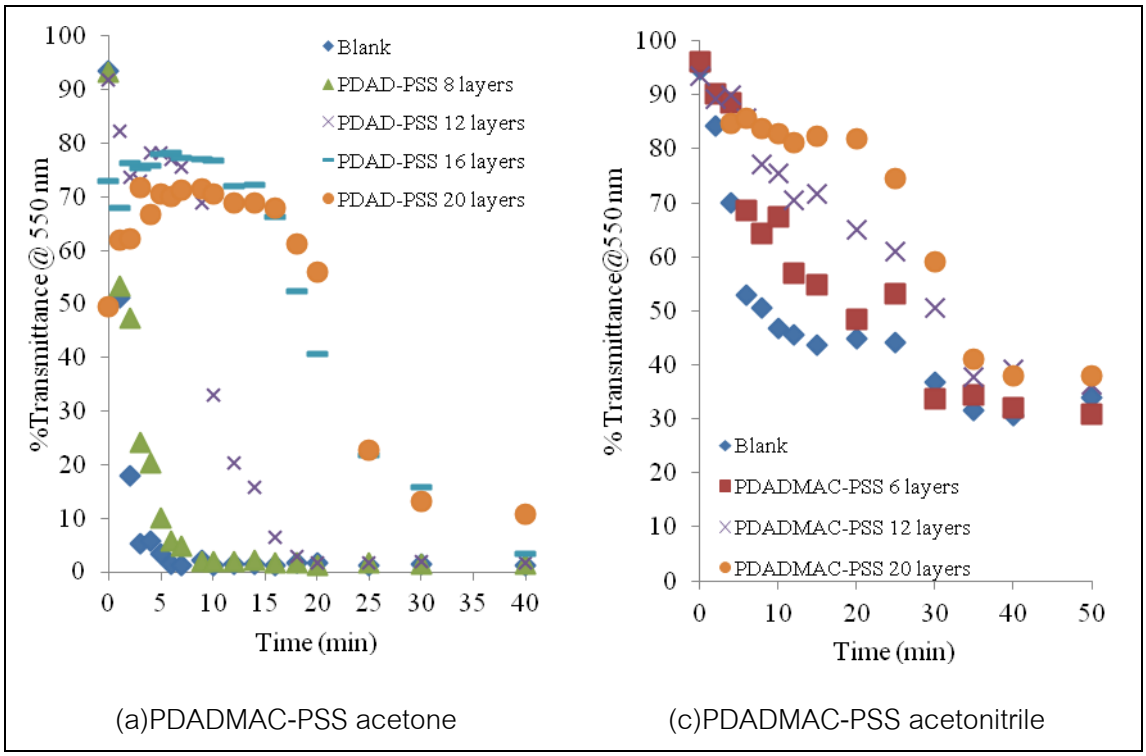

Figure 4.42 Percent transmittance of PMMA substrates coated with 0, 6, 12 and 20 layers of PDADMAC-PSS(a) and chitosan–alginate(b) when dipped in acetone and

PDADMAC-PSS(c) and chitosan–alginate(d) when dipped in acetonitrile as a function of time.

In order to protect the PMMA surface from organic solvent, polyelectrolyte multilayers are used here as a hydrophilic barrier. Because of their ionic structures, these coatings tend to repel hydrophobic solvent and here, two types of PEM thin films, PDADMAC/PSS and chitosan/alginate, were tested in two types of organic solvent. Put some references regarding the explaination why the electrostatic repel solvent and who used it. PSS PDAD is very hydrophylic then why it cannot block the solvent. The choice of these two types of PEM was driven by the fact that the first PDADMAC/PSS pair is made of synthetic polymer commonly used in PEM studies while chitosan/alginate are bio-polymer. The ionic character as well as the presence of a large amount of hydroxyl groups along the biopolymer repeat unit was hypothesized to provide a stronger hydrophilic character and therefore better protection against non-polar solvent when compare the standard PDADMAC/PSS pair. Tho choice of using these organic solvent is commonly used as organic phase in bioanalysis as well as organic synthesis.

PDADMAC-PSS was coated on PMMA substrate with uncontrolled pH condition. Simultaneously, pH 5.5 condition was used for chitosan-alginate coated PMMA substrate. Figure 4.42 showed comparison of the solvent resistance between the chitosan-alginate and PDADMAC-PSS multilayers thin films on PMMA substrates. Chitosan-alginate films are obtained stepwise by the electrostatic interaction of the carboxylic groups of alginate chains and amino groups of chitosan. Chitosan amino group is protonated at low pH. Amino group is converted to ammonium group and the positive charges are obtained. The pKa of chitosan is around 6.3, therefore, chitosan displays a polycationic behavior at pH 5.5. For alginate is a weak anionic polyeletrolyte. The negative charges of alginate depend on pH condition. The pKa of alginate is from 3.38 to 3.65, at pH above the pKa presents positively charges chains. So, a pH value of 5.5 was used for chitosan–alginate as it represents the condition under which both polyelectrolytes are well ionized and near their respective pKa. Chitosan-alginate and PDADMAC-PSS coated PMMA substrates were investigated the protecting solvent by

dipping in to acetonitrile or acetone as a function of time. The loss of transparency as a result of the solvent diffusion can be characterized for each coating when compared with the bare PMMA sample. From figure 4.42 it can be seen that the percent transmission through the bare PMMA decreases rapidly as a result of the solvent diffusion which leads to swelling and produce an opaque PMMA film. In contrast, when increasing the number of deposited layers for both PDADMAC/PSS (Figure 4.42 a, c) and chitosan/alginate (Figure 4.42 b, d) films, the transparency is maintained for 18 to 20 min for acetone testing and 25 to 30 min for acetronitrile testing, respectively. It can be seen that for both PEM coating, the solvent protection provided when using 6 layers is poor and is due to the incomplete coating of the PMMA surface. This can be explained by the low charge density of PMMA making it difficult for the polyelectrolytes to anchor on the surface. Nevertheless when 20 layers of chitosan–alginate or PDADMAC/PSS were deposited, the chitosan/alginate pair performed better and pictures of the different PMMA samples after 15 min are shown in figure 4.43. It can be seen that the bare PMMA is totally opaque, the PDADMAC/PSS coated is starting to become opaque but the chitosan/alginate sample remains transparent.

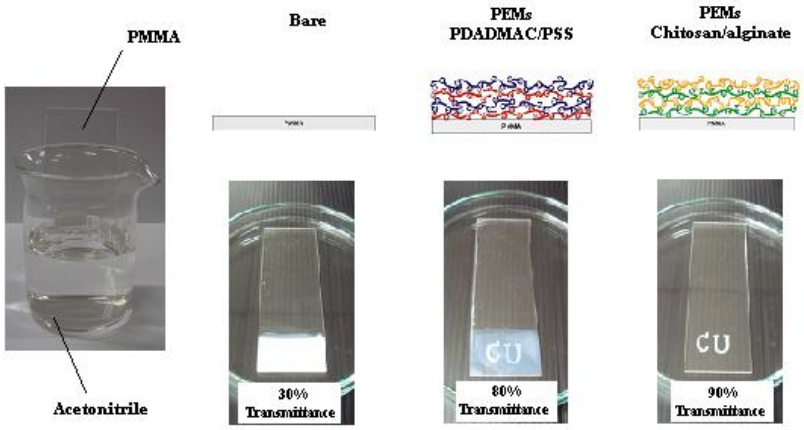

Figure 4.43 Scheme of PEMs coated PMMA substrates immerse in acetonitrile with the sample images at 15 min.

The thickness of the prepared film from both PDADMAC/PSS and chitosan/alginate after 20 layers was measured by measuring its step height of scratching the film as showed in figure 4.44. It was found 400 nm and 100 nm for PDADMAC/PSS and chitosan/alginate, respectively.

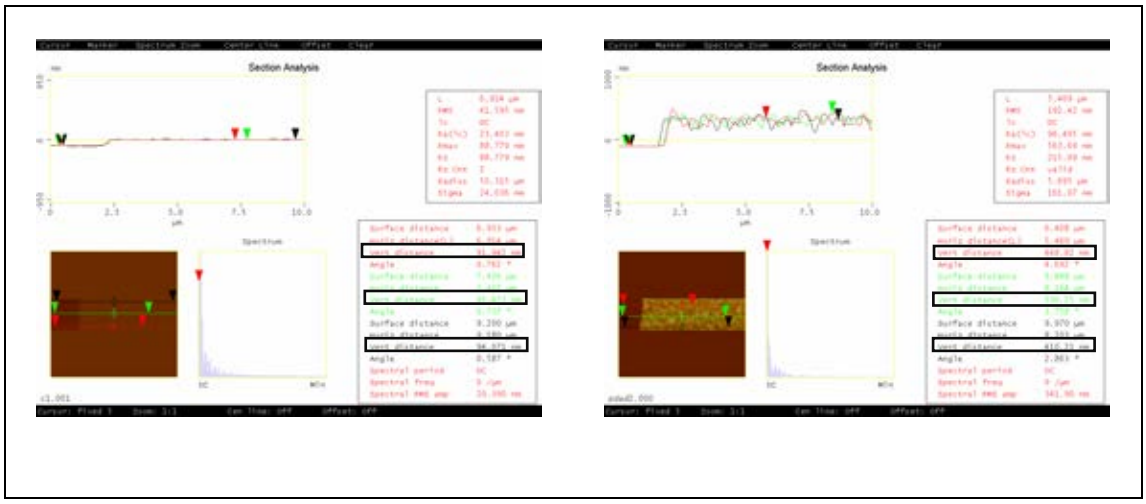

Figure 4.44 The comparison thin film thickness of PDADMAC/PSS and chitosan/alginate 20 layers.

Interestingly, although the chitosan/alginate film had a thickness of about a quarter of the PDADMAC/PSS film, its resistance to the solvent was found to be better. This confirms the superior solvent protection provided by the chitosan/alginate films. In contrast, the PDMS sample remained transparent when dipped in organic solvent due to their cross linked nature. The effect of solvent interaction is then limited to swelling which leads to loss of contact between the microchip part and leakage. Therefore to the observation of the changing in weight as a result of solvent adsorption was chosen. PDMS samples were exposed to chloroform vapor and their weight recorded as a function of time for various number of chitosan/alginate layers (Figure 4.45).

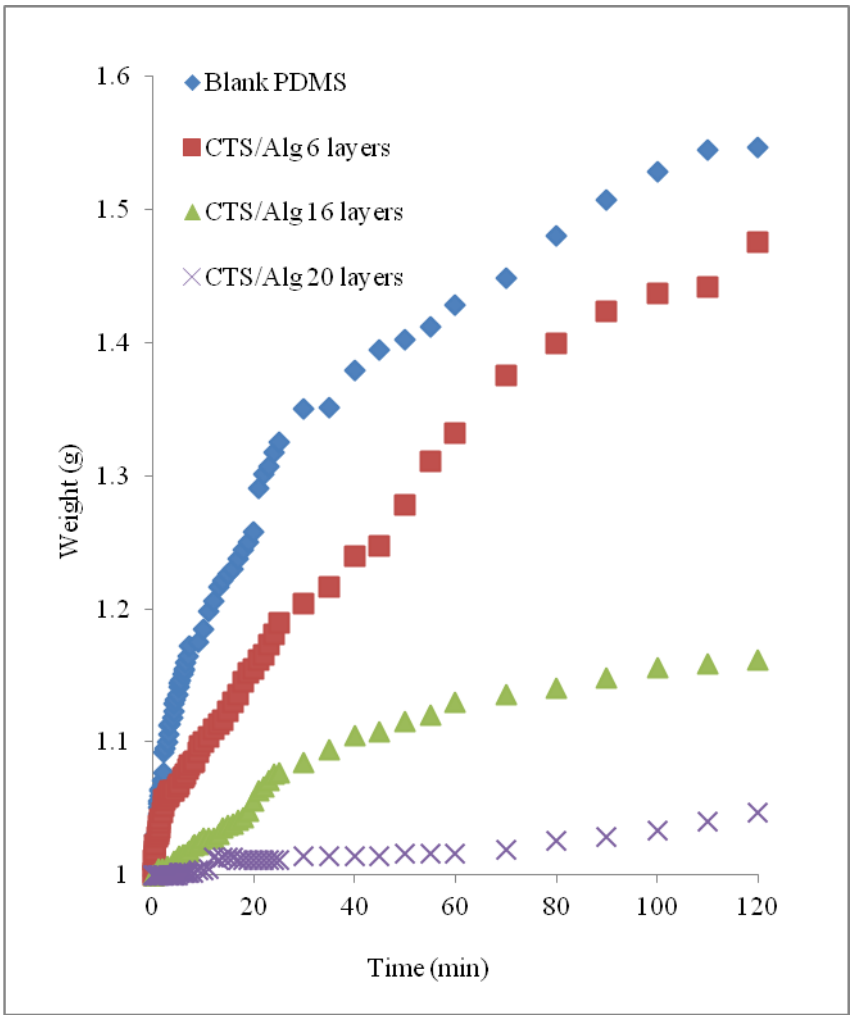

Figure 4.45 Weight investigation of chitosan (CTS)-alginate (Alg) coated PDMS with various number of layer under exposure to chloroform vapor (inset: Pictures of bare and 20 layers coated PDMS under exposure to chloroform vapor condition at 1 hr).

The chitosan/alginate pair was chosen as it provides the best solvent protection. It can be seen that the bare PDMS sample had a 55% weight increase after 2 h exposure but that the weight of the coated sample with 20 layers chitosan/alginate only increased by 5% for the same exposure time. The benefit of the coating is clearly seen and it is the hydrophilic nature of the biopolymer that is thought to be responsible to the low diffusion of the chloroform vapor.

CHAPTER V
CONCLUSIONS

In this work, metal nanoparticles were prepared by chemical reduction method. Anionic polyelectrolytes have been used to stabilize silver nanoparticles and sodium citrate has been used to stabilize and reduce gold nanoparticles. Electrostatic property of stabilizing agents provided stable solution and allowed to fabricate multilayers thin films via layer-by-layer self assembly technique. The growth of films was monitored using UV-Vis spectra of the substrate after each dipping step. The resistivity of metal nanoparticles multilayers thins film was found to be strongly dependent on the concentration of stabilizing agent used in nanoparticles synthesis. The multilayer thin film electrode fabricated with the gold nanoparticles using 30 mM sodium citrate as reducing and stabilizing reagents had the best stability and conductivity as low as bluk of gold and were used for the micro-electrode design.A simple and inexpensive method for fabricating microelectrodes with gold nanoparticles using 30 mM sodium citrate has been presented by layer-by-layer flow deposition technique. The FE-SEM and AFM images showed that gold nanoparticles could be successfully formed on a glass substrate and that the resulting microelectrode was uniform. The AC current detection of potassium chloride (KCl) solution showed the resulting of good efficiency detection. The gold nanoparticles electrodes also presented good reproducibility by testing ten electrodes and run to run of an electrode. In addition, the microelectrode can be easily integrated into microfluidic devices.

The high conductive thin film revealed an easily scratch of thin film electrode. The PEMs coating electrodes have been presented as good protecting layer on electrodes from scratching of electrode which were not affect the detection performance. This method has also been used to detect carbaryl.

A rapid and simple technique for an organic solvent resistant was also presented. Surface coating and controllable hydrophilic surface were demonstrated which provided flexibility technique for various applications.

Suggestions

More work is clearly needed in order to study the specific behavior of the metal nanoparticles electrodes. The modifying the type of coating can also use to fabricate thin film electrode via this technique. Many other types polyelectrolytes and nanomaterials could suggest such as nanorods, composite, conducting polymer, modified carbon nanotubes.

Decouplers can be used to allow placing the ground electrode and thus electrically separate the systems in order to use electrode under electrical potential.

REFERENCES

[1] Aubry N., Singh P. Recent advances in microfluidics. Mechanics Research Communications 36 (2009):1-1.

[2] Chung T.D., Kim H.C. Recent advances in miniaturized microfluidic flow cytometry for clinical use. Electrophoresis 28 (2007):4511-4520.

[3] Ferguson B.S., Buchsbaum S.F., Swensen J.S., Hsieh K., Lou X.H., Soh H.T. Integrated Microfluidic Electrochemical DNA Sensor. Analytical Chemistry 81 (2009):6503-6508.

[4] Lin Y.H., Wu H., Timchalk C.A., Thrall K.D. Integrated microfluidics/electrochemical sensor system for monitoring of environmental exposures to toxic chemicals. Abstracts of Papers of the American Chemical Society 223 (2002):U77-U77.

[5] Uhrig K., Kurre R., Schmitz C., Curtis J.E., Haraszti T., Clemen A.E.M., et al. Optical force sensor array in a microfluidic device based on holographic optical tweezers. Lab on a Chip 9 (2009):661-668.

[6] Luan L., Evans R.D., Jokerst N.M., Fair R.B. Integrated optical sensor in a digital microfluidic platform. Ieee Sensors Journal 8 (2008):628-635.

[7] Shafiee H., Sano M.B., Henslee E.A., Caldwell J.L., Davalos R.V. Selective isolation of live/dead cells using contactless dielectrophoresis (cDEP). Lab on a Chip 10 (2010):438-445.

[8] Kuban P., Hauser P.C. Evaluation of microchip capillary electrophoresis with external contactless conductivity detection for the determination of major inorganic ions and lithium in serum and urine samples. Lab on a Chip 8 (2008):1829-1836.

[9] Kohlheyer D., Eijkel J.C.T., Schlautmann S., van den Berg A., Schasfoort R.B.M. Bubble-free operation of a microfluidic free-flow electrophoresis chip with integrated Pt electrodes. Analytical Chemistry 80 (2008):4111-4118.

[10] Hong C., Bao D., Thomas M.S., Clift J.M., Vullev V.I. Print-and-peel fabrication of microelectrodes. Langmuir 24 (2008):8439-8442.

[11] Kovarik M.L., Torrence N.J., Spence D.M., Martin R.S. Fabrication of carbon microelectrodes with a micromolding technique and their use in microchip-based flow analyses. Analyst 129 (2004):400-405.

[12] Choi J.W., Rosset S., Niklaus M., Adleman J.R., Shea H., Psaltis D. 3-dimensional electrode patterning within a microfluidic channel using metal ion implantation. Lab on a Chip 10 (2010):783-788.

[13] Dong H., Li C.M., Zhang Y.F., Cao X.D., Gan Y. Screen-printed microfluidic device for electrochemical immunoassay. Lab on a Chip 7 (2007):1752-1758.

[14] Redha Z.M., Baldock S.J., Fielden P.R., Goddard N.J., Brown B.J.T., Haggett B.G.D., et al. Hybrid Microfluidic Sensors Fabricated by Screen Printing and Injection Molding for Electrochemical and Electrochemiluminescence Detection. Electroanalysis 21 (2009):422-430.

[15] Fischer D.J., Vandaveer W.R., Grigsby R.J., Lunte S.M. Pyrolyzed photoresist carbon electrodes for microchip electrophoresis with dual-electrode amperometric detection. Electroanalysis 17 (2005):1153-1159.

[16] Zhang L., Shen Y.H., Xie A.J., Li S.K., Wang C. One-step synthesis of silver nanoparticles in self-assembled multilayered films based on a Keggin structure compound. Journal of Materials Chemistry 18 (2008):1196-1203.

[17] Buso D., Palmer L., Bello V., Mattei G., Post M., Mulvaney P., et al. Self-assembled gold nanoparticle monolayers in sol-gel matrices: synthesis and gas

sensing applications. Journal of Materials Chemistry 19 (2009):2051-2057.

[18] Franzen S., Gerber R.W., Leonard D.N. Conductive thin film multilayers of gold on glass formed by self-assembly of multiple size gold nanoparticles. Thin Solid Films 517 (2009):6803-6808.

[19] Steen W.A., Schwartz D.T. A route to diverse combinatorial libraries of electroactive nickel hexacyanoferrate. Chemistry of Materials 15 (2003):2449-2453.

[20] Liao K.T., Chen C.M., Huang H.J., Lin C.H. Poly(methyl methacrylate) microchip device integrated with gold nanoelectrode ensemble for in-column biochemical reaction and electrochemical detection. Journal of Chromatography A 1165 (2007):213-218.

[21] Riekkola M.L., Parshintsev J., Ruiz-Jimenez J., Petaja T., Hartonen K., Kulmala M. Comparison of quartz and Teflon filters for simultaneous collection of size-separated ultrafine aerosol particles and gas-phase zero samples. Analytical and Bioanalytical Chemistry 400 (2011):3527-3535.

[22] Lo Nostro P., Falletta E., Bonini M., Fratini E., Lo Nostro A., Pesavento G., et al. Clusters of poly(acrylates) and silver nanoparticles: Structure and applications for antimicrobial fabrics. Journal of Physical Chemistry C 112 (2008):11758-11766.

[23] Dubas S.T., Potiyaraj P., Kumlangdudsana P. Synthesis of silver chloride nanocrystal on silk fibers. Materials Letters 61 (2007):2464-2466.

[24] Ramaraj R., Maduraiveeran G., Tamilmani V. Silver quantum dots for selective detection of mercuric ions. Current Science 100 (2011):199-204.

[25] Suh J.S., Lee S., Gu G.H. A simple method to fabricate silver colloid clusters for surface-enhanced Raman scattering. Chemical Physics Letters 511 (2011):121-125.

[26] Biswas P., Sahu M. Single-step processing of copper-doped titania nanomaterials in a flame aerosol reactor. Nanoscale Research Letters 6 (2011):1-14.

[27] Paik U., Kim J.Y., Hackley V.A. Rheological and electrokinetic behavior associated with concentrated nanosize silica hydrosols. Materials Chemistry and Physics 91 (2005):205-211.

[28] Kimura K., Liu S.M., Yang Y., Sato S. Enhanced photoluminescence from Si nano-organosols by functionalization with alkenes and their size evolution. Chemistry of Materials 18 (2006):637-642.

[29] Murphy C.J., Gole A.M., Hunyadi S.E., Orendorff C.J. One-dimensional colloidal gold and silver nanostructures. Inorganic Chemistry 45 (2006):7544-7554.

[30] Zheng J.W., Li X.W., Gu R.N., Lu T.H. Comparison of the surface properties of the assembled silver nanoparticle electrode and roughened silver electrode. Journal of Physical Chemistry B 106 (2002):1019-1023.

[31] Schatz G.C., Zhao J., Pinchuk A.O., Mcmahon J.M., Li S.Z., Ausman L.K., et al. Methods for Describing the Electromagnetic Properties of Silver and Gold Nanoparticles. Accounts of Chemical Research 41 (2008):1710-1720.

[32] Lead J.R., Fabrega J., Luoma S.N., Tyler C.R., Galloway T.S. Silver nanoparticles: Behaviour and effects in the aquatic environment. Environment International 37 (2011):517-531.

[33] Dubas S.T., Wacharanad S., Potiyaraj P. Tunning of the antimicrobial activity of surgical sutures coated with silver nanoparticles. Colloids and Surfaces a-Physicochemical and Engineering Aspects 380 (2011):25-28.

[34] Dubas S.T., Pimpan V. Green synthesis of silver nanoparticles for ammonia sensing. Talanta 76 (2008):29-33.

[35] Murphy C.J., Sau T.K. Seeded high yield synthesis of short Au nanorods in aqueous solution. Langmuir 20 (2004):6414-6420.

[36] Murphy C.J., Caswell K.K., Bender C.M. Seedless, surfactantless wet chemical synthesis of silver nanowires. Nano Letters 3 (2003):667-669.

[37] Dubas S.T., Limsavarn L., Sritaveesinsub V. Polyelectrolyte assisted silver nanoparticles synthesis and thin film formation. Materials Letters 61 (2007):3048-3051.

[38] Kelly K.L., Coronado E., Zhao L.L., Schatz G.C. The optical properties of metal nanoparticles: The influence of size, shape, and dielectric environment. Journal of Physical Chemistry B 107 (2003):668-677.

[39] El-Sayed M.A., Eustis S. Why gold nanoparticles are more precious than pretty gold: Noble metal surface plasmon resonance and its enhancement of the radiative and nonradiative properties of nanocrystals of different shapes. Chemical Society Reviews 35 (2006):209-217.

[40]https://vpn.chula.ac.th/+CSCO+c0756767633A2F2F6A6A6A2E6676747A6E6E7971657670752E70627A++/materials-science/nanomaterials/silver-nanoparticles.html.

[41] Evanoff D.D., Chumanov G. Synthesis and optical properties of silver nanoparticles and arrays. Chemphyschem 6 (2005):1221-1231.

[42] Cao G. NANOSTRUCTURES AND NANOMATERIALS Synthesis, Properties and Applications: Imperial College Press, 2004.

[43] Roucoux A., Schulz J., Patin H. Reduced transition metal colloids: A novel family of reusable catalysts? Chemical Reviews 102 (2002):3757-3778.

[44] Schmid G., West H., Mehles H., Lehnert A. Hydrosilation reactions catalyzed by supported bimetallic colloids. Inorganic Chemistry 36 (1997):891-895.

[45] Laoufi I., Saint-Lager M.C., Lazzari R., Jupille J., Robach O., Garaudee S., et al. Size and Catalytic Activity of Supported Gold Nanoparticles: An in Operando Study during CO Oxidation. Journal of Physical Chemistry C 115 (2011):4673-4679.

[46] Dey K.K., Panda B.R., Paul A., Basu S., Chattopadhyay A. Catalytic gold nanoparticle driven pH specific chemical locomotion. Journal of Colloid and Interface Science 348 (2010):335-341.

[47] Mayer A.B.R., Johnson R.W., Hausner S.H., Mark J.E. Colloidal silver nanoparticles protected by water-soluble nonionic polymers and "soft" polyacids. Journal of Macromolecular Science-Pure and Applied Chemistry A36 (1999):1427-1441.

[48] Jana N.R., Gearheart L., Murphy C.J. Evidence for seed-mediated nucleation in the chemical reduction of gold salts to gold nanoparticles. Chemistry of Materials 13 (2001):2313-2322.

[49] Leone S.R., Abate Y., Schwartzberg A., Strasser D. Nanometer-scale size dependent imaging of cetyl trimethyl ammonium bromide (CTAB) capped and uncapped gold nanoparticles by apertureless near-field optical microscopy. Chemical Physics Letters 474 (2009):146-152.

[50] John Turkevich P.C.S.a.J.H. A study of the nucleation and growth processes in the synthesis of colloidal gold Discuss Faraday Soc, 11 (1951):55-75.

[51] Harriman A.T., J. M.; Millward, G. R. . Catalytic and structural properties of iridium-iridium dioxide colloids New Journal of Chemistry 11 (1987):757-762

[52] Furlong D.N.L., Anton; Sasse, Wolfgang H. F.; Sanders, John V. . Colloidal platinum sols Preparation, characterization, and stability towards salt Journal of the Chemical Society, Faraday Transactions 1: Physical Chemistry in Condensed Phases 80 (1984):571-588.

[53] Tano T.E., Kunio; Meguro, Kenjiro Preparation of organopalladium sols by thermal decomposition of palladium acetate Journal of Colloid and Interface Science 133 (1989):530-533

[54] Esumi K.S., Maki; Tano, Takafumi; Torigoe, Kanjiro; Meguro, Kenjiro Dispersion of uniformly sized palladium particles in organic solvents Colloids and Surfaces a-Physicochemical and Engineering Aspects 55 (1991):9-14

[55] Esumi K., Itakura T., Torigoe K. Preparation of Organo Palladium Sols from Palladium Complexes in Various Alcohols. Colloids and Surfaces a-Physicochemical and Engineering Aspects 82 (1994):111-113.

[56] Robert Prucek L.K.a.J.H. Silver Colloids-Methods of Preparation and Utilization ACTA UNIVERSITATIS PALACKIANAE OLOMUCENSIS CHEMICA 43 (2004):1-12.

[57] Grieser F., Hobson R., Sostaric J., Mulvaney P. Sonochemical reduction processes in aqueous colloidal systems. Ultrasonics 34 (1996):547-550.

[58] J. S. Bradley E.W.H., S. Behal, C. Klein, A. Duteil, B. Chaudret. Preparation and characterization of organosols of monodispersed nanoscale palladium. Particle size effects in the binding geometry of adsorbed carbon monoxide. Chem Mater 4 (1992):1234–1239.

[59] de Caro D., Bradley J.S. Investigation of the surface structure of colloidal platinum by infrared spectroscopy of adsorbed CO. New Journal of Chemistry 22 (1998):1267-1273.

[60] Berns R.S. Principles of color technology. John Wiley&Sons; 2000.

[61] Chirea M., Garcia-Morales V., Manzanares J.A., Pereira C., Gulaboski R., Silva F. Electrochemical characterization of polyelectrolyte/gold nanoparticle multilayers self-assembled on gold electrodes. Journal of Physical Chemistry B 109 (2005):21808-21817.

[62] Lin L., Qiu P.H., Cao X.N., Jin L.T. Colloidal silver nanoparticles modified electrode and its application to the electroanalysis of Cytochrome c. Electrochimica Acta 53 (2008):5368-5372.

[63] Gero Decher J.B.S. Multilayer Thin Films: Wiley-VCH Verlag GmbH & Co. KGaA, 2002.

[64] Herbert Dautzenberg B.P. Polyelectrolytes: Formation,Characterization and Application. New York Hanser Publishers, 1994.

[65] Dubas S.T., Schlenoff J.B. Factors controlling the growth of polyelectrolyte multilayers. Macromolecules 32 (1999):8153-8160.

[66] Darhuber A.A., Troian S.M. Principles of microfluidic actuation by modulation of surface stresses. Annual Review of Fluid Mechanics 37 (2005):425-455.

[67] Yeh C.H., Zhao Q.L., Lee S.J., Lin Y.C. Using a T-junction microfluidic chip for monodisperse calcium alginate microparticles and encapsulation of nanoparticles. Sensors and Actuators a-Physical 151 (2009):231-236.

[68] Zhang X. H.S.J. Micro-Fluidic and Lab-on-a-ChipTechnology. Ernst Schering Foundation Symposium Proceedings 3 (2007):21-37.

[69] Yi C.Q., Zhang Q., Li C.W., Yang J., Zhao J.L., Yang M.S. Optical and electrochemical detection techniques for cell-based microfluidic systems. Analytical and Bioanalytical Chemistry 384 (2006):1259-1268.

[70] Jennifer E. R. P.B., Rebecca H., Cynthia, Zimmerman, Clare S., Rebecca M., and Christopher C. A Low Cost Microfluidic Microarray System for Typing Y Chromosome SNPs 2009 p. 1-45.

[71] Kumar C.S. Microfluidic Devices in Nanotechnology: Fundamental Concepts: John Wiley & Sons, Inc., 2010.

[72] http://en.wikipedia.org/wiki/Hagen%E2%80%93Poiseuille_equation/23-08-2010.

[73] Schwarz M.A., Hauser P.C. Recent developments in detection methods for microfabricated analytical devices. Lab on a Chip 1 (2001):1-6.

[74] Belder D., Ludwig M., Kohler F. High-speed chiral separations on a microchip with UV detection. Electrophoresis 24 (2003):3233-3238.

[75] Belder D., Schulze P., Ludwig M., Kohler F. Deep UV laser-induced fluorescence detection of unlabeled drugs and proteins in microchip electrophoresis. Analytical Chemistry 77 (2005):1325-1329.

[76] Henry C.S. Microchip Capillary Electrophoresis Methods and Protocols. Methods and Protocols: Humana Press Inc., 2006.

[77] Pumera M. Contactless conductivity detection for microfluidics: Designs and applications. Talanta 74 (2007):358-364.

[78] Haddad P.R., Guijt R.M., Evenhuis C.J., Macka M. Conductivity detection for conventional and miniaturised capillary electrophoresis systems. Electrophoresis 25 (2004):4032-4057.

[79] Qiang W., Zhai C., Lei J.P., Song C.J., Zhang D.M., Sheng J., et al. Disposable microfluidic device with ultraviolet detection for highly resolved screening of illicit drugs. Analyst 134 (2009):1834-1839.

[80] Xu B.J., Yang M., Wang H., Zhang H.L., Jin Q.H., Zhao J.L., et al. Line laser beam based laser-induced fluorescence detection system for microfluidic chip electrophoresis analysis. Sensors and Actuators a-Physical 152 (2009):168-175.

[81] Bruening M.L., Harris J.J. Electrochemical and in situ ellipsometric investigation of the permeability and stability of layered polyelectrolyte films. Langmuir 16 (2000):2006-2013.

[82] Wang K., Dai H., Leng T., Mehenti N.Z., Harris J.S., Fishman H.A. Fabrication and characterization of a carbon nanotube microelectrode array for retinal prostheses. Investigative Ophthalmology & Visual Science 45 (2004):U379-U379.

[83] Lacher N.A., Lunte S.M., Martin R.S. Development of a microfabricated palladium decoupler/electrochemical detector for microchip capillary electrophoresis using a hybrid glass/poly(dimethylsiloxane) device. Analytical Chemistry 76 (2004):2482-2491.

[84] Wang J., Tian B.M., Sahlin E. Integrated electrophoresis chips/amperometric detection with sputtered gold working electrodes. Analytical Chemistry 71 (1999):3901-3904.

[85] Martin R.S., Kovarik M.L., Torrence N.J., Spence D.M. Fabrication of carbon microelectrodes with a micromolding technique and their use in microchip-based flow analyses. Analyst 129 (2004):400-405.

[86] Kadara R.O., Jenkinson N., Banks C.E. Characterization and fabrication of disposable screen printed microelectrodes. Electrochemistry Communications 11 (2009):1377-1380.

[87] Lenihan J.S., Ball J.C., Gavalas V.G., Lumpp J.K., Hines J., Daunert S., et al. Microfabrication of screen-printed nanoliter vials with embedded surface-modified electrodes. Analytical and Bioanalytical Chemistry 387 (2007):259-265.

[88] Ji Z.Y., Li H.X., Liu Y.L., Hu W.P. Electroplating silver tetracyanoquinodimethane between gold micro-gap electrodes for the fabrication of coplanar devices, a new way to integrate material synthesis and devices fabrication within one step. Applied Physics a-Materials Science & Processing 91 (2008):301-303.

[89] Halperin S.A. The difference between surface resistance and surface resistivity. Ee-Evaluation Engineering 35 (1996):46-&.

[90] Gutiérrez M.P., Li H., Patton J. Thin Film Surface Resistivity. (2002).

[91] http://en.wikipedia.org/wiki/Van_der_Pauw_method/12-10-10.

[92] Ladam G., Schaad P., Voegel J.C., Schaaf P., Decher G., Cuisinier F. In situ determination of the structural properties of initially deposited polyelectrolyte multilayers. Langmuir 16 (2000):1249-1255.

[93] Galloway M., Stryjewski W., Henry A., Ford S.M., Llopis S., McCarley R.L., et al. Contact conductivity detection in poly(methyl methacylate)-based microfluidic devices for analysis of mono- and polyanionic molecules. Analytical Chemistry 74 (2002):2407-2415.

[94] ASTM D 3359 Standard Test Methods for Measuring Adhesion by Tape Test.

[95] Dubas S.T., Pimpan V. Humic acid assisted synthesis of silver nanoparticles and its application to herbicide detection. Materials Letters 62 (2008):2661-2663.

[96] Karak N., Konwarh R.K., R., Gogoi B., Philip R., Laskar M.A. Biomimetic preparation of polymer-supported free radical scavenging, cytocompatible and antimicrobial "green" silver nanoparticles using aqueous extract of Citrus sinensis peel. Colloids and Surfaces B-Biointerfaces 84 (2011):338-345.

[97] Nath S.S., Das R., Chakdar D., Gope G., Bhattacharjee R. Synthesis of silver nanoparticles and their optical properties. Journal of Experimental Nanoscience 5 (2010):357-362.

[98] Frank A.J., Cathcart N., Maly K.E., Kitaev V. Synthesis of Silver Nanoprisms with Variable Size and Investigation of Their Optical Properties: A First-Year

Undergraduate Experiment Exploring Plasmonic Nanoparticles. Journal of Chemical Education 87 (2010):1098-1101.

[99] Sileikaite A., Puiso J., Prosycevas I., Tamulevicius S. Investigation of Silver Nanoparticles Formation Kinetics During Reduction of Silver Nitrate with Sodium Citrate. Materials Science-Medziagotyra 15 (2009):21-27.

[100] Tan Y.W., Wang Y., Jiang L., Zhu D.B. Thiosalicylic acid-functionalized silver nanoparticles synthesized in one-phase system. Journal of Colloid and Interface Science 249 (2002):336-345.

[101] http://www.scitopics.com/Zeta_potential.html/14-08-2011.

[102] Kotov N.A., Correa-Duarte M.A., Giersig M., Liz-Marzan L.M. Control of packing order of self-assembled monolayers of magnetite nanoparticles with and without SiO2 coating by microwave irradiation. Langmuir 14 (1998):6430-6435.

[103] Kotov N.A., Ostrander J.W., Mamedov A.A. Two modes of linear layer-by-layer growth of nanoparticle-polylectrolyte multilayers and different interactions in the layer-by-layer deposition. Journal of the American Chemical Society 123 (2001):1101-1110.

[104] Dubas S.T., Farhat T.R., Schlenoff J.B. Multiple membranes from "true" polyelectrolyte multilayers. Journal of the American Chemical Society 123 (2001):5368-5369.

[105] Ung T., Liz-Marzan L.M., Mulvaney P. Optical properties of thin films of Au@SiO2 particles. Journal of Physical Chemistry B 105 (2001):3441-3452.

[106] Banhart J. Relativistic and non-relativistic electron transport in disordered alloys .2. Applications to palladium alloyed with copper, silver and gold. Philosophical Magazine B-Physics of Condensed Matter Statistical

Mechanics Electronic Optical and Magnetic Properties 77 (1998):105-119.

[107] Henry C.S., Liu Y., Wipf D.O. Conductivity detection for monitoring mixing reactions in microfluidic devices. Analyst 126 (2001):1248-1251.

[108] http://en.wikipedia.org/wiki/Electrolysis_of_water.

[109] Kok W.T., Sahin Y. SOLID-STATE FIELD DECOUPLER FOR OFF-COLUMN DETECTION IN CAPILLARY ELECTROPHORESIS. Analytical Chemistry 65 (1993):2497-2501.

[110] Hauser P.C., Kuban P. Fundamentals of electrochemical detection techniques for CE and MCE. Electrophoresis 30 (2009):3305-3314.

[111] Soper S.A., Galloway M., Stryjewski W., Henry A., Ford S.M., Llopis S., et al. Contact conductivity detection in poly(methyl methacylate)-based microfluidic devices for analysis of mono- and polyanionic molecules. Analytical Chemistry 74 (2002):2407-2415.

[112] Miller M.D., Bruening M.L. Correlation of the swelling and permeability of polyelectrolyte multilayer films. Chemistry of Materials 17 (2005):5375-5381.

[113] Bruening M.L., Miller M.D. Correlation of the swelling and permeability of polyelectrolyte multilayer films. Chemistry of Materials 17 (2005):5375-5381.

[114] Fernandez-Calvino D., Soler-Rovira P., Polo A., Arias-Estevez M., Plaza C. Influence of humified organic matter on copper behavior in acid polluted soils. Environmental Pollution 158 (2010):3634-3641.

[115] David C., Mongin S., Rey-Castro C., Galceran J., Companys E., Garces J.L., et al. Competition effects in cation binding to humic acid: Conditional affinity

spectra for fixed total metal concentration conditions. Geochimica Et Cosmochimica Acta 74 (2010):5216-5227.

[116] Matsuda M., Kaminaga A., Hayakawa K., Takisawa N., Miyajima T. Surfactant binding by humic acids in the presence of divalent metal salts. Colloids and Surfaces a-Physicochemical and Engineering Aspects 347 (2009):45-49.

[117] Ghabbour E.A., Shaker M., El-Toukhy A., Abid I.M., Davies G. Thermodynamics of metal cation binding by a solid soil-derived humic acid: Binding of Fe(III), Pb(II), and Cu(II). Chemosphere 63 (2006):477-483.

[118] Fang F., Kanan S., Patterson H.H., Cronan C.S. A spectrofluorimetric study of the binding of carbofuran, carbaryl, and aldicarb with dissolved organic matter. Analytica Chimica Acta 373 (1998):139-151.

[119] Hall D.G., Nguyen R. Toxicity of pesticides to Tamarixia radiata, a parasitoid of the Asian citrus psyllid. Biocontrol 55 (2010):601-611.

[120] Auroux P.A., Iossifidis D., Reyes D.R., Manz A. Micro total analysis systems. 2. Analytical standard operations and applications. Analytical Chemistry 74 (2002):2637-2652.

[121] Shoji S. Review of micro total analysis systems (mu-TAS). Electrochemistry 68 (2000):188-191.

[122] Xie Y.C., Xu Y., Yung K.L., Huang L.B., Lee M.H. Photolamination bonding for PMMA microfluidic chips. Microsystem Technologies-Micro-and Nanosystems-Information Storage and Processing Systems 16 (2010):1887-1891.

[123] Easley C.J., Benninger R.K.P., Shaver J.H., Head W.S., Piston D.W. Rapid and inexpensive fabrication of polymeric microfluidic devices via toner transfer masking. Lab on a Chip 9 (2009):1119-1127.

[124] Fu G., Tor S.B., Loh N.H., Hardt D.E. Fabrication of robust tooling for mass production of polymeric microfluidic devices. Journal of Micromechanics and Microengineering 20 (2010).

[125] Lee J.N., Park C., Whitesides G.M. Solvent compatibility of poly(dimethylsiloxane)-based microfluidic devices. Analytical Chemistry 75 (2003):6544-6554.

[126] Sun X.H., Peeni B.A., Yang W., Becerril H.A., Woolley A.T. Rapid prototyping of poly(methyl methacrylate) microfluidic systems using solvent imprinting and bonding. Journal of Chromatography A 1162 (2007):162-166.

[127] Porras S.P., Kenndler E. Are the asserted advantages of organic solvents in capillary electrophoresis real? A critical discussion. Electrophoresis 26 (2005):3203-3220.

[128] Hung L.H., Lin R., Lee A.P. Rapid microfabrication of solvent-resistant biocompatible microfluidic devices. Lab on a Chip 8 (2008):983-987.

[129] Lee J., Kim M.J., Lee H.H. Surface modification of poly(dimethylsiloxane) for retarding swelling in organic solvents. Langmuir 22 (2006):2090-2095.